This is to certify that the
dissertation entitled

MESOSTRUCTURED SILICA FOR THE REINFORCEMENT
OF THERMOSET EPOXY POLYMERS

presented by

IN PARK

has been accepted towards fulfillment
of the requirements for the

Ph.D. degree in Department of Chemistry

Thomas J. Pinnavaia
Major Professor's Signature

January 10, 2006
Date

MESOSTRUCTURED SILICA FOR THE REINFORCEMENT OF THERMOSET EPOXY POLYMERS

By

In Park

A DISSERTATION

Submitted to
Michigan State University
in partial fulfillment of the requirements
for the degree of

DOCTOR OF PHILOSOPHY

Department of Chemistry

2006

ABSTRACT

MESOSTRUCTURED SILICA FOR THE REINFORCEMENT OF THERMOSET EPOXY POLYMERS

By

In Park

Large-pore mesoporous silicas with wormhole framework structures have been assembled through hydrogen-bonding pathways from sodium silicate or tetraethylorthosilicate as the silica source and amine-terminated Jeffamine surfactants of the type $H_2NCH(CH_3)CH_2[OCH_2CH(CH_3)]_xNH_2$ as the structure-directing porogen. Depending on the molecular weight of the *α,ω*-diamine surfactant (x = 33 and 68 for Jeffamine D2000 and D4000, respectively) and the synthesis temperature (25–65°C), the mean pore size distributions of the mesostructured silicas (denoted MSU-J) were centered between 4.9 and 14.3 nm.

The as-made and calcined forms of MSU-J (5.3 nm pore size) have been used to form rubbery epoxy mesocomposites containing 1.0–12 wt% silica. The tensile modulus, strength, elongation, and toughness for the mesocomposites formed from as-made and calcined forms of MSU-J silica are systematically reinforced by up to 4.8, 5.7, 1.6, and 8.5 times, respectively, in comparison to the pure epoxy polymer. Moreover, the reinforcement benefits are realized without the need for organic modification of the silica surface. The oxygen permeability of the mesocomposites prepared form as-made MSU-J silica increases dramatically at loadings ≥5.0 wt%, whereas the compositions made from the calcined form of the mesostructure show no permeation dependence on silica loading.

Mechanically improved thermoset epoxy mesocomposites have also been prepared from calcined silica foam, MSU-F which exhibits large cell size of 26.5 nm, window size of 14.9 nm and high pore volume of 2.2 cm^3/g. Despite no organic modifier in its pore the calcined MSU-F silica foam is well dispersed in the epoxy matrix due to its very large pore diameter and low intrinsic density. The tensile modulus, strength, elongation, and toughness for the resulting rubbery epoxy mesocomposites are systematically enhanced by 3.7, 6.8, 2.2, and 20.6 times, respectively, at relatively low silica loading (9 wt%) compared to the silica-free rubbery epoxy polymer. The remarkable mechanical enhancements are contributed by the large window and cell sizes of the MSU-F silica foam which are comparable to the layer separation (>10 nm) of the exfoliated clay layers in the polymer-epoxy nanocomposites. Moreover, little or no sacrifice of thermal stability and transparency were observed in the rubbery–MSU-F mesocomposites.

ACKNOWLEDGEMENTS

First, I would like to express my appreciation to Professor Thomas J. Pinnavaia for his thoughtful guidance for the last 4 and half years. I thank the Lord for being his student and for learning from him a lot of things that I need to be a Ph. D. or an independent researcher. I'd also tell former and current members in our group that you are so lucky because you had (or have) an intelligent and kind advisor.

Also, I would like to give thanks to the former and current group members. Costas, my mentor, taught me how to use a polisher and the MOCON instrument and how to prepare epoxy polymers and clay papers. Pete took me good pizza places and fishing stores in Lansing area. Dr. Kim helped me synthesize mesostructures. DK has always been willing to help me a lot when I got troubles especially my early years in the US. Sebastian has not hesitated to answer my English questions. Siqi is a really good partner to discuss tensile properties and preparation process with. Junho and I have shared good and bad things happening to us. Marc is one of the most diligent and kindest people I have ever seen. Zharong, Hui, and Sun are so nice to me. I am also grateful to Soong and Kyoungsoo for answering my organic questions.

I fully understand that this thesis could not have been completed without my wife and son's sacrifice. Thus I would like to dedicate this humble thesis to Haikyung and Jihwan. Do you guys know how much I love you? You can never know it!!!

TABLE OF CONTENTS

CHAPTER 1

CHAPTER 2

CHAPTER 3

CHAPTER 4

LIST OF TABLES

LIST OF FIGURES

CHAPTER 1

INTRODUCTION

1.1 Supramolecular Assembly of Mesoporous Materials

1.1.1 Electrostatic Pathways

In 1992, Mobil researchers reported the discovery of the novel family of molecular sieves (M41S) prepared by supramolecular assembly through electrostatic interactions between cationic surfactant micelles and anionic inorganic precursors.[1] These mesoporous (alumino)silicates exhibits regular and well-defined pore sizes of 15–100 Å, very high surface area (>1000 m^2/g) and hydrocarbon sorption capacities (>0.7 cc/g). The applications of these materials are based on their microstructures which allow molecules access to large internal surfaces that enhance catalytic activity and adsorptive capacity.[2] MCM-41, one of the members of the M41S family, possesses a two-dimensionally ordered hexagonal array (*p6m*) of uniform mesopores. Its pore size is easily controlled by surfactant chain lengths or/and adding a pore expander (1,3,5-trimethylbenzene, TMB). Also a cubic (MCM-48, *Ia3d*) and a lamellar (MCM-50, *p2*) phase were prepared by varying the surfactant to silicon molar ratio (Figure 1.1).

A proposed mechanism for the formation of M41S is a liquid crystal templating (LCT) which has two possible pathways.[2] One is that the inorganic precursor species are deposited on a preexisting hexagonal liquid crystal phase and the other is that the inorganic species and the surfactant micellar rods are

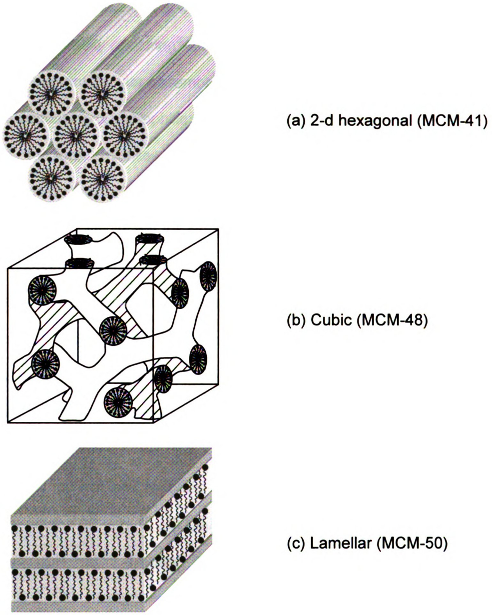

(a) 2-d hexagonal (MCM-41)

(b) Cubic (MCM-48)

(c) Lamellar (MCM-50)

Figure 1.1 Three structure types observed for silica-surfactant mesophases: (a) MCM-41 (hexagonal), (b) MCM-48 (bicontinuous cubic), and (c) MCM-50 (lamellar). In each type there is a periodic arrangement of pores (or layers) while the inorganic walls (or sheets) are amorphous.

combined to render a hexagonal structure. However a number of mechanisms, such as charge density matching[3] and folding sheet[4, 5], have been proposed to elucidate the supramolecular assembly of the mesoporous materials. Generally, surfactants containing a hydrophilic head group and a hydrophobic tail group are assembled to form micelles or micellar arrays which directs inorganic mesostructures on the surface of the surfactant structure[6] (Figure 1.2[7]).

Various synthetic routes for inorganic mesostructures can be categorized by reaction conditions such as interactions between the structure-directing agent (surfactant or porogen) and the inorganic precursor, pH conditions, types of surfactants, etc. In the case of M41S mesostructured molecular sieves, cationic quaternary ammonium surfactants (S^+) were used under basic pH conditions. Electrostatic interaction between S^+ and anionic inorganic precursors (I^-) is involved in this pathway.

Huo and co-workers reported another electrostatic route ($S^+X^-I^+$) with intermediate anions (X^-, e.g. Cl^-, Br^-) under acidic conditions below the isoelectric point of silica (pH ~2).[7-9] Through this pathway, a new family (SBA-1 (cubic, *Pm3n*), SBA-2 (3d hexagonal, $P6_3/mmc$) and SBA-3 (MCM-41 type)) was synthesized from gemini surfactants in acidic media. The formation of amphiphilic liquid-crystal arrays was described in terms of the local effective *g* packing parameter[9] (defined in Figure 1.3) in order to explain and predict product structures and phase transitions. As the *g* value increases, the surface curvature of micelles decreases so that a lamellar phase is favorable when the *g* value approaches unity.

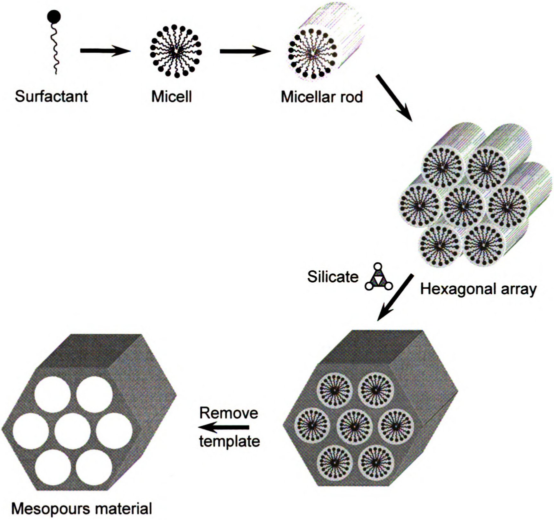

Figure 1.2 Schematic representation of the general formation of mesostructures from inorganic precursors and surfactants. Inorganic precursor species are associated with surface of surfactant micellar structures to form an ordered inorganic framework by condensation and polymerization of inorganic precursors.

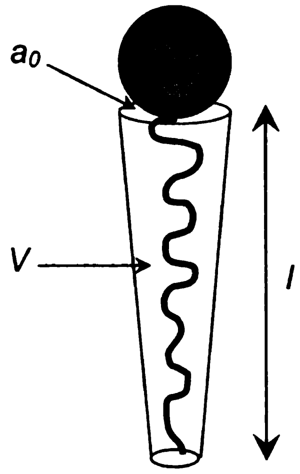

V: the total volume of the surfactant chains

a_0: the effective head group area at the micelle surface

l: the kinetic surfactant tail length

g	mesophase
⅓	cubic (*Pm3n*)
½	hexagonal (*p6m*)
½ – ⅓	cubic (*Ia3d*)
1	lamellar

Figure 1.3 Schematic view of a surfactant and values for calculation of the local effective packing parameter, $g = V/a_0l$. (Inset table) the critical g values at which mesophase transitions occur.

1.1.2 Neutral Templating Pathways

A neutral templating route for preparing mesoporous molecular sieves (HMS) is demonstrated based on hydrogen-bonding interactions and self-assembly between neutral primary amine micelles (S^o) and neutral inorganic precursors (I^o).[10] Unlike cylinder-like framework of MCM-41, HMS materials possess wormhole framework morphology with nearly uniform pore diameters. The S^oI^o templating pathway produces mesoporous materials with thicker framework walls and substantially higher thermal stability[11] compared to charge-matching derived silicates. Another benefit of the HMS materials is improved textural mesoporosities[12] owing to the very small elementary particle domain size in comparison with M41S and SBA materials templated by quaternary ammonium cations of equivalent chain length. This synthetic strategy using relatively weak S^oI^o interaction also allows for the facile, environmentally benign recovery of the cost-intensive template by simple solvent extraction methods. Unlike the tubular hexagonal pores (MCM-41 type) the wormhole pores of HMS are three-dimensionally interconnected, confirmed by a strong peak in the XRD pattern of SNU-2 carbon prepared by using Al-HMS as a template.[13, 14]

The neutral amine surfactant templating pathway under neutral pH conditions generates silica molecular sieves with lamellar frameworks and hierarchical vesicular particle morphology (MSU-V[15] and MSU-G[16]). MSU-V silicas with gallery-confined micropores/mesopores (1.3–2.7 nm) have been assembled in the interlayered regions of multilamellar vesicles formed from a neutral diamine bolaamphiphiles ($H_2N(CH_2)_nNH_2$, n = 12–22). Electrically neutral gemini surfactants of the type $C_nH_{2n-1}NH(CH_2)_2NH_2$ (n = 10–14) and silica precursors produces another family of silica vesicles (MSU-G). The high SiO_4 crosslinking of MSU-G silicas allows for unprecedented thermal (up to 1000°C) and hydrothermal (more than 150 hours at 100°C) stabilities. Both of the molecular sieves with vesicular silica morphology retain the lamellar framework structures after surfactant are removed due to interlayer pillars.

The hydrogen-bonding pathway was expanded to nonionic surfactants (N^o). MSU-X silica molecular sieves have been prepared from tetraethylorthosilicate (TEOS) in the presence of low-cost, nontoxic, and biodegradable polyethylene oxide (PEO) surfactants, which act as the structure-directing agents.[17] Cost-effective and water-soluble sodium silicates have also been used as an inorganic precursor for preparation of MSU-X type mesostructures (designated MSU-X').[18] This N^oI^o templating pathway to mesostructures uses hydrogen bonding interactions between the hydrophilic surfaces of a flexible rod- or worm-like inorganic oxide framework. Disordered channel structures with uniform diameters ranging from 2.0 to 5.8 nanometers have been obtained by varying the size and structure of the surfactant molecules. Increasing synthesis temperature weakens the hydrogen-bonding interactions and consequently the curvature of the micelle decreases so that the framework pore size is expanded up to approximately two times (65°C compared to 25°C).[19] Metal-substituted silica and pure alumina mesostructures have also been prepared by the hydrolysis of the corresponding alkoxides in the presence of PEO surfactants.[20]

1.1.3 Mesocellular Silica Foams

Another group of nonionic surfactants, amphiphilic triblock copolymers (typically P123, $(PEO)_{20}(PPO)_{70}(PEO)_{20}$, polyethylene oxide–polypropylene oxide–polyethylene oxide) have been used to prepare well-ordered hexagonal mesoporous silica structures (SBA-15) in acidic aqueous solutions (pH <1).[21] The pore size of SBA-15 is expanded up to 30 nm by adding a swelling agent (TMB). Under nearly neutral pH conditions, hexagonally ordered mesoporous silicas (denoted MSU-H) have also been synthesized from the same surfactant and water-soluble sodium silicates.[22] The assembly pathway under neutral pH allows MSU-H to possess a higher degree of crosslinking due to little or no charge present on the silica framework walls.

Increasing the TMB-P123 ratio sufficiently induces a phase transformation from SBA-15 to mesocellular foams (MCF).[23] The MCF phase possesses interconnected spherical pore system with windows or openings. Detail analysis on nitrogen sorption isotherms and transmission electron microscopy (TEM) demonstrated that the cylinder pore system at the low TMB-polymer ratios (0.1–0.2, mass ratio) transforms to the spherical pores at the high ratios (>0.3) through intermediate phases with spherical nodes.[24] Increasing the TMB content leads to the formation of microemulsion droplets with a mean surface curvature similar to that of the cylindrical micelles (Figure 1.4[24]). Transition from MSU-H to MSU-F (silica foams) prepared under nearly neutral pH conditions has also been reported.[22] Physical properties of selected mesostructured materials are listed in Table 1.1.

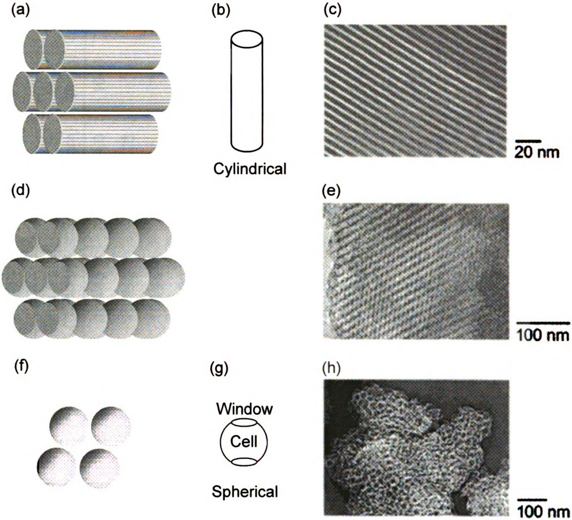

Figure 1.4 Morphological transitions for P123-templated materials progressively swollen by TMB (1,3,5-trimethylbenzene) of the silica products templated by the micellar arrays: micelle arrays (a, d, f); silica pore morphologies (b, g); and TEM images (c, e, h). In the absence of TMB, cylindrical silica pores (b) are formed from cylindrical micelles (a), as confirmed by the TEM image (c). Spherical micelles (f) and the resulting cellular silica foam with windows (g, h) are prepared at a TMB/P123 ratio of 5.0. Intermediate phases with buckling pore morphology are obtained at a 0.21 ratio (d, e).

Table 1.1 Physical properties for selected mesostructured silicas prepared by supramolecular assembly pathways.

†	Mesophase	Route (pH)[a]	Surfactant (Cosolvent)	Inorganic precusor	Temp./time (°C/hour)	d[b] (nm)	P.S.[c] (nm)	S_{BET}[d] (m^2/g)	P.V.[e] (cm^3/g)
MCM-41[25]	2d hexagonal	S^+I^- (b)	CTA^+[f]	SS[g]	100/48	4.0	4.0	1040	0.6
MCM-48[25]	Cubic	S^+I^- (b)	CTA^+	SS	100/48	3.3	2.8	[h]	0.6
MCM-50[25]	Lamellar	S^+I^- (b)	CTA^+	SS	100/48	3.6	[i]	[i]	[i]
SBA-2[7]	3d hexagonal	$S^+X^-I^+$ (a)	$C_{n\text{-}s\text{-}1}$[j]	TEOS	100/20	[h]	~30[k]	~600[k]	~0.8[k]
SBA-15[26]	2d hexagonal	$S^+X^-I^+$ (a)	P123	TEOS	35/24, 100/24	10.5	8.9	850	1.17
MCF[23]	Cellular Foam	$S^+X^-I^+$ (a)	P123 (TMB)	TEOS	35/20, 120/20	[l]	36 (18)[m]	625	2.4
HMS[27]	Wormhole	S^oI^o (n)	$C_{12}H_{23}NH_2$	TEOS	25/20	3.8	2.9	1121	0.78
MSU-X[17]	Wormhole	N^oI^o (n)	T15-S-30[n]	TEOS	25/17	7.9	4.5	780	[h]
MSU-V[28]	Lamellar vesicle	S^oI^o (n)	C_{18}[o]	TEOS	55/48	3.4	2.7	926	0.58
MSU-G[16]	Lamellar vesicle	S^oI^o (n)	$C^o_{12\text{-}2\text{-}0}$[p]	TEOS	100/48	5.7	3.2	412	[h]
MSU-H[22]	2d hexagonal	N^oI^o (n)	P123	SS	60/15	10.3	9.8	625	1.24
MSU-F[29]	Cellular Foam	N^oI^o (n)	P123 (TMB)	SS	25/24, 100/24	[l]	35 (23)[m]	468	2.39

[†] The d spacing, pore size, S_{BET}, and pore volume were measured with calcined materials. [a] (b): basic, (a): acidic, and (n): neutral pH conditions. [b] Basal spacing, d_{100} for 2d hexagonal, wormhole, and lamellar vesicles; d_{211} for cubic structures. [c] Pore size. [d] BET surface area. [e] Pore volume. [f] $C_{16}H_{33}N(CH_3)_3^+$. [g] Sodium silicate. [h] Values are not provided in the reference. [i] The MCM-50 lamellar structure is collapsed after the surfactant is removed. [j] $C_nH_{2n-1}N^+(CH_3)_2C_sH_{2s-1}N^+(CH_3)_3$ (n = 12, 14, 16, or 18, s = 2, 3, or 6). [k] The values are mean values out of ranges that the reference shows. [l] The cellular foams do not exhibit X-ray reflections from powder XRD patterns due to their extremely large pores. [m] Cell size (window size). [n] $C_{11\text{-}15}H_{23\text{-}31}\text{-}(EO)_{30}$. [o] 1,12-diaminododecane. [p] $C_{12}H_{25}NH(C_2H_5)NH_2$.

1.2 Polymer-Based Nanocomposites

1.2.1 Smectite Clays

The hydrous layer silicates commonly known as clay minerals are part of the larger family of phyllosilicates.[30] Clay minerals are composed of two-dimensional octahedron layers and tetrahedral layers. Depending on the number of layers, clay minerals are commonly separated into two subgroups, 1:1 layered and 2:1 layered silicates.[31] In case of the 1:1 type, the layers are formed by coupling of only one tetrahedral sheet to an octahedral sheet. Layers of the 2:1 layered type clay minerals consist of a central octahedral sheet and two tetrahedral sheets, as shown in Figure 1.5[31]. Substitutions by ions of lesser charge produce resultant negative charges on the layers which are balanced by gallery cations. The layers of talc and pyrophyllite (See Table 1.2) are electrically neutral. Substitution of Al^{3+} by Mg^{2+} generates negative charges on the octahedral sheets in layers of montmorillonite which is most common member of smectite clays. Other smectite clays shown in Table 1.2 have negative charges on the octahedral sheets (beidelite and saponite) or the tetrahedral sheet (hectorite) in similar manner to that of montmorillonite. The overall charge is balanced with hydrated cations in the clay gallery and the cations can be replaced with other cations by utilizing ion-exchange reactions which allow for modification of the interlayer region.

The smectite clay minerals are capable of osmotic swelling in polar solvent (usually water) to give very high spacings (>>100 Å) between the layers. The osmotic swelling is depending on factors such as layer charge density, type

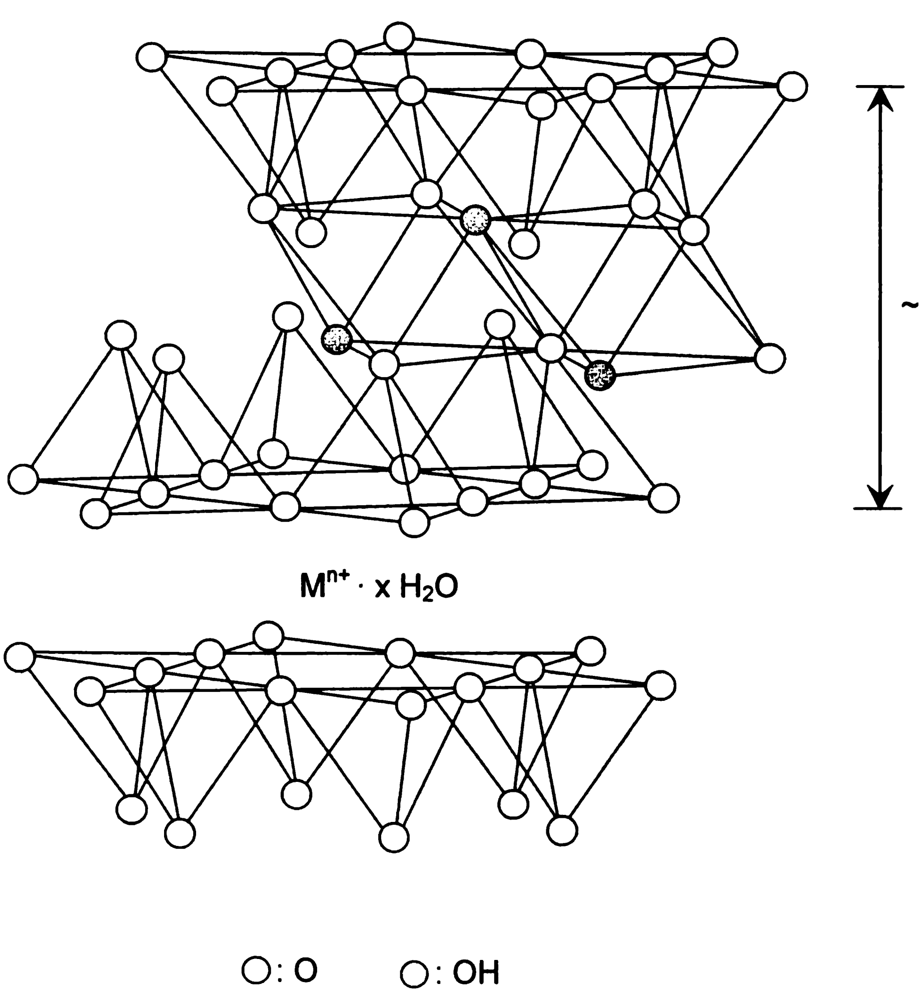

Figure 1.5 Schematic representation of the idealized structure of a smectite clay mineral. Normally, silicon atoms primarily occupy tetrahedral positions. In dioctahedral 2:1 structures, the octahedral interspaces are either two-thirds occupied by M^{3+} ions (especially Al^{3+}) whereas in trioctahedral structures they are completely occupied by M^{2+} cations, especially Mg^{2+}. Aluminum may substitute for silicon in tetrahedral positions and magnesium, iron, or lithium atoms may replace metal ions in octahedral sites.

of interlayer cations, and position of layer charge.[32] Under appropriate conditions individually swollen smectite layers (exfoliation or delamination) are completely dispersed in a certain matrix.

Table 1.2 Elemental compositions of common 2:1 type smectites. In dioctahedral smectite clays two-third of the octahedral sites are occupied by metal ions. Trioctahedral smectites possess all octahedral positions filled by metal ions. Interlayer cations are all assumed to be monovalent but cations of various charge may occupy the interlayer position.[30]

Mineral group	Dioctahedral	Trioctahedral
Talc-pyrophyllite	Pyrophyllite: $Al_2Si_4O_{10}(OH)_2$	Talc: $Mg_6Si_4O_{10}(OH)_2$
Smectites ($x \sim 0.2$–0.6)†	Montmorillonite: $(M_x^+ nH_2O)$ $(Al_{2-x}Mg_x)Si_4O_{10}(OH)_2$	Hectorite: $(M_x^+ nH_2O)$ $(Mg_{3-x}Li_x)Si_4O_{10}(OH)_2$
	Beidellite: $(M_x^+ nH_2O)$ $Al_2(Si_{4-x}Al_x)O_{10}(OH)_2$	Saponite: $(M_{x-y}^+ nH_2O)((Mg_{3-y})$ $(Al,Fe)_x)(Si_{4-x}Al_x)O_{10}(OH)_2$

† x is charge per formula unit ($O_{10}(OH)_2$).

1.2.2 Polymer-Clay Nanocompsites

Layered silicates have been widely used to improve the mechanical and barrier properties of organic polymers. Toyota researchers first developed polymer-smectite clay nanocomposites by uniformly dispersed individual silicate layers in a nylon-6 matrix.[33, 34] Protonated ε-caprolactam was intercalated and polymerized in the galleries of montmorillonte. The unlimited swelling of the clay layers in the polymer matrix provided reinforced mechanical properties[35], such as modulus (which increased by 200%), strength (increased by 50%) and heat distortion temperature (increased by 80 °C). The reinforcement realized for nylon-6 was attributed to the large surface area (~750 m^2/g) and high aspect ratio (>200) of the clay.[36] Such properties allow the clay nanolayers, when dispersed in polymer matrix, to carry out a significant component of the applied load.[37] A recent theoretical study demonstrated that high aspect ratio and high intrinsic modulus (400 GPa) of the clay nanolayers facilitate the reinforcement in mechanical properties.[38] Moreover the high aspect ratio of the impermeable clay nanolayers provides a tortuous pathway (details discussed in 1.2.5 section) for decomposed versatile components, to enhance heat distortion temperature of the polymer.

In order to generalize the exfoliation of clay nanolayers in other polymers the inorganic exchange ions in the galleries of the native clay are generally replaced by a long-chain organic modifier (usually, alkylammonium surfactants) to provide the surface of the clay with hydrophobic environment, which can compatibilize the clay surface and the hydrophobic polymer matrix.[36] The nanocomposite concept has been applied to a variety of organic polymer systems.

Polymer-clay nanocomposites can be generally classified into three types based on the structures of clay layers in the polymer matrix (Figure 1.6).[39] In contrast to conventional composites (Figure 1.6 a) formed from clay tactoids with

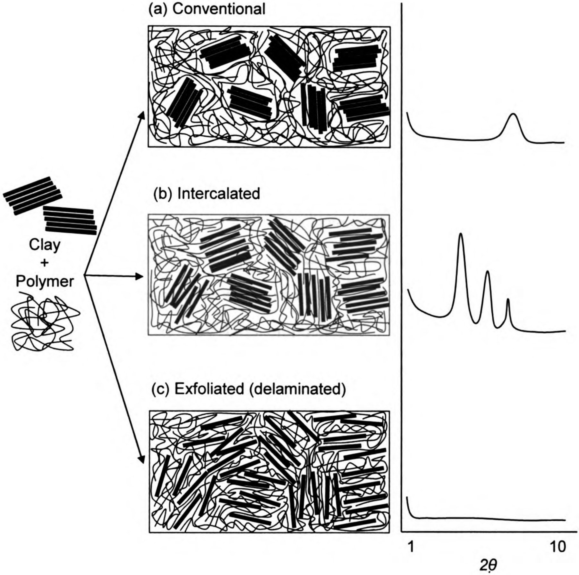

Figure 1.6 Schematic illustrations of polymer-clay composite structures. Rectangular bars represent clay layers with ~1 nm thickness; (a) conventional composites, (b) intercalated nanocomposites, and (c) exfoliated (delaminated) nanocomposites. The corresponding powder XRD patterns for composites at low angle region (*2θ* = 1–10°) are also illustrated.

no intercalation of the polymer into the clay structure, intercalated nanocomposites (Figure 1.6 b) are prepared when one or a few polymer chains are inserted into the clay galleries with retained layer ordering. In the exfoliated nanocomposites (Figure 1.6 c) the clay nanolayers are completely dispersed and the separation between nanolayers may be uniform or disordered in the continuous polymer matrix. Exfoliated nanocomposites allow for higher homogeneity and more improved interfacial interactions between the layers and the matrix, unlike conventional and intercalated composites which have greatly reduced interfacial interactions with the polymer.

1.2.3 Thermoset Epoxy-Clay Nanocomposties

Crosslinked epoxy polymers are known for their high chemical resistance, good adhesion, attractive optical properties and flexibility.[40] The term "resin or thermoset plastic" is applied to both prepolymer and its cured polymer. The most common structure of epoxy resins are based on bisphenol A (structure 1-1).[41] To generate thermoset epoxy polymer network, the epoxy resins are cured (or crosslinked) by curing agents. Polyamines are the most common curing agent with reaction involving ring-opening addition of amine (reaction 1-2). Carboxylic acids and anhydrides have also been used as curing agents. In this thesis two types of epoxy resins (diglycidyl ether of bisphenol As, EPON 826 and 828, (structures 1-3)) were used in combination with diamine curing agents (α,ω-diamine-terminated polypropylene oxide, Jeffamine D230 and D2000, (structures 1-4)).

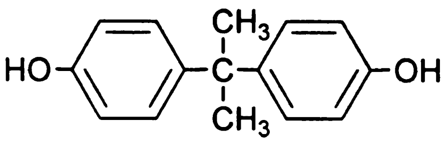

(1-1)

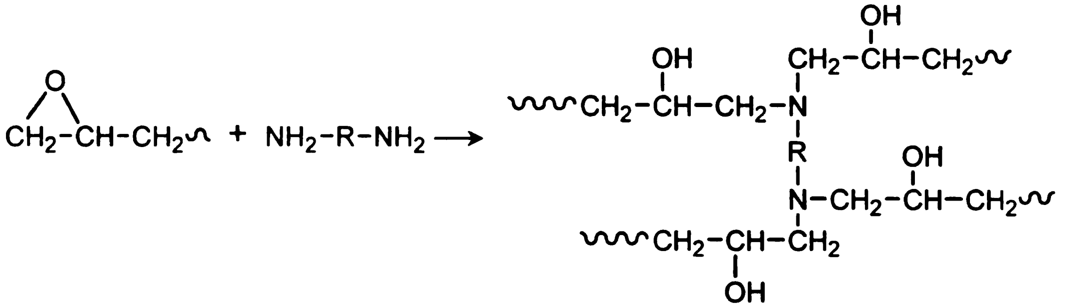

(1-2)

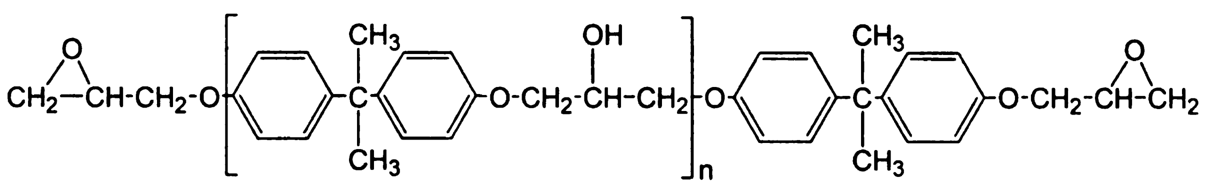

EPON 826; n = 0 (90%), 1 (10%)
EPON 828; n = 0 (88%), 1 (10%), 2 (2%)

(1-3)

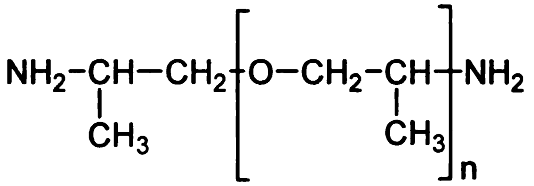

$$NH_2\text{-}\underset{CH_3}{CH}\text{-}CH_2\left[O\text{-}CH_2\text{-}\underset{CH_3}{CH}\right]_n NH_2$$

Jeffamine D230; n = 5.6, M_w ~200
Jeffamine D2000; n = 33.1, M_w ~2000

(1-4)

The first example of an exfoliated clay-epoxy nanocomposite structure[42] was prepared using protonated alkylammonium ions intercalated in montmorillonite. The intercalate facilitates the polymerization-delamination process. In the absence of an amine curing agent the acidity of the exchanged onium ions plays the role of a catalyst for the cationic ring-opening self-polymerization of the epoxy to form a polyether (reaction 1-5).[43] In the presence of amine curing agent the acidic intergallery onium ions also catalyze the polymerization reaction in the clay gallery at rates that are competitive with the extragallery polymerization rate.[39] The competitive polymerization rates facilitate clay exfoliation, which is confirmed by the observation of only intercalated composites formed from nonacidic ammonium ions. Other factors that affects the exfoliation of clays are the chain-length of the organic modifiers and the layer charge density of the pristine clays.[39]

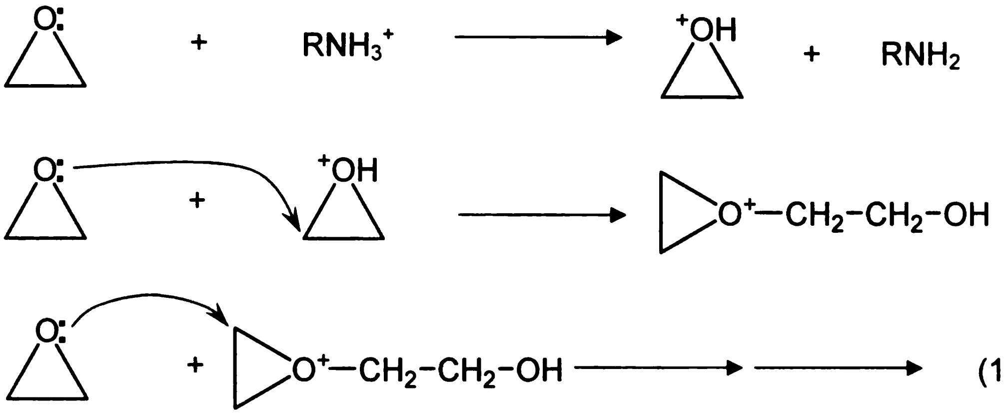

(1.5)

Exfoliated silicate–epoxy nanocomposites can show remarkable improvement in mechanical properties. A glassy thermoset epoxy nanocomposite containing 4 v/v% exfoliated montmorillonite shows a 60% increase in storage modulus compared to the pure epoxy.[44] A rubbery epoxy nanocomposite containing 23 wt% montmorillonite exhibits more than 10-fold improvement in tensile modulus and strength and 40–60% elongation-at-break.[45] Generally ,intercalated clay nanocomposites are less effective than exfoliated analogues in improving mechanical properties[39] and transparency[46]. Recently, protonated α, ω-diamines were used as clay surface modifiers and curing agents and exfoliated montmorillonite–epoxy nanocomposites were successfully prepared through the acid-catalyzed curing reaction shown in the reaction scheme (1.6).[47] This approach reduces the need for an organic modifier and limits the plasticizing effect caused by long-chain organic modifier. Carbon nanofibers[48] and exfoliated graphite[49] have also been used as reinforcement agents. However, the resulting nanocomposites manifest less improvement in mechanical properties than that of clay counterparts at the same loading of the agents.

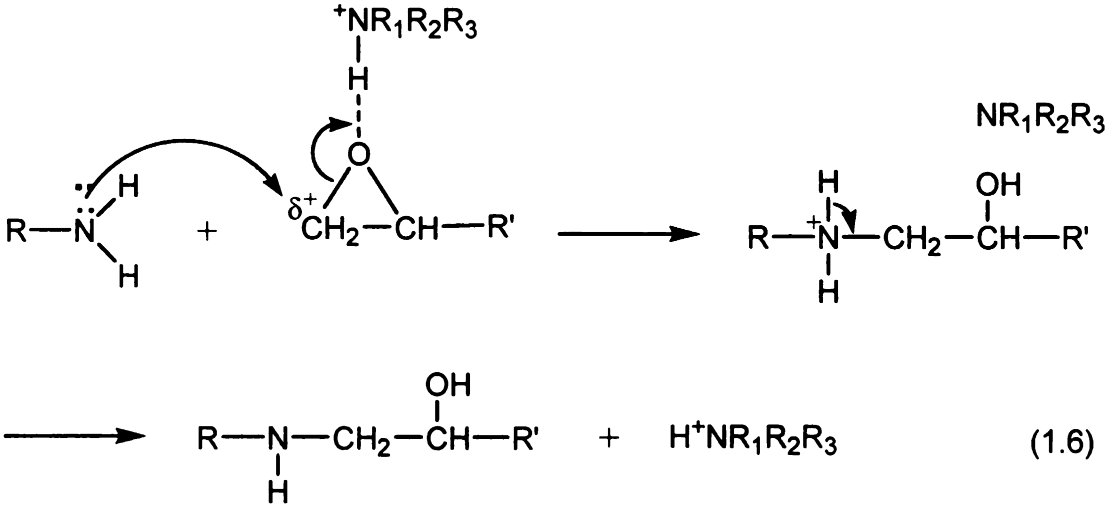

(1.6)

1.2.4 Mesocomposites

Mesoporous silica materials with large pore size are promising hosts for the construction of nanocomposites with organic polymers.[50] For example, one dimensional channels of hexagonal MCM-41 allow conjugated polymer chains such as polydiacetylene[51], polyvinylene[52] and polythiophene[53] to align within the pores so that the resulting nanocomposites exhibit unusual chromatic changes, polarized luminescence, and high stability after 20 voltametric cycles, respectively. However, only a few studies have been published describing polymer-based nanocomposites containing mesoporous silicas to improve mechanical[54-56] and gas permeability properties[57].

Kojima *et al.*[54] reported that Nylon 6,6/FSM silica composites (35 wt% FSM silica loading) could be prepared above 2 MPa pressure, which provided a driving force for nylon 6,6 chains to insert into the pores of FSM. The resulting composites exhibited about a two-fold larger storage modulus in the viscoelastic experiments than that of pure nylon 66 processed under the same conditions. Collapse of FSM framework structure was not observed under 30 MPa pressure, as confirmed by XRD and TEM. However, even higher loadings of FSM particles showed only 2-fold enhancement of storage modulus from the composites. A mesostructured organosilica[55] and a silylated MCM-48[56] were used as reinforcing agents for poly((3-trimethoxysilyl)propylmethacrylate) (PTMSPMA) and poly(vinyl acetate) (PVAc), respectively. Approximately 140% and 700% increases were observed in tensile strength and tensile modulus, respectively, for the 28.2 wt% silica-loaded PTMSPMA composite, but the elongation and the toughness of the composite were sacrificed. In case of the PVAc-based composite containing 4.3 wt% silylated MCM-48, tensile modulus, strength, and toughness were increased by 300%, 80%, and 40 %, respectively along with a 33% decrease in elongation.

1.2.5 Gas Permeability

The high aspect ratio (200-2000) of clay nanolayers provides enhanced barrier characteristics as well as reduced solvent uptake, chemical resistance and flame retardance.[36] A simple model[58] (shown in Figure 1.7 a) has been used to explain the reduction of gas permeability by the impermeable exfoliated clay platelets (Figure 1.7 b) which present a tortuous path (Figure 1.7) to the permeant gases. In the tortuous path mechanism the relative permeability is $P_c / P_o = 1 / \tau$, where P_c and P_0 are the permeabilities of the composite and unfilled polymer and τ is the tortuosity factor defined by the ratio of distance a molecule must travel to get through the polymer film to thickness of the film. The expression for the tortuosity factor in the case where all the platelets are aligned are shown in Figure 1.7 is

$$\tau = 1 + \frac{1}{2}\alpha\phi \tag{1.6}$$

where ϕ is the volume fraction of the platelets and α is the aspect ratio of the plates. This mechanism neglects horizontal variations and disordered arrangement of the platelets.[59] The more developed version of the tortuosity factor[60] appropriate for the three-dimensional, disordered arrange of platelets has been given as

$$\tau = 1 + \frac{1}{4}\mu\alpha^2\phi^2(1-\phi) \tag{1.7}$$

where μ is a geometric factor depending on the size and shape of the platelets and on the extent of positional disorder.

Polymer membranes for gas separation require high permeability coefficients as well as high selectivity coefficients.[61] Highly selective zeolites have been used as absorbents in rubbery or glassy polymer-based membranes to improve gas separation performance.[62-65] Approximately a two-fold increase of oxygen gas permeability was observed for zeolite/polymer composite membranes.[63, 65] High zeolite loadings (53 v/v% and 50 wt%), however, are required to achieve the enhancement of oxygen permeabilities. For lower zeolite loadings (0–30 wt%), the oxygen permeability coefficients of the composite materials generally decrease along with the increase of zeolite loadings[62, 64, 65] due to insufficient pore channel networks. Non-selective interfacial voids caused

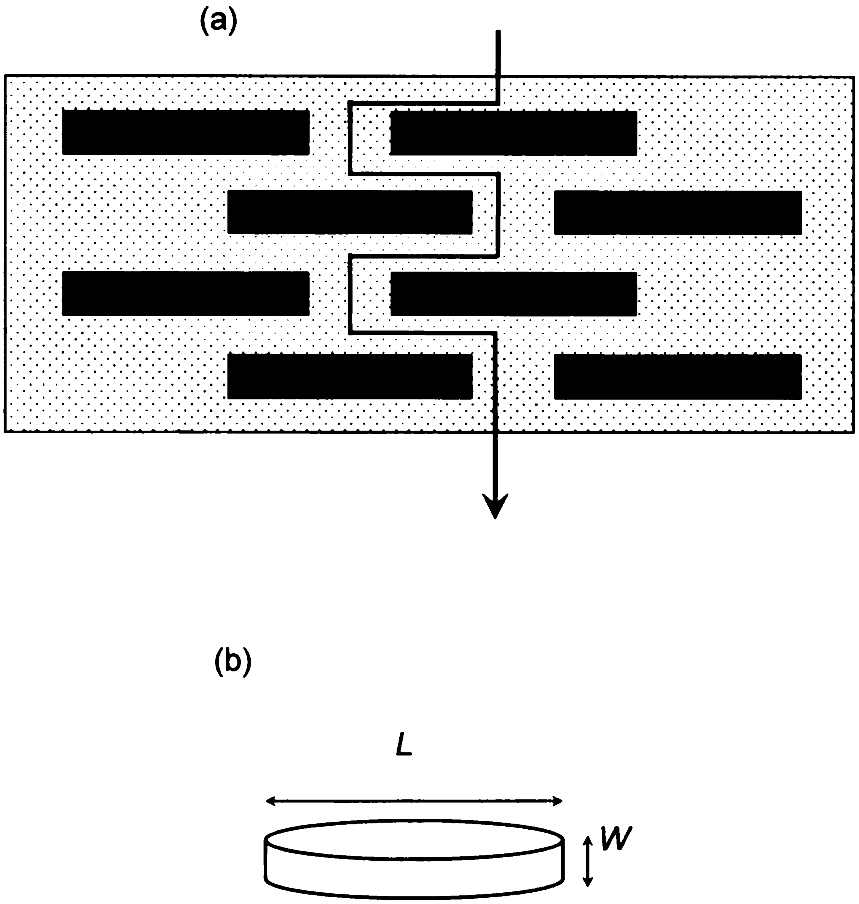

Figure 1.7 A model (a) for the tortuous path of a diffusing molecule through a polymer filled with oriented impermeable disks (b) with aspect ratio, $\alpha = L / W$.

by the weak interaction between the zeolite surface and the polymer matrix do not provide significant permselectivity improvements.[66] The meager interfacial interaction between the polymer chains and the inorganic additive surface also results in poor dimensional properties for the polymer composites.

A study of the mechanical properties of natural zeolite-epoxy composites showed that the tensile strength, Young's modulus and impact strength decrease with increase in the zeolite loadings, confirming the poor adhesion between the zeolite surface and polymer chains.[67] Wetting polymer chains at the surface of the reinforcing agents are needed in order to achieve the high mechanical stability that is demanded for good membrane performance.[68]

Only a few examples describing polymer-based membranes containing mesostructured silicas have been reported to show improved performance for gas separation membranes. The Addition of 30 wt% MCM-41 silica to a polysulfone (PSF) resulted in a 155% increase in permeability for oxygen gas without loss of the O_2/N_2 selectivity due to the increase in diffusivity from nonselective voids.[57] As MCM-41 loading increased, however, the MCM-41/PSF composite membranes became more brittle, despite FT-IR evidence for hydrogen-bonding interaction between PSF and MCM-41. The mesoporous silica-polymer membrane concept was expanded to include amine-functionalized DAM-1(MCM-41 type silica)-polyimide membranes[69]. Approximately 260% and 45% increases in oxygen permeability and O_2/N_2 selectivity were observed at 30 wt% and 20 wt% loadings, respectively. However the weak mechanical properties of the DAM-1-polyimide membranes were a drawback, indicating the poor interaction between the polymer and the mesoporous silica.

1.3 Research Goals and Significance

Although intercalated/exfoliated clay-polymer nanocomposites exhibit improved properties such as mechanical, thermal and barrier properties the hydrophilic nature of the clay surface must be modified with organic modifiers in order to compatibilize the hydrophobic polymer chains. Despite using organic modifiers on the surfaces of clays to improve the compatibility of the clay with the polymer, primarily intercalated or partially exfoliated clay structures have been obtained for many polymer systems.[70, 71] Also, many efforts, such as changing processing methods[46], using solvents[72], and selecting organic modifiers[39] have been made to facilitate induce exfoliation of the smectite clays in polymer matrices. Despite these efforts, it is still extremely difficult to routinely exfoliate clay nanolayers in a polymer matrix.

Mesoporous silicas may be promising candidates reinforcing organic polymers owing to their high surface area and high pore volume. However, earlier studies aimed at using mesoporous silica as a reagent have not been successful and the characterizations of the mesocomposites are not clear. Thus we will herein propose that relatively large pore size (5–30 nm) can provide polymer chains with facilitated access to the inner silica wall without the need for organic surfactants in the pores. The framework pore diameters of mesostructured silicas are comparable to the gallery heights of the clay layer structures in polymer media. Moreover the pore diameters are easily expandable by temperature, surfactants, co-surfactant and pore expanders to distances that exceed the basal spacing of exfoliated clay layers (>10 nm). As a result, mesostructured silica can afford cost- and labor-effective process for preparation of reinforced polymer nanocomposites.

In this thesis MCM-41 type mesostructures are excluded as viable reinforcing agents due to the limiting size and one-dimensional nature of the cylindrical pores, which is not suitable for filling by polymer chains. For analogous reasons cubic mesoporous silica (MCM-48, 3.5 nm pore size) with bicontinous pore networks is not expected to be a useful candidate because the MCM-48 does not disperse in thermoset epoxy matrices[73]. The relatively small pore size and low pore volume (high bulk density) of the MCM-48 may be the cause of the poor dispersion of the silica. Thus, we must take into account large pore size and high pore volume as well as three-dimensional pore structure to select beneficial candidates for the improvement of mesostructure dispersion and polymer properties. Moreover mesostructures prepared under electro-statically neutral assembly conditions are preferred because the surfactants used to template the mesostructures can be easily removed by ethanol extraction.

One of the objectives in this work is to synthesize of large-pore wormhole mesostructures and study their use as reinforcing agents for improvement of mechanical properties of thermoset epoxy polymers, which have been widely used in a variety of applications including coatings, adhesives and electronics. A mesocellular foam (MSU-F) prepared under a nearly neutral pH condition will be also explored as a reinforcement agent of thermoset epoxy system.

1.4 References

(1) Kresge, C. T.; Leonowicz, M. E.; Roth, W. J.; Vartuli, J. C.; Beck, J. S. *Nature* **1992**, *359*, 710.

(2) Beck, J. S.; Vartuli, J. C.; Roth, W. J.; Leonowicz, M. E.; Kresge, C. T.; Schmitt, K. D.; Chu, C. T. W.; Olson, D. H.; Sheppard, E. W.; Mccullen, S. B.; Higgins, J. B.; Schlenker, J. L. *J. Am. Chem. Soc.* **1992**, *114*, 10834.

(3) Monnier, A.; Schuth, F.; Huo, Q.; Kumar, D.; Margolese, D.; Maxwell, R. S.; Stucky, G. D.; Krishnamurty, M.; Petroff, P.; Firouzi, A.; Janicke, M.; Chmelka, B. F. *Science* **1993**, *261*, 1299.

(4) Inagaki, S.; Fukushima, Y.; Kuroda, K. *J. Chem. Soc. Chem. Comm.* **1993**, 680.

(5) Yanagisawa, T.; Shimizu, T.; Kuroda, K.; Kato, C. *Bull. Chem. Soc. Jpn.* **1990**, *63*, 988.

(6) Ying, J. Y.; Mehnert, C. P.; Wong, M. S. *Angew. Chem. Int. Ed.* **1999**, *38*, 56.

(7) Huo, Q. S.; Margolese, D. I.; Stucky, G. D. *Chem. Mater.* **1996**, *8*, 1147.

(8) Huo, Q. S.; Margolese, D. I.; Ciesla, U.; Demuth, D. G.; Feng, P. Y.; Gier, T. E.; Sieger, P.; Firouzi, A.; Chmelka, B. F.; Schuth, F.; Stucky, G. D. *Chem. Mater.* **1994**, *6*, 1176.

(9) Huo, Q. S.; Leon, R.; Petroff, P. M.; Stucky, G. D. *Science* **1995**, *268*, 1324.

(10) Tanev, P. T.; Pinnavaia, T. J. *Science* **1995**, *267*, 865.

(11) Tanev, P. T.; Pinnavaia, T. J. *Chem. Mater.* **1996**, *8*, 2068.

(12) Zhang, W. Z.; Pauly, T. R.; Pinnavaia, T. J. *Chem. Mater.* **1997**, *9*, 2491.

(13) Lee, J.; Yoon, S.; Oh, S. M.; Shin, C. H.; Hyeon, T. *Adv. Mater.* **2000**, *12*, 359.

(14) Lee, J.; Han, S.; Hyeon, T. *J. Mater. Chem.* **2004**, *14*, 478.

(15) Tanev, P. T.; Pinnavaia, T. J. *Science* **1996**, *271*, 1267.

(16) Kim, S. S.; Zhang, W. Z.; Pinnavaia, T. J. *Science* **1998**, *282*, 1302.

(17) Bagshaw, S. A.; Prouzet, E.; Pinnavaia, T. J. *Science* **1995**, *269*, 1242.

(18) Kim, S. S.; Pauly, T. R.; Pinnavaia, T. J. *Chem. Comm.* **2000**, 835.

(19) Prouzet, E.; Pinnavaia, T. J. *Angew. Chem. Int. Ed.* **1997**, *36*, 516.

(20) Bagshaw, S. A.; Pinnavaia, T. J. *Angew. Chem. Int. Ed.* **1996**, *35*, 1102.

(21) Zhao, D. Y.; Feng, J. L.; Huo, Q. S.; Melosh, N.; Fredrickson, G. H.; Chmelka, B. F.; Stucky, G. D. *Science* **1998**, *279*, 548.

(22) Kim, S. S.; Pauly, T. R.; Pinnavaia, T. J. *Chem. Comm.* **2000**, 1661.

(23) Schmidt-Winkel, P.; Lukens, W. W.; Zhao, D. Y.; Yang, P. D.; Chmelka, B. F.; Stucky, G. D. *J. Am. Chem. Soc.* **1999**, *121*, 254.

(24) Lettow, J. S.; Han, Y. J.; Schmidt-Winkel, P.; Yang, P. D.; Zhao, D. Y.; Stucky, G. D.; Ying, J. Y. *Langmuir* **2000**, *16*, 8291.

(25) Vartuli, J. C.; Schmitt, K. D.; Kresge, C. T.; Roth, W. J.; Leonowicz, M. E.; Mccullen, S. B.; Hellring, S. D.; Beck, J. S.; Schlenker, J. L.; Olson, D. H.; Sheppard, E. W. *Chem. Mater.* **1994**, *6*, 2317.

(26) Zhao, D. Y.; Huo, Q. S.; Feng, J. L.; Chmelka, B. F.; Stucky, G. D. *J. Am. Chem. Soc.* **1998**, *120*, 6024.

(27) Pauly, T. R.; Pinnavaia, T. J. *Chem. Mater.* **2001**, *13*, 987.

(28) Tanev, P. T.; Liang, Y.; Pinnavaia, T. J. *J. Am. Chem. Soc.* **1997**, *119*, 8616.

(29) Karkamkar, A.; Kim, S. S.; Pinnavaia, T. J. *Chem. Mater.* **2003**, *15*, 11.

(30) Bailey, S. W. In *Crystal Structures of Clay Minerals and Their X-Ray Identification*, Edited by Brindley, G. W. Brown, G., Mineralogical Society, London, **1980**.

(31) Pinnavaia, T. J. *Science* **1983**, *220*, 365.

(32) McEwan, D. M. C.; Wilson, M. J. In *Crystal Structures of Clay Minerals and Their X-Ray Identification*, Edited by Brindley, G. W. Brown, G., Mineralogical Society, London, **1980**.

(33) Fukushima, Y.; Okada, A.; Kawasumi, M.; Kurauchi, T.; Kamigaito, O. *Clay Miner.* **1988**, *23*, 27.

(34) Okada, A.; Kawasumi, M.; Usuki, A. *Mat. Res. Soc. Symp. Proc.* **1990**, *171*, 45.

(35) Kojima, Y.; Usuki, A.; Kawasumi, M.; Okada, A.; Fukushima, Y.; Kurauchi, T.; Kamigaito, O. *J. Mater. Res.* **1993**, *8*, 1185.

(36) LeBaron, P. C.; Wang, Z.; Pinnavaia, T. J. *Appl. Clay Sci.* **1999**, *15*, 11.

(37) Weon, J. I.; Sue, H. J. *Polymer* **2005**, *46*, 6325.

(38) Fornes, T. D.; Paul, D. R. *Polymer* **2003**, *44*, 4993.

(39) Lan, T.; Kaviratna, P. D.; Pinnavaia, T. J. *Chem. Mater.* **1995**, *7*, 2144.

(40) Lange, J.; Nicolas, B.; Galy, J.; Gerard, J. F. *Polymer* **2002**, *43*, 5985.

(41) Odian, G. *Principles of Polymerization*. 3rd ed. Wiley, New York, **1993**.

(42) Wang, M. S.; Pinnavaia, T. J. *Chem. Mater.* **1994**, *6*, 468.

(43) Lan, T.; Kaviratna, D.; Pinnavaia, T. J. *J. Phys. Chem. Solids* **1996**, *57*, 1005.

(44) Messersmith, P. B.; Giannelis, E. P. *Chem. Mater.* **1994**, *6*, 1719.

(45) Lan, T.; Pinnavaia, T. J. *Chem. Mater.* **1994**, *6*, 2216.

(46) Brown, J. M.; Curliss, D.; Vaia, R. A. *Chem. Mater.* **2000**, *12*, 3376.

(47) Triantafillidis, C. S.; LeBaron, P. C.; Pinnavaia, T. J. *J. Solid State Chem.* **2002**, *167*, 354.

(48) Richard, P.; Prasse, T.; Cavaille, J. Y.; Chazeau, L.; Gauthier, C.; Duchet, J. *Mater. Sci. Eng. A* **2003**, *352*, 344.

(49) Fukushima, H. *Ph. D. Thesis*, Michigan State University, East Lansing, **2001**.

(50) Shi, J. L.; Hua, Z. L.; Zhang, L. X. *J. Mater. Chem.* **2004**, *14*, 795.

(51) Lu, Y. F.; Yang, Y.; Sellinger, A.; Lu, M. C.; Huang, J. M.; Fan, H. Y.; Haddad, R.; Lopez, G.; Burns, A. R.; Sasaki, D. Y.; Shelnutt, J.; Brinker, C. J. *Nature* **2001**, *410*, 913.

(52) Nguyen, T. Q.; Wu, J. J.; Doan, V.; Schwartz, B. J.; Tolbert, S. H. *Science* **2000**, *288*, 652.

(53) Li, G. T.; Bhosale, S.; Wang, T. Y.; Zhang, Y.; Zhu, H. S.; Fuhrhop, K. H. *Angew. Chem. Int. Ed.* **2003**, *42*, 3818.

(54) Kojima, Y.; Matsuoka, T.; Takahashi, H. *J. Appl. Polymer Sci.* **1999**, *74*, 3254.

(55) Ji, X. L.; Hampsey, J. E.; Hu, Q. Y.; He, J. B.; Yang, Z. Z.; Lu, Y. F. *Chem. Mater.* **2003**, *15*, 3656.

(56) He, J.; Shen, Y. B.; Yang, J.; Evans, D. G.; Duan, X. *Chem. Mater.* **2003**, *15*, 3894.

(57) Reid, B. D.; Ruiz-Trevino, A.; Musselman, I. H.; Balkus, K. J.; Ferraris, J. P. *Chem. Mater.* **2001**, *13*, 2366.

(58) Nielsen, L. E. *J. Macromol. Sci. (Chem.)* **1967**, *A1*, 929.

(59) Fredrickson, G. H.; Bicerano, J. *J Chem Phys* **1999**, *110*, 2181.

(60) Cussler, E. L.; Hughes, S. E.; Ward, W. J.; Aris, R. *J. Membrane Sci.* **1988**, *38*, 161.

(61) Maier, G. *Angew. Chem. Int. Ed.* **1998**, *37*, 2961.

(62) Jia, M. D.; Peinemann, K. V.; Behling, R. D. *J. Membrane Sci.* **1991**, *57*, 289.

(63) Duval, J. M.; Folkers, B.; Mulder, M. H. V.; Desgrandchamps, G.; Smolders, C. A. *J. Membrane Sci.* **1993**, *80*, 189.

(64) Gur, T. M. *J. Membrane Sci.* **1994**, *93*, 283.

(65) Suer, M. G.; Bac, N.; Yilmaz, L. *J. Membrane Sci.* **1994**, *91*, 77.

(66) Zimmerman, C. M.; Singh, A.; Koros, W. J. *J. Membrane Sci.* **1997**, *137*, 145.

(67) Lee, J. Y.; Shim, M. J.; Kim, S. W. *Polym. Eng. Sci.* **1999**, *39*, 1993.

(68) Stern, S. A. *J. Membrane Sci.* **1994**, *94*, 1.

(69) Balkus, K. J.; Cattanach, K.; Musselman, I. H.; Ferraris, J. P. *Mater. Res. Soc. Symp. Proc.* **2003**, *752*, 91.

(70) Robello, D. R.; Yamaguchi, N.; Blanton, T.; Barnes, C. *J. Am. Chem. Soc.* **2004**, *126*, 8118.

(71) Shen, M. M.; Lu, M. G.; Chen, Y. L.; Ha, C. Y. *Polym Int* **2005**, *54*, 1163.

(72) Choi, Y. S.; Ham, H. T.; Chung, I. J. *Chem. Mater.* **2004**, *16*, 2522.

(73) Park, I.; Pinnavaia, T. J. *Unpublished data*, **2004**.

CHAPTER 2

ASEMBLY OF LARGE-PORE SILICA MESOPHASES WITH WORMHOLE FRAMEWORK STRUCTURES FROM α,ω-DIAMINEPOROGENS

2.1 Introduction

Supramolecular assembly pathways based on hydrogen-bonding interactions between electrically neutral amine surfactants and electrically neutral silica precursors typically afford mesostructures with wormhole framework motifs.[1] Compared to the highly ordered monolithic mesophases prepared through electrostatic templating pathways, wormhole mesostructures typically exhibit improved activity as heterogeneous catalysts for condensed phase reactions due to the three-dimensional pore network and an improved textural mesoporosity that minimize diffusion and facilitate access to reaction sites on the pore surfaces.[2-6] Neutral amine templating offers the additional advantage of facile recovery of surfactants by solvent extraction methods.[1,7-9] Also, the use of amine surfactant micelles as mesostructure-directing agents is not limited to silicate frameworks. Mesoporous forms of certain transition-metal oxides also have been prepared using amine surfactants.[7-9]

Despite the advantages of amine surfactants for the hydrogen-bonding assembly of highly accessible mesostructured silicas, the average framework pore sizes have been limited to the range 1.6–3.1 nm.[1] An expansion of framework pore sizes up to 4.5 nm can be achieved for some wormhole silicas through the incorporation of a cosolvent, such as 1,3,5-trimethylbenzene, in the hydrophobic interior region of the micelle.[10,11] Even greater mesopore accessibility and catalytic activity can be anticipated for these wormhole framework structures if the framework pore sizes can be expanded beyond these limiting values and into the >10 nm range.

We report herein a new group of large pore mesoporous silicas, denoted MSU-J, with three-dimensional wormhole framework structures prepared through hydrogen-bonding pathways. Our approach is based on the use of amineterminated polypropylene oxide (PPO) Jeffamine surfactants of the type $H_2NCH(CH_3)CH_2[OCH_2CH(CH_3)]_xNH_2$ as the structure-directing porogen. We show that pore sizes and pore volumes up to 14.3 nm and 2.29 cm^3/g, respectively, can be achieved, depending on the synthesis conditions and the molecular weight of the surfactant. The resulting pore sizes and BET surface areas are comparable to those of SBA-15 silicas, but unlike SBA-15, the mesopores are three-dimensionally connected.

2.2 Experimental

Jeffamine D2000 and D4000 surfactants (abbreviated to D2000 and D4000, respectively) were obtained from Huntsman Corp. and used without further purification as structure-directing porogens. Commercially available sodium silicate (Aldrich, 27% SiO_2, 14% NaOH) solution and TEOS (Aldrich) were used as the silica precursors.

In a typical synthesis of MSU-J from sodium silicate, an amount of acid (HCl) equivalent to the formal hydroxide content of the sodium silicate precursor was added to an aqueous solution of the surfactant. The desired quantity of sodium silicate was added to the surfactant solution under vigorous stirring at ambient temperature, and the mixture with a pH of 8.0-8.5 was allowed to age in a heated water bath at the desired synthesis temperature for 20 h with stirring. The surfactant was then removed from the washed, air-dried solids by calcination at 600°C for 4 h in air.

MSU-J molecular sieves also were prepared with TEOS used as a silica precursor in water/ethanol solvent mixture. The surfactant was dissolved in ethanol, and then the desired amount of water was added under stirring. TEOS was added to the surfactant solution. The molar composition of the reaction mixture was 1.0:0.125:220:17 TEOS:D2000:H_2O:EtOH. The assembly conditions were the same as those used in the preparation of MSU-J mesostructures made from sodium silicate.

X-ray diffraction (XRD) patterns were obtained on a Rigaku Rotaflex 200B diffractometer equipped with Cu K_α X-ray radiation and a curved crystal graphite monochromator operating at 45 kV and 100 mA. Transmission electron microscopy (TEM) images were taken on a JEOL JEM-100CX II microscope with a CeB_6 filament and an accelerating voltage of 120 kV. Sample grids of calcined mesoporous silicas were prepared via sonication of powdered sample in EtOH for 10 min and evaporating 2 drops of the suspension onto a carbon-coated, holey film supported on a 3 mm, 300 mesh copper grid.

2.3 Results and discussion

Tetraethyl orthosilicate (TEOS) and alkylamine surfactants are known to be effective reagents for the supramolecular assembly of wormhole framework structures through hydrogen- bonding interactions between the amine headgroups of the micelles and the silanol groups of the TEOS hydrolysis products.[1,10,11] Sodium silicate also can be used for the preparation of silica mesophases through supramolecular hydrogen-bonding mechanisms, provided that the formal hydroxide ion content of the solution is balanced through the addition of an acid to achieve a reaction mixture at a near-neutral pH.[12] In the present work both reagents were used as the silica source for the amine-directed assembly of very large pore wormhole mesostructures.

To optimize the framework pore size of the mesostructured products, we selected two high molecular weight α,ω-diamine surfactants of the type $H_2NCH(CH_3)CH_2[OCH_2CH(CH_3)]_xNH_2$ as the structure-directing porogens. The derivatives with hydrophobic propylene oxide segments corresponding to $x \sim 33$ and 68 have approximate molecular weights of 2000 and 4000, respectively. Reflecting these average molecular weights, the surfactants are marketed under the trade names Jeffamine D2000 and Jeffamine D4000.

Numerous survey experiments indicated the optimum reaction stoichiometry for the assembly of MSU-J mesostructures from sodium silicate to be 1.0:0.83:0.125:0.83:230 SiO_2:NaOH:D2000 (or 0.062 for D4000):HCl:H_2O, as judged by N_2 adsorption isotherms and the corresponding textural properties of the assembly products. For TEOS as the silica precursor, the optimal reaction

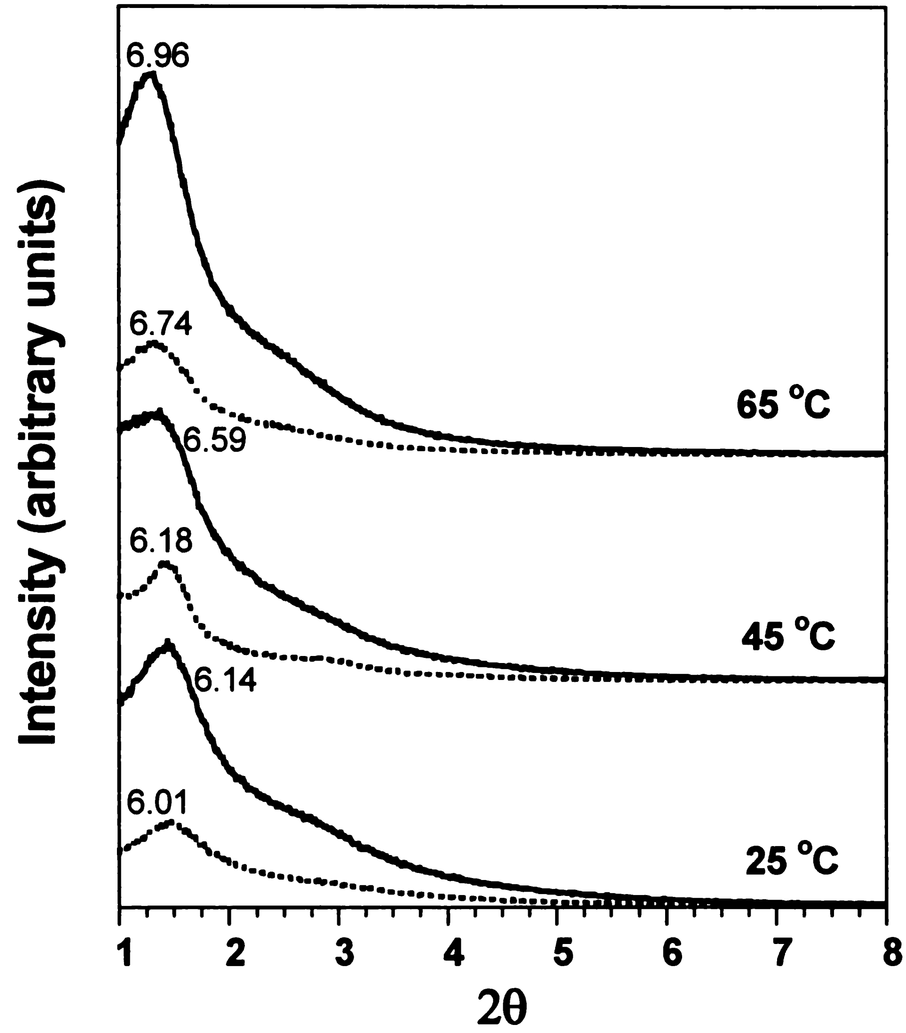

Figure 2.1 X-ray diffraction patterns of as-synthesized (·····) and calcined (—) MSU-J silica molecular sieves using D2000 as templating agents and sodium silicate as a silica source under neutral pH conditions at 25, 45, and 65°C. The numbers are the pore-pore correlation distances in nanometer (nm) units.

stoichiometry was 1.0:0.125:220:17 TEOS:D2000:H_2O:EtOH.

Figure 2.1 illustrates X-ray diffraction (XRD) patterns of as-synthesized and calcined MSU-J silicas prepared from the sodium silicate and D2000 surfactant at temperatures of 25, 45, and 65°C. Each sample exhibits an intense and relatively broad reflection in the 2θ range 1-1.5° with a weak, broad shoulder appearing at 2-3°. The absence of multiple *hkl* reflections indicates that the framework pore system is lacking in long-range order, but the well-expressed low-angle reflection is consistent with the average correlation distance between pores in a wormhole framework structure. Relatively broad XRD reflections (not shown) also were observed for MSU-J silicas synthesized from TEOS and D2000 at 60°C and from sodium silicate and D4000 at 45 and 65°C. In case of MSU-J silicas with pores > 8 nm, no XRD reflections could be detected at a 2θ angle higher than 1° due to the detection limit of our wide-angle X-ray diffractometer.

The presence of a wormhole framework structure for each of the mesostructured products was verified by TEM images, examples of which are shown in Figure 2.2. Although we were not able to observe a low-angle XRD peak for mesostructures with a pore size > 8 nm, the pore structures shown in the TEM images of this product (Figure 2.2c,d) confirm the wormhole structure and the relatively regular porosity.

N_2 adsorption-desorption isotherms and Barrett-Joyner-Halenda (BJH) framework pore-size distributions (inset) for calcined MSU-J phases synthesized from TEOS are presented in Figure 2.3. Filling of the framework-confined

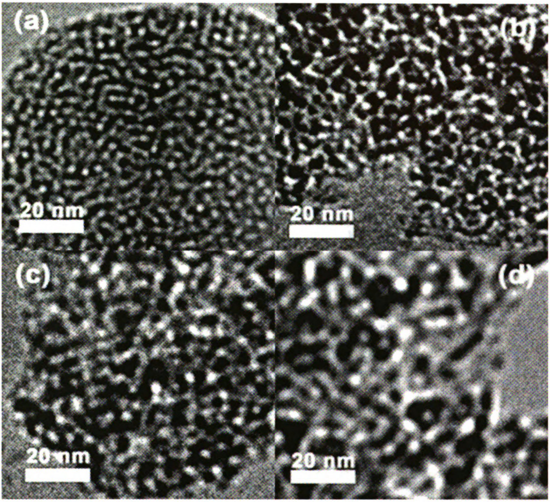

Figure 2.2 TEM images of calcined MSU-J silicas synthesized with the Jeffamine surfactants and the silica sources; (a) D2000 and sodium silicate at 25°C, (b) D2000 and TEOS at 45°C, (c) D2000 and TEOS at 60°C, and (d) D4000 and sodium silicate at 65°C. Average pore sizes are 5.3, 7.5, 11.9, and 14.3 nm for (a), (b), (c), and (d), respectively.

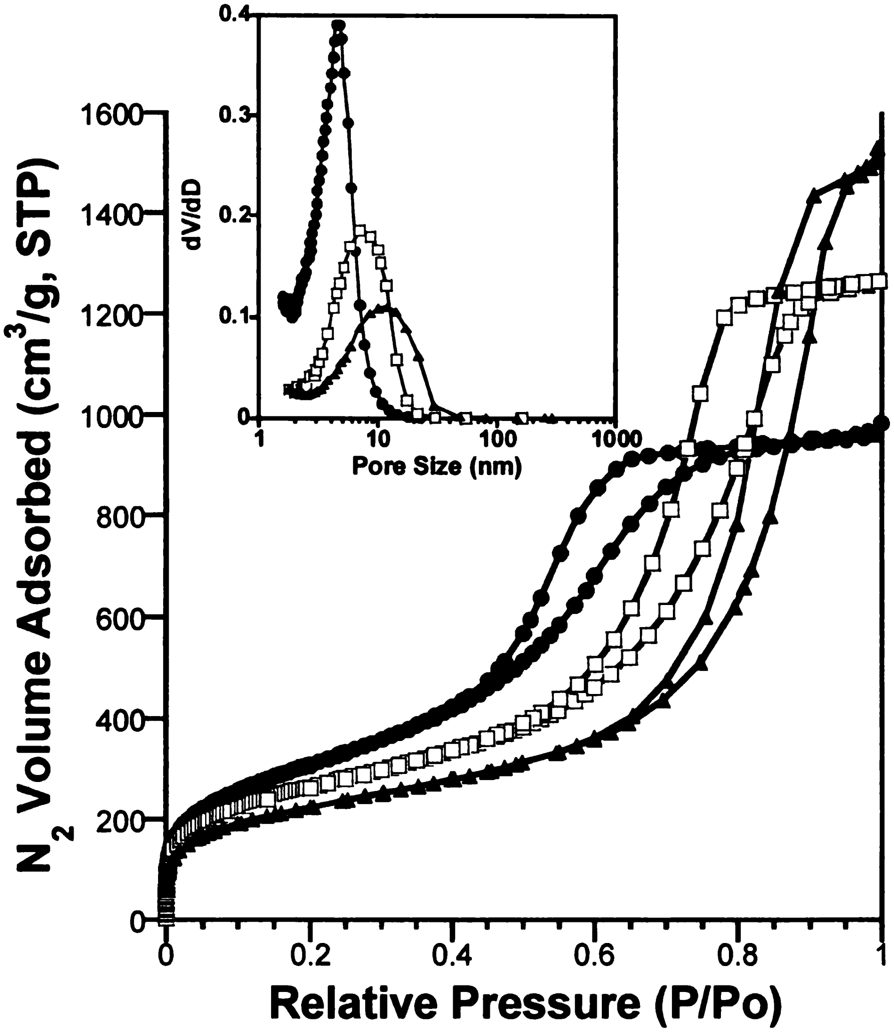

Figure 2.3 N_2 adsorption-desorption isotherms of MSU-J silica molecular sieves assembled from TEOS in the presence of D2000 as a structure director at different synthesis temperatures and calcined at 600 °C for 4 h. The insert provides BJH framework pore size distributions determined from the adsorption branches of the N_2 isotherms (•, □, and ▲ for 25, 45, and 60°C, respectively).

mesopores occurred at P/P_0) 0.5–0.9. As seen from the BJH plots, the pore size increases from 4.9 at 25°C to 11.9 nm at 60°C. The TEM images of the calcined MSU-J mesostructures assembled from TEOS and D2000 at 45 and 60°C in (see Figure 2.2, parts b and c, respectively) reveal pore sizes consistent with those obtained from the pore-size distributions calculated on the adsorption branches of the nitrogen adsorption isotherms.

As shown by the nitrogen isotherms and pore-size distributions in Figure 2.4, the pore volumes and pore sizes of MSU-J materials assembled from sodium silicate and D2000 surfactant are less sensitive to the assembly temperature in comparison to the mesostructures assembled from TEOS. The silicate oligomers generated from these two precursors are presumed to differ in molecular weight and in the extent of cross linking. Also, differences in the ionic strengths of the sodium silicate and TEOS reaction mixtures are likely to contribute to differences in pore sizes of the resulting mesostructures. These differences in precursor structure are manifested in differences in the temperature dependence of the framework pore sizes, as well as the porepore correlation distance.

As expected on the basis of polypropylene oxide chain length, the pore sizes of mesostructures assembled from D4000 are larger than those assemble from D2000 at the same synthesis temperature. Table 1 provides the BET surface areas and pore volumes of calcined MSU-J wormhole mesostructures. The pore diameter expands with increasing synthesis temperature over the range 25-65°C from 5.3 to 6.7 nm with sodium silicate as the silica source. The use of

TEOS as the silica source results in even larger average pore sizes of 7.5 and 11.9 nm at assembly temperatures of 45 and 60°C, respectively. The increases are accompanied by expected decreases in the BET surface areas. The largest average pore size (14.3 nm) is observed for the mesostructure assembled at 60°C from D4000 and sodium silicate.

Table 2.1 Textural properties of calcined MSU-J silicas with wormhole framework structures.

Silica source	Surfactant	Synthesis temp. (°C)	S_{BET} (m^2/g)	d (nm)[b]	BJH pore size (nm)	Wall thickness (nm)[d]	Pore volume (cm^3/g)
SS[a]	D2000	25	947	6.1(6.0)	5.3	0.8	1.41
SS	D2000	45	899	6.6(6.2)	6.0	0.6	1.49
SS	D2000	65	805	7.0(6.7)	6.6	0.4	1.49
TEOS	D2000	25	1127	6.6(6.0)	4.9	1.7	1.53
TEOS	D2000	45	962	8.2(7.2)	7.5	0.7	1.96
TEOS	D2000	60	798	-[c]	11.9	-	2.29
SS	D4000	45	756	-[c]	8.0	-	1.56
SS	D4000	65	408	-[c]	14.3	-	1.37

[a] SS = sodium silicate. [b] The d values in parentheses are for as-synthesized MSU-J mesostructures. [c] XRD reflections were not resolved for these samples. [d] The wall thickness was determined by subtracting the BJH pore size from the pore-pore correlation distance.

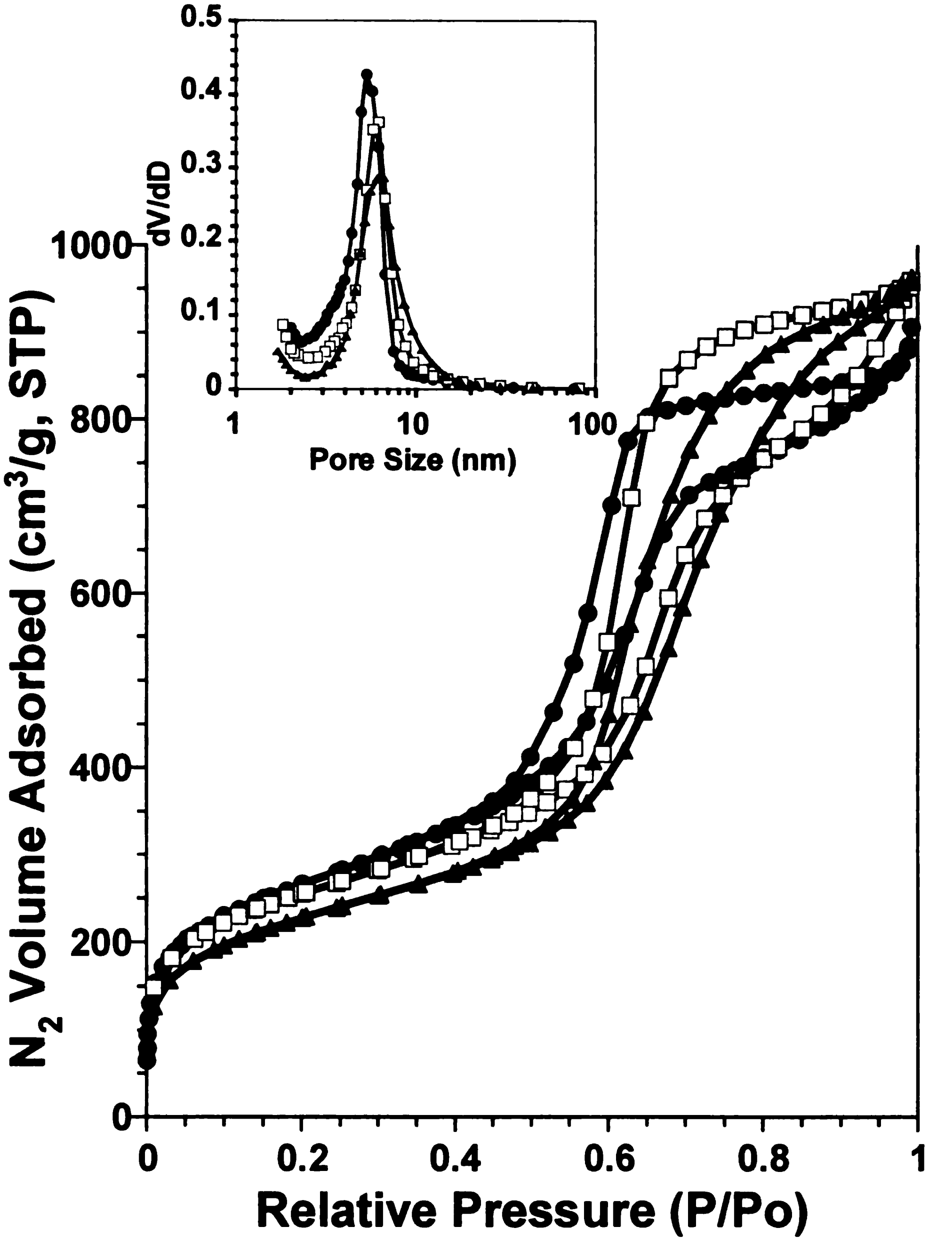

Figure 2.4 N_2 adsorption-desorption isotherms of MSU-J silica molecular sieves assembled from sodium silicate in the presence of D2000 as a structure director at different synthesis temperatures and calcined at 600 °C for 4 h. The insert provides BJH framework pore size distributions determined from the adsorption branches of the N_2 isotherms (●, □, and ▲ for 25, 45, and 65°C, respectively).

The temperature dependence of MSU-J pore sizes is related to a decrease in H-bonding at the silica-surfactant interface with increasing temperature. As the framework cross-linking is enhanced through further condensation of silanol groups at higher temperature, the polarity of the interface is decreased.[11] Consequently, the loss of hydrogen bonding structure between the surfactant and silica aggregates at the I°S° interface will decrease the effective headgroup area (a_0) and increase the surfactant packing parameter (g) $V/(la_0)$, where V is the volume of the surfactant molecule and l is the surfactant length.). The resulting decrease in micelle curvature results in an increase in thepore size. The maximum chain lengths of D2000 and D4000 are approximately 12 and 25 nm, respectively, when the propylene oxide units of the structure-directing agents are placed in a "stretched" all-trans conformation, as indicated by reverse Monte Carlo simulation.[13] The more likely conformations of the PPO chains include kinks that allow for hairpin configurations in the structure-directing micelles. In accord with this expectation, the largest pore sizes observed for MSU-J silicas are smaller than would be predicted by the maximum surfactant chain lengths.

The pore-size maxima for hexagonal MCM-41[14] and SBA-15[15,16] mesostructures has been widely examined and characterized. In the case of MCM-41 electrostatically assembled from quaternary ammonium ion surfactants, the framework pore sizes can be increased from values in the 3-4 nm range up to values approaching ~ 7 nm by increasing the assembly temperature over the range 100-150°C.[17] Also, SBA-15 silicas prepared under strongly acidic conditions in the presence of a triblock copolymer (Pluronic 123) exhibit pore sizes of 4.7-10.6 nm, depending on reaction and postsynthesis reaction conditions.[18,19] Thus, the average pore sizes observed for the wormhole framework structures in the present work span the values found for large-pore MCM-41 and SBA-15. Only mesostructured micellar foam structures exhibit larger pore sizes. However, foam structures require the use of much more complex microemulsions[18,19] and latex polymers[20] as porogens. Also, the BET surface areas of MSU-J silicas (408-1127 m^2/g) are comparable to those of SBA-15 (630–1040 m^2/g). Moreover, MSU-J silicas have larger framework pore volumes (1.37–2.29 cm^3/g) in comparison to SBA-15 materials (0.56-1.23 cm^3/g).

In addition to spanning the pore sizes characteristic of large-pore MCM-41 and SBA-15, the mesostructures reported herein add a new dimensionality to the family of large pore mesostructures. Being wormhole frameworks, the mesopores in MSU-J materials are fully three-dimensional, which can be an advantage over the one-dimensional pore system of MCM-41, particularly in facilitating access to the framework walls under diffusion-controlled conditions. SBA-15 formally has a three-dimensional pore system, but the mesopores are one-dimensional and linked primarily through micropores. Secondary mesopores that link the primary mesopores can be formed in some SBA-15 derivatives, but the secondary mesopores represent less than 6% of the total pore volume.[21] Because MCM-41 and SBA-15 are assembled through electrostatic assembly pathways, the pore-size distributions for these mesostructures are typically narrower than the distributions for wormhole framework structures assembled through hydrogen-bonding pathways. The broader pore-size distributions for MSU-J silicas, however, do not represent a substantial disadvantage for most catalytic or adsorption applications, save perhaps for separations of macromolecules on the basis of size.

2.4 Summary

Wormhole mesostructures assembled through neutral pH pathways typically exhibit improved activity as heterogeneous catalysts, an improved textural mesoporosity and facile recovery of surfactants by solvent extraction methods. Despite the advantages of wormhole mesostructured materials, the average framework pore sizes have been limited to the range 1.6–4.5 nm.

Large-pore mesoporous silicas with wormhole framework structures have been assembled through hydrogen-bonding pathways from sodium silicate or tetraethylorthosilicate as the silica source and amine-terminated Jeffamine surfactants of the type $H_2NCH(CH_3)CH_2[OCH_2CH(CH_3)]_xNH_2$ as the structure-directing porogen. Depending on the molecular weight of the α,ω-diamine surfactant (x = 33 and 68 for Jeffamine D2000 and D4000, respectively) and the synthesis temperature (25–65°C), the mean pore size distributions of the mesostructured silicas (denoted MSU-J) were centered between 4.9 and 14.3 nm. The resulting pore sizes and BET surface areas are comparable to those of SBA-15 silicas, but unlike SBA-15, the mesopores are three-dimensionally connected. Also, the BET surface areas of MSU-J silicas (408-1127 m^2/g) are comparable to those of SBA-15 (630–1040 m^2/g). Moreover, MSU-J silicas have larger framework pore volumes (1.37–2.29 cm^3/g) in comparison to SBA-15 materials (0.56-1.23 cm^3/g). MSU-J wormhole mesostructures represent the largest pore sizes observed to date for a fully three–dimensional mesoporous framework assembled from a single micellar porogen.

2.5 References

(1) Tanev, P. T.; Pinnavaia, T. J. *Science* **1995**, *267*, 865.

(2) Sayari, A. *Chem. Mater.* **1996**, *8*, 1840.

(3) Kloetstra, K. R.; vanBekkum, H.; Jansen, J. C. *Chem. Commun.* **1997**, 2281.

(4) Reddy, J. S.; Sayari, A. *J. Chem. Soc. Chem. Commun.* **1995**, 2231.

(5) Lee, J.; Yoon, S.; Oh, S. M.; Shin, C. H.; Hyeon, T. *AdV. Mater.* **2000**, *12*, 359.

(6) Lee, J.; Han, S.; Hyeon, T. *J. Mater. Chem.* **2004**, *14*, 478.

(7) Antonelli, D. M.; Ying, J. Y. *Angew. Chem. Int. Ed.* **1996**, *35*, 426.

(8) Sun, T.; Ying, J. Y. *Nature* **1997**, *389*, 704.

(9) Kondo, J. N.; Takahara, Y.; Lu, D. L.; Domen, K. *Chem. Mater.* **2001**, *13*, 1200.

(10) Zhang, W. Z.; Pauly, T. R.; Pinnavaia, T. J. *Chem. Mater.* **1997**, *9*, 2491.

(11) Pauly, T. R.; Pinnavaia, T. J. *Chem. Mater.* **2001**, *13*, 987.

(12) Kim, S. S.; Pauly, T. R.; Pinnavaia, T. J. *Chem. Commun.* **2000**, 835.

(13) Carlsson, P.; Swenson, J.; Borjesson, L.; Torell, L. M.; McGreevy, R. L.; Howells, W. S. *J. Chem. Phys.* **1998**, *109*, 8719.

(14) Kresge, C. T.; Leonowicz, M. E.; Roth, W. J.; Vartuli, J. C.; Beck, J. S. *Nature* **1992**, *359*, 710.

(15) Zhao, D. Y.; Feng, J. L.; Huo, Q. S.; Melosh, N.; Fredrickson, G. H.; Chmelka, B. F.; Stucky, G. D. *Science* **1998**, *279*, 548.

(16) Zhao, D. Y.; Huo, Q. S.; Feng, J. L.; Chmelka, B. F.; Stucky, G. D. *J. Am. Chem. Soc.* **1998**, *120*, 6024.

(17) Corma, A.; Kan, Q. B.; Navarro, M. T.; PerezPariente, J.; Rey, F. *Chem. Mater.* **1997**, *9*, 2123.

(18) Yang, C. M.; Zibrowius, B.; Schmidt, W.; Schuth, F. *Chem. Mater.* **2003**, *15*, 3739.

(19) Matos, J. R.; Mercuri, L. P.; Kruk, M.; Jaroniec, M. *Chem. Mater.* **2001**, *13*, 1726.

(20) Lukens, W. W.; Yang, P. D.; Stucky, G. D. *Chem. Mater.* **2001**, *13*, 28-34.

(21) Galarneau, A.; Cambon, H.; Di Renzo, F.; Ryoo, R.; Choi, M.; Fajula, F. *New J. Chem.* **2003**, *27*, 73.

CHAPTER 3

EPOXY-SILICA MESOCOMPOSITES WITH ENHANCED TENSILE PROPERTIES AND OXYGEN PERMEABILITY

3.1 Introduction

Inorganic particles with a domain size less than 100 nm in at least one dimension can enhance the tensile properties of a polymer through beneficial interactions at the polymer–particle interface.[1] Layered silicate clays in exfoliated form have been widely investigated in recent years as reinforcing agents, as well as barrier and flame retardation agents, for a variety of organic polymer systems.[2-4] Unlike conventional composites formed from monolithic particles, clay nanocomposites are formed through the complete dispersion (exfoliation) of the nanolayers that comprise the clay tactoids. This exfoliation process provides a large surface area (~750 m^2/g) and a high particle aspect ratio (≥ 200)[5] that normally cannot be achieved with monolithic particles.

Mesostructured silica and other metal oxides[6] represent another class of inorganic material that more recently has been considered for polymer composite formation. These solids have controllable nanopores (2–10 nm) and surface areas that are even higher than exfoliated clays, though the particle morphology tends to be isotropic. Mesostructured silica with a large mesopore size has shown promise for the formation of novel polymer composites.[7] For example, the one dimensional channels of hexagonal MCM-41 have been used to direct the polymerization of conjugated polymers such as polydiacetylene[8], polyvinylene[9, 10] and polythiophene[11]. The alignment of the polymers within the pores can result in unusual chromatic changes, polarized luminescence, and stability after multiple cyclovoltametric cycles. Nevertheless, there has been only a few attempts to improve the mechanical[12-14] and permeability properties[15] of a polymer using mesoporous silica as an adjuvant.

Although embedded nanoparticles can improve both the barrier and the mechanical properties of a polymer for potential applications in packaging,[16] it generally is much more difficult to enhance the permeability of a polymer for gas separation applications without compromising polymer strength.[17] Porous zeolite molecular sieve and mesostructured silica particles have been shown to improve the permeability polymer-based membranes.[15, 18-22, 23] For example, the addition of 30% (w/w) MCM-41 to polysulfone boosts the oxygen permeability by 155% without a loss in O_2/N_2 selectivity due to increased diffusivity through nonselective voids.[15] However, the composite membranes became increasingly brittle with increasing mesostructured silica loading. Similar improvements in permeability at the expense of strength have been observed for amine-functionalized polyimide membranes[23] embedded with mesostructured silica.

We recently reported a large pore mesostructured silica, denoted MSU-J,[24] assembled from tetraethylorthosilicate as the silica source and the α, ω-diamine polypropylene oxide $H_2NCH(CH_3)CH_2[OCH_2CH(CH_3)]_xNH_2$ (x = ~33, trade named Jeffamine D2000) as the structure-directing agent. The latter amine, which is commercially available under the trade name Jeffamine D2000, also has been use as a cross-linking agent[25-27] for the formation of rubbery epoxy polymers. In the present study we investigate the properties of as-made, amine-intercalated MSU-J mesostructured silica for the synthesis of epoxy–silica mesocomposites. For comparison purposes we also have used the surfactant-free calcined version of MSU-J silica for epoxy composite formation. The three-dimensional wormhole[28, 29] pore network (average pore size 5.3 nm) and the high surface area (~ 950 m^2/g) of MSU-J silica is shown to substantially improve the tensile properties of the polymer. Also, we report the unexpected enhancement in the oxygen permeation properties for composite compositions derived from as-made MSU-J mesostructures. The observed enhancement in oxygen permeability may find use for the design of composite membranes based on mesostructured forms of silica.

3.2 Experimental

Epoxy resin EPON 828, a diglycidyl ether of bisphenol (Resolution Performance Products, M_w ~377), was used for the preparation of epoxy - MSU-J silica mesocomposites. The α, ω diamine–functionalized polypropylene oxide $H_2NCH(CH_3)CH_2[OCH_2CH(CH_3)]_xNH_2$ (x = ~33) with an average molecular weight of ~2000 was obtained from Huntsman Chemical Co. under the trade name Jeffamine D2000. The amine was used both as an epoxy curing agent and as a structure-directing agent for the synthesis of MSU-J silica. Sodium silicate (27% SiO_2, 14% NaOH solution) was purchased from Aldrich and used as a silica precursor for the preparation of MSU-J mesostructured silica.

The Jeffamine D2000 porogen was mixed with an amount of aqueous HCl solution equivalent to the hydroxide content of the sodium silicate solution. The silica source was added to the porogen solution under vigorous stirring at ambient temperature and the mixture was allowed to age at 25°C for 20 h. The optimum molar composition for the formation of as-made MSU-J was 1.0 SiO_2 : 0.83 NaOH : 0.125 Jeffamine D2000 : 0.83 HCl : 230 H_2O. The porogen-intercalated as-made mesostructured product, denoted as-made MSU-J, was recovered by filtration and dried in air at ambient temperature. A porogen–free analog of the mesostructure, denoted calcined MSU-J, was obtained by calcination of as-made MSU-J at 600°C for 4 h. The as-made and calcined forms of the mesostructures were ground to a powder for future use.

A pre-determined amount of as-made or calcined MSU-J silica was added to the epoxy resin and mixed at 50°C for 10 min. The amount of Jeffamine D2000 curing agent needed to achieve an overall NH : epoxide stoichiometry of 1 : 1 was then added to the mixture and mixed at 50 °C for another 10 min. For composites prepared from the as-made mesostructure, the Jeffamine D2000 present in the pores of the mesostructure was counted as contributing to the curing process. The resulting suspensions were out-gassed under vacuum and transferred to an aluminum mold. Pre-curing of the nanocomposite was carried out under nitrogen gas flow at 75°C for 3 h, followed by an additional 3 h cure at 125°C to complete the cross-linking.

In order to compare the optical transparency of an epoxy–as-made MSU-J mesocomposite against a conventional epoxy - epoxy nanocomposite, an octadecylammonium-modified montmorillonite (ODA-MMT, Nanocor Inc.) was used as a reinforcing agent. Approximately 65% of the cation exchange sites of the ODA-MMT clay are occupied by ODA cations and the remaining sites are occupied by protons. A procedure analogous to that used to prepare the as-made MSU-J–epoxy mesocomposites was used to prepare the clay composites.

X-ray diffraction (XRD) patterns were obtained on a Rigaku Rotaflex 200B diffractometer equipped with Cu K_{α} X-ray radiation and a curved crystal graphite monochromator operating. Samples of the liquid epoxy-silica mixture were prepared by pouring the suspension onto filter paper mounted on a glass slide and blotting away the excess liquid. Cured nanocomposites were examined by mounting a rectangular flat specimen into an aluminum X-ray sample holder. XRD patterns with equivalent intensities were obtained for the upper and lower surfaces of the cured mesocomposites containing 12 wt% silica, thus verifying the uniform dispersion of mesostructured silica in the epoxy matrix.

Transmission electron microscopy (TEM) images were taken on a JEOL JEM-100CX II microscope with a CeB_6 filament and an accelerating voltage of 120 kV. Sample grids of calcined mesoporous silicas were prepared via sonication of a powdered sample in ethanol for 10 min and evaporating 2 drops of the suspension onto a holey carbon film supported on a 3 mm, 300 mesh copper grid.

Tensile measurements on individually molded samples were performed at ambient temperature according to ASTM standard D3039 using an SFM-20 United Testing System. The dog-bone shaped specimens used in the tensile testing were 28 mm long in the narrow region, 3 mm thick, and 3 mm wide along the center of the casting. At least four stress-strain data points with good precision were obtained and the results averaged. For a typical instance, the errors in modulus and strength for the composites containing 12%(w/w) as-made MSU-J silica are ± 1.2 and ± 0.50, respectively, based on the 95% confidence interval for the mean values. The original cross-sectional area at zero strain was used to compute toughness.

Oxygen permeability data were recorded on a MOCON Oxtran 2/60 oxygen permeability instrument with a test gas containing 100% oxygen, nitrogen (containing 2 vol% hydrogen) as a carrier gas. Film samples with a thickness between 0.9 and 1.5 mm, area of 0.317 cm^2, were cast from an aluminum disk mold, and were loaded in the testing cells with adhesive aluminum foil masks.

Thermogravimetric analyses (TGA) were performed using a computer controlled Shimadzu TGA-50 thermal analyzer. Typically, a 50 mg sample was placed in a pyrex bucket and heated an ambient temperature to 800 °C at a rate of 5 °C/min in a nitrogen flow of 50 mL/min.

Positronium Annihilation Lifetime Spectroscopy (PALS) was performed with a standard fast timing spectrometer with a 0.30 ns time resolution. A ^{22}Na source that emits about 10^6 positrons/s is sealed between two thin sheets of Ni foil and then sandwiched between two identical sheets (each sheet is about 2 cm square) of the sample to be studied. Positrons are emitted from the source simultaneously with a 1270 keV gamma ray (detected as the "start" signal) and some 80% penetrate the sealing foil and stop in the target sample. About 30% of the positrons stopping in the neat epoxy form positronium, the bound state of the positron and electron, which tends to localize in free volume voids. Subsequent annihilation of the positronium produces 511 keV radiation detected as the "stop" signal and the time between each start and stop signal pair is recorded as a time histogram. This lifetime spectrum is fitted for exponential lifetime components wherein the lifetime and intensity are related to void size and porosity.

3.3 Results

A large pore mesostructured silica with a wormhole framework structure, denoted MSU-J, was assembled from sodium silicate and Jeffamine D2000 as the structure-directing porogen according to previously described methods.[24] The pore diameter (5.3 nm), pore volume (1.41 cm^3/g) and a surface area (947 m^2/g) were determined by a N_2 adsorption isotherm following calcination of the as-made mesostructure at 600°C. It is presumed that the as-made mesostructure, which contains 58% (w/w) Jeffamine D2000 porogen in the framework mesopores, has similar textural properties.

Both the as-made and the calcined forms of the mesostructure were used in forming rubbery epoxy mesocomposites. The mesocomposites formed from as-made MSU-J have the Jeffamine D2000 curing agent initially partitioned between the silica mesophase and the pre-polymer resin. For the mesocomposites formed from the porogen–free calcined form of MSU-J, however, all the curing agent is contained initially in the bulk pre-polymer prior to the curing reaction.

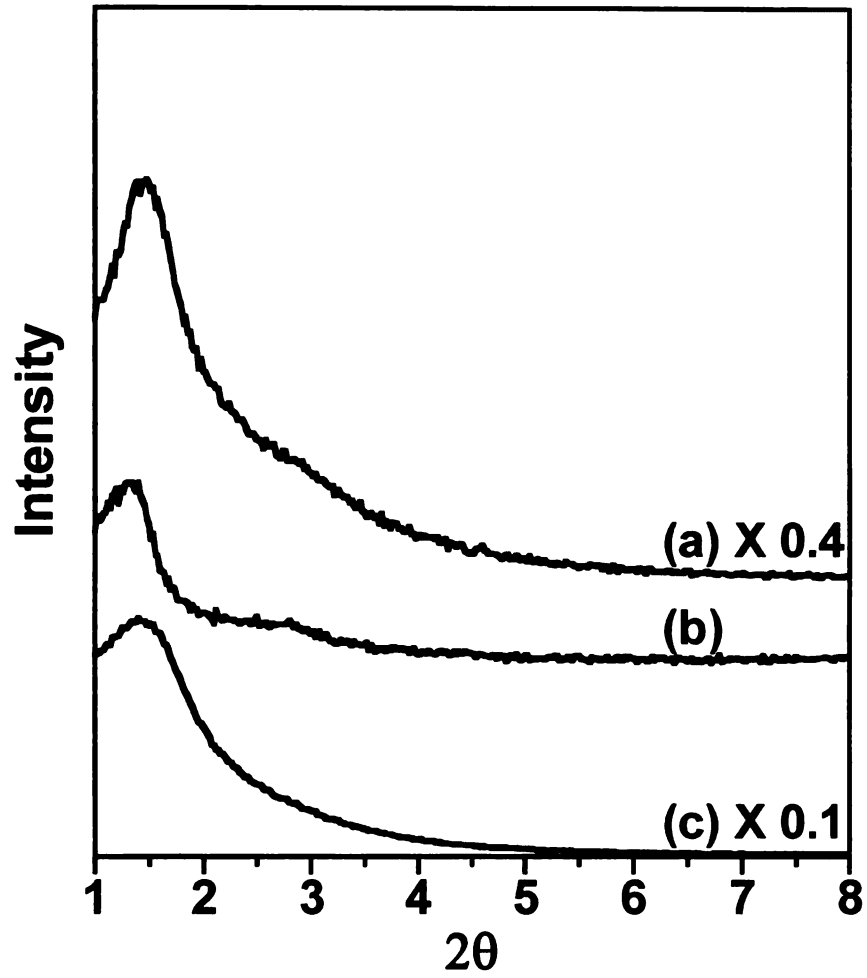

Figure 3.1 Small angle powder X-ray diffraction patterns: (a) as-made MSU-J mesostructure containing 58% (w/w) intercalated Jeffamine D2000; (b) epoxy–silica mesocomposite (12 wt% silica) formed from as-made MSU-J; (c) mesostructured silica recovered through calcination at 600°C of a mesocomposite containing 12% (w/w) silica.

Figure 3.1 compares the small angle XRD patterns for the as-made MSU-J mesostructure (curve a) with the pattern of the mesostructure dispersed at the 12% (w/w) level in a cured epoxy composite (curve b). The presence of a low angle reflection, corresponding to a d-spacing of 6.0 nm, is indicative of the average pore–pore correlation distance for a wormhole framework. The wormhole framework structure is verified by the TEM shown in Figure 3.2a. The loss of diffraction intensity upon dispersion of the mesostructure in the cured composite is attributable to contrast matching between the silica walls and cured polymer formed in the mesopores. Evidence supporting the contrast matching effect is provided by the increase in intensity observed upon removal of the polymer through calcination (curve c). Analogous XRD scattering behavior was observed for the calcined MSU-J–epoxy composite system. These XRD data, along with the TEM image of Figure 3.2b of the recovered mesostructure, clearly show that the wormhole framework structure of MSU-J is retained in a epoxy matrix upon cross-linking at 125 °C.

Tensile data were obtained from dog-bone-shaped specimens containing 1.0–12 wt% as-made and calcined MSU-J silica. A comparison of stress-strain curves (more accurately load-displacement curves because the load is not normalized with respect to cross sectional area of the specimens) as a function of silica loadings for the rubbery epoxy mesocomposites is provided in Figure 3.3. Both forms of the mesostructure provide composites with improved mechanical performance. The modulus, strength, elongation and toughness of the epoxy composites prepared from the as-made and calcined forms of the silica generally

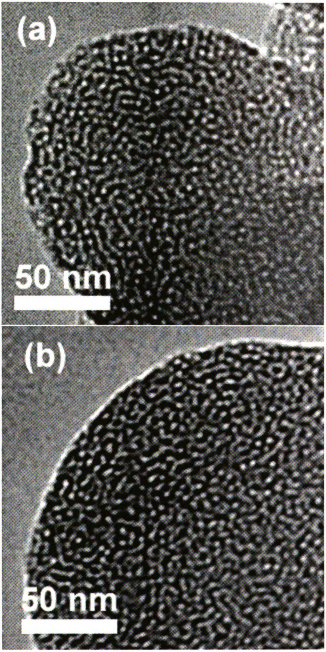

Figure 3.2 TEM images of (a) calcined MSU-J silica and (b) the silica obtained through calcination at 600°C a cured epoxy–silica mesocomposite (12 wt% silica) formed from as-made MSU-J silica.

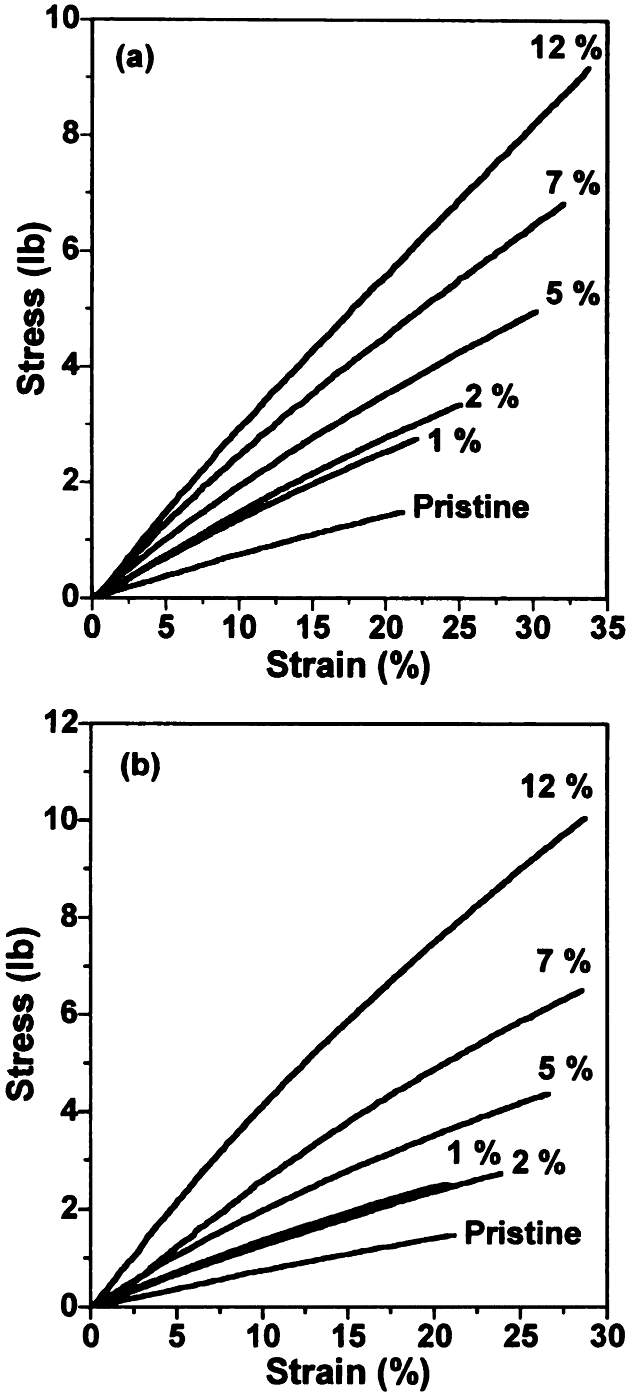

Figure 3.3 Comparison of stress-strain curves for pristine epoxy and MSU-J/epoxy mesocomposites containing different loadings of (a) as-made MSU-J silica and (b) calcined MSU-J silica.

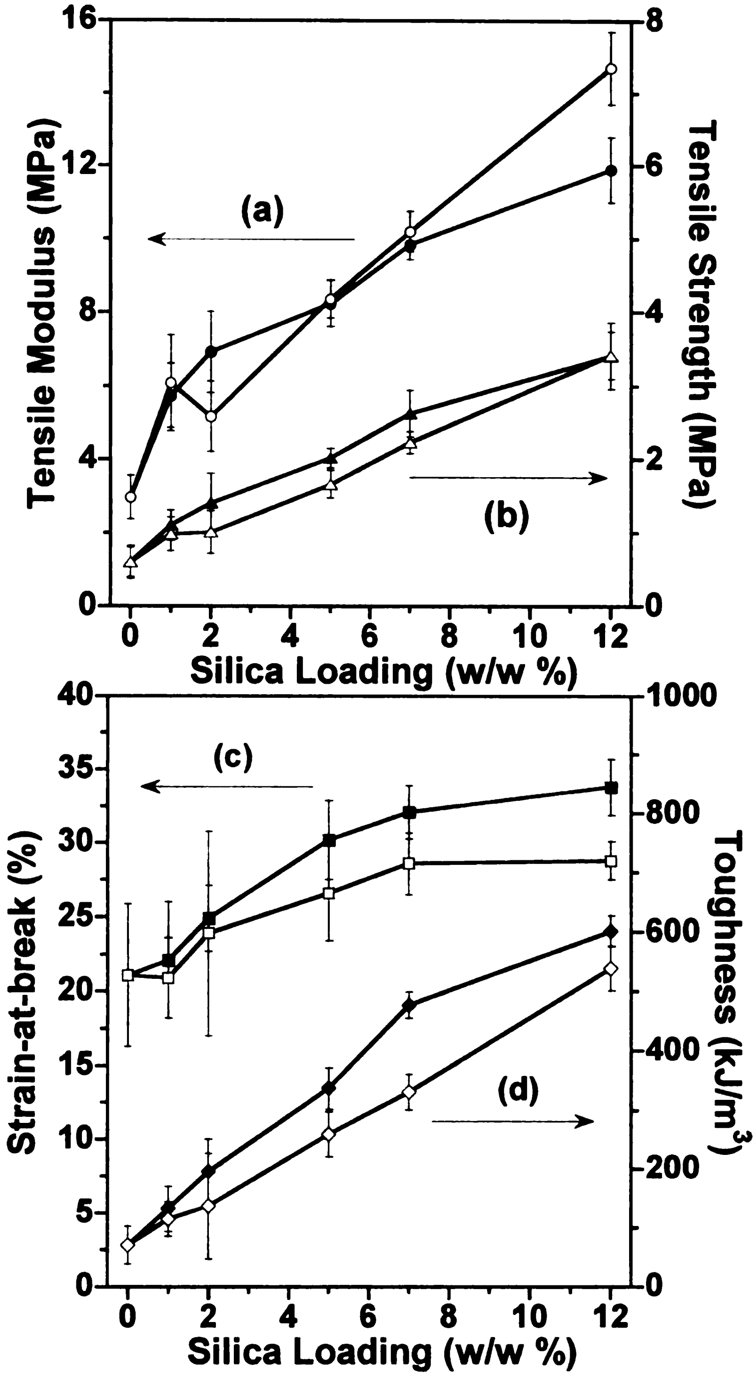

Figure 3.4 Loading dependence of the (a) tensile modulus (b) tensile strength (c) strain-at-break and (d) toughness for epoxy mesocomposites prepared from MSU-J silica. The solid and open data points are for the composites prepared from as-made and calcined MSU-J silica, respectively.

increase with increasing silica loadings (Figure 3.4). Table 3.1 summarizes the values of tensile properties obtained at different silica loadings. Note that the composites formed from the as-made silica have a higher elongation at-break, so that the toughness of the composites increases more rapidly with increasing silica loading in comparison to the composites formed from calcined MSU-J.

The most significant difference in the properties of the mesocomposites formed from as-made and calcined MSU-J silica is observed in the oxygen permeability profiles of the composites. Figure 3.5 presents the O_2 permeability of the rubbery epoxy composites as a function of as-made and calcined MSU-J silica loadings. The oxygen permeability for the nanocomposites prepared from the calcined mesostructure is nearly independent of the silica content of the epoxy matrix over the entire loading range 0–12% (w/w) silica. The as-made MSU-J system, in contrast, shows behavior similar to the calcined silica composites only at low silica loadings (1–3 wt%). An abrupt and significant increase in oxygen permeability occurs at 5 wt% loading. Relative to the pristine polymer, a 5- to 6-fold increase in oxygen permeability is observed over the silica loading range 7–12% (w/w). Oxygen permeability increases of this magnitude are unprecedented among polymer-based nanocomposites containing dispersed porous particulates.

PALS results for the neat epoxy and two samples of the as-made MSU-J silica composites (2% and 10% w/w) are quite definitive. The neat epoxy displays a very typical 2.7 ns positronium lifetime (with a relative intensity of 20%) that corresponds to 0.7 nm diameter voids inherent to the material. The two spectra from the MSU-J silica composites are almost identical except that the 10% w/w film has a relative intensity of the 2.7 ns lifetime of only 18%. The 10% drop in relative intensity corresponds to the 10% of positrons that stop in the silica phase which does not have a 2.7 ns lifetime. There is no indication of any longer positronium lifetimes as would be expected if the silica pores where vacant (5 nm pores would correspond to lifetimes in the 50–80 ns range). Special long time-range PALS runs with high sensitivity to such long lifetimes were performed and an *upper limit* of 0.15% relative intensity could be set on any such components (i.e. less than 1% of the 20% positronium intensity measured in the neat epoxy). Heating in vacuum to 150 °C to drive off any absorbed water from environmental exposure yielded identical spectra. The PALS data are completely consistent with no voids in the as-made MSU-J silica mesocomposites, other than those microvoids inherent to the cured epoxy. The silica pores are fully occupied by cured polymer.

Another significant result derived from the epoxy–MSU-J mesocomposite systems relative to natural epoxy clay nanocomposites is the optical transparency of the mesocomposites. Figure 3.6 illustrates that the mesocomposite containing 10% (w/w) as-made MSU-J silica is substantially more transparent than an ODA-MMT composite containing the same loading of montmorillonite clay. The mesocomposites made from calcined MSU-J have a similar transparency. Thus, in comparison to clay nanoparticles, the refraction index of the MSU-J silica more nearly matches that of the epoxy matrix. The

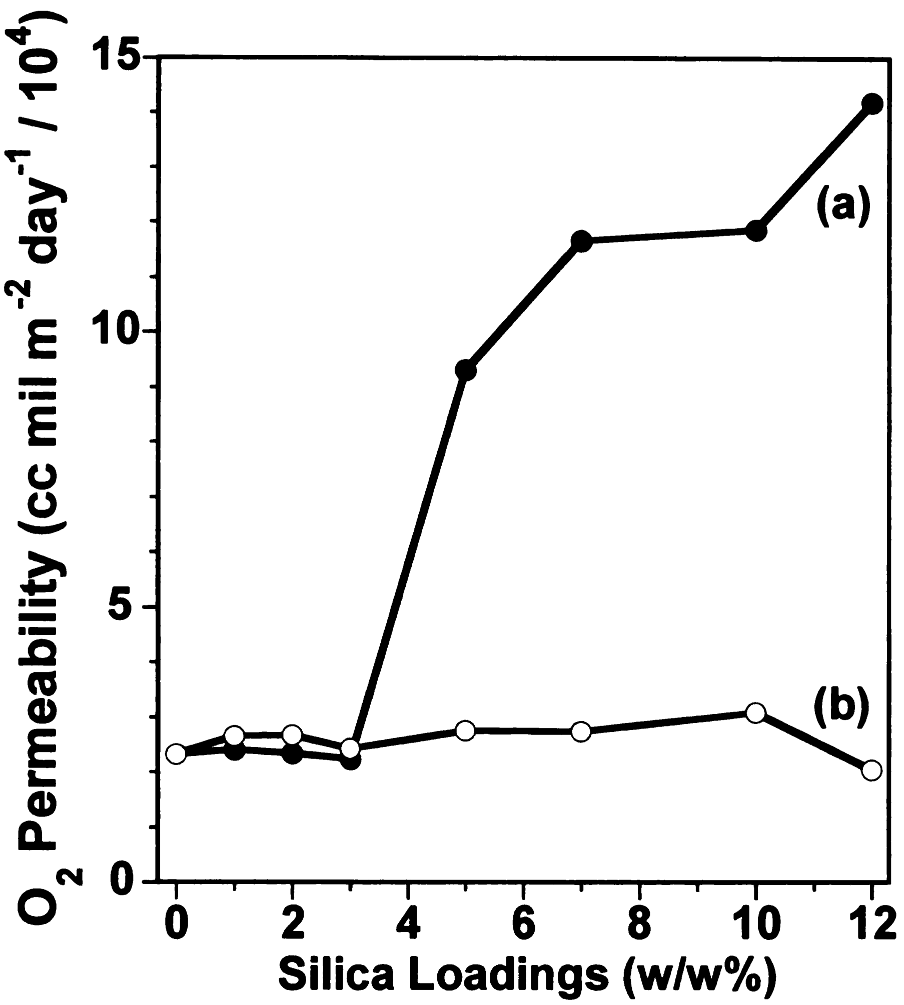

Figure 3.5 Dependence of oxygen permeability on silica loadings for epoxy mesocomposites prepared from (a) as-made MSU-J silica and (b) calcined MSU-J silica.

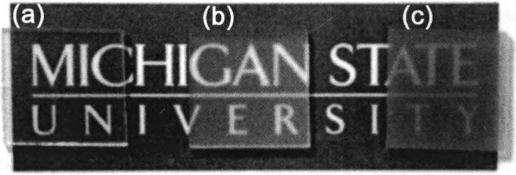

Figure 3.6 Optical image illustrating differences in the transparency of (a) pristine epoxy polymer and epoxy composites prepared from (b) as-made MSU-J silica at 10% (w/w) loading and (c) octadecylammonium-modified montmorillonite (ODA-MMT) at 10% (w/w) silicate loading.

thermal stability of the mesocomposites formed from as-made MSU-J is enhanced in comparison to the pristine polymer.

As illustrated in Figure 3.7, the temperature needed to achieve a weight loss of 1.5% is increased by 50 °C relative to the pristine epoxy polymer. Along with the delayed first degradation stage, the maximum degradation rate is shifted from 365 °C for the pristine epoxy to 396 °C for the mesocomposite containing 12% (w/w) as-made MSU-J silica, as determined from the first derivative of the TGA curves. Additionally, the charring processes, which starts at approximately 400 °C in both cases, is extended up to 800 °C for the as-made MSU-J composite at a 12% (w/w) loading.

3.4 Discussion

The XRD and TEM results shown in Figures 3.1 and 3.2 clearly establish retention of the mesophase phase structure upon dispersal of as-made and calcined MSU-J silica in a cured epoxy matrix. Little or no settling of the mesophase was observed during the polymer curing process, because the intensity of the Bragg reflections from the upper and lower surfaces of the cured composite specimens were equivalent over the entire range of silica loadings.

The substantial improvements in the modulus, strength and toughness achieved for the MSU-J mesocomposites in comparison to the pristine polymer (c.f. Table 3.1) most likely are a consequence of strong interfacial interactions and adhesion between the epoxy matrix and silica mesophase. It is important to note that favorable interfacial interactions are realized in these mesocomposites

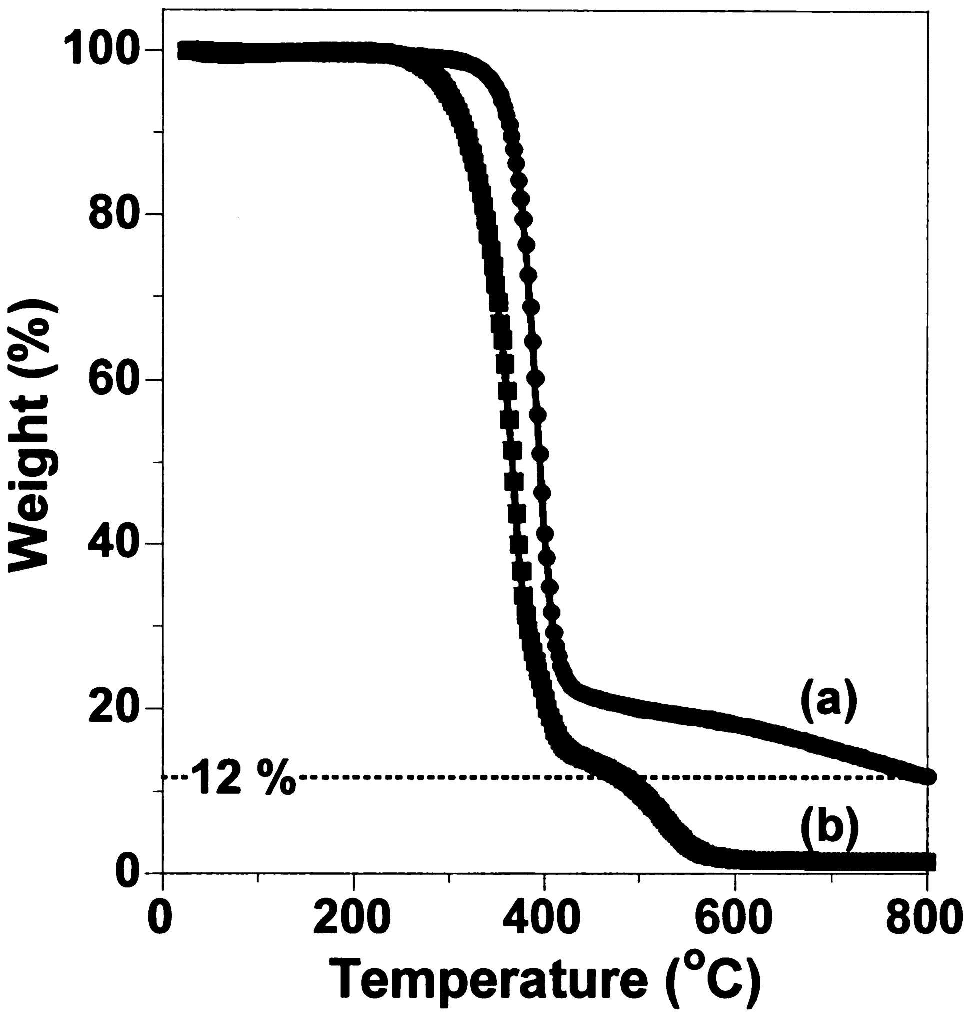

Figure 3.7 Thermogravimetric analysis curves in air for (a) the epoxy mesocomposite prepared from as-made MSU-J silica at a loading of 12% (w/w) silica and (b) the pristine epoxy polymer.

without the need for organic modification of the silica surface. The high surface area of the MSU-J silica (~950 m^2/g) facilitates such interfacial interactions. Similar improvements in tensile moduli, strengths and strain-at-breaks have been observed for rubbery epoxy–organoclay nanocomposites.[30-32] The 4- to 5.5-fold increase in modulus at 12% (w/w) MSU-J loading is comparable to the 6-fold benefit in modulus provided by organoclay nanoparticles at an equivalent loading. Moreover, the benefit in tensile properties occurs with little or no sacrifice in transparency (c.f. Figure 3.6) or thermal stability properties (c.f. Figure 3.7).

In the case of exfoliated clay nanocomposites, the anisotropic clay platelets in the cured matrix can be partially aligned in the direction of the stress and further enhance the tensile properties.[30] This strain-induced alignment of particles is less significant for the more isotropic MSU-J silica particles. Differences in particle morphology and alignment under applied stress may be the reason why the elongation-at-break is limited to 34% for the mesocomposites formed from as-made MSU-J, whereas for nanocomposites formed from exfoliated clay platelets the elongation-at-break is 50% at the same 12% (w/w) loading.[30] In any case, unlike conventional reinforced composites which sacrifice elasticity and toughness in exchange for benefits in modulus and strength,[32-34] mesostructured silica and exfoliated clay are unique in providing substantially improved tensile properties at relatively low particulate loadings.

We note that previous attempts to use three-dimensional mesostructured silica as a polymer reinforcing agent have not demonstrated mechanical improvements comparable to those achieved with exfoliated organoclays. For instance, Nylon 66 composites containing 35% (w/w) of a mesostructured silica denoted FSM[12] exhibited only a two-fold increase in modulus. A mesostructured organosilica[13] and a silylated cubic MCM-48[14] mesostructure have been used as reinforcing agents for poly((3-trimethoxysilyl)propylmethacrylate) and poly(vinyl acetate), respectively. The latter composites exhibited improvements in tensile strength and modulus, but the elongation at break was sacrificed despite efforts to achieve compatible particle–polymer interfaces through extensive organic modification of the silica surface.

The oxygen permeabilities of the mesocomposites formed from calcined MSU-J silica is independent of the particulate loading up to 12% (w/w) loading, as expected for a uniform dispersion of more or less isotropic particles in the polymer matrix (c.f. Figure 3.5, curve (b)). However, the composite formed from as-made MSU-J silica shows an enhancement in oxygen permeability at a silica loading ≥ 5% (w/w) silica (c.f. Figure 3.5, curve (a)). Both composite systems show no evidence for the presence of free volume, as judged by PALS. That is, the mesopores of the embedded silica in both mesocomposites systems are fully occupied by cured polymer. Thus, the enhancement in oxygen permeability for the mesocomposites made from as-made MSU-J silica cannot be attributed to diffusion through vacant pores in the mesostructured silica.

The main difference between the composites formed from as-made and calcined MSU-J silica lies in the initial distribution of the amine curing agent at the initial stages of the polymerization process. For as-made MSU-J, the amine is partitioned between the mesopores and the bulk resin, whereas for the calcined silica, the curing agent initially resides exclusively in the resin. The latter distribution of curing agent should lead to a uniform chain cross-linking throughout the polymer matrix. Although protonated amines act as an acid catalyst for epoxy-amine polymerization in the gallery regions of clays,[35] the silica-intercalated amine in as-made MSU-J is electrically neutral[36] and acid catalysis is not anticipated. However, the partitioning of the curing agent between the silica phase and the bulk pre-polymer may affect the rates for diffusion of resin and curing agent into and out of the pores and lead to a non-uniform chain cross-linking, particularly in the silica - polymer interface region.[37-39] As illustrated in Figure 3.8, a decrease in chain cross-linking near the silica interface would provide a "corona" or an "interface" of more permeable polymer around the silica particles and provide a percolation pathway for enhanced oxygen permeation. This proposed decrease in chain cross-linking density and concomitant increase in polymer flexibility in the interface region may also help explain why the mesocomposites prepared from as-made MSU-J silica are notably tougher than those prepared from the calcined form of the mesostructure (c.f. Table 3.1). Moreover, ^{29}Si MAS NMR spectroscopy (not shown) indicates the framework cross-linking to be lower in as - made MSU-J (Q^3/Q^4 = 0.89) than in calcined MSU-J silica (Q^3/Q^4 = 0.36). A lower degree of framework cross-linking for as-made MSU-J may provide the silica reinforcing agent with more flexibility, thus increasing toughness at he expense of modulus.

We note that zeolite–loaded polymer membranes[19,21,22] have been reported wherein the oxygen permeability increases via a percolation pathway at

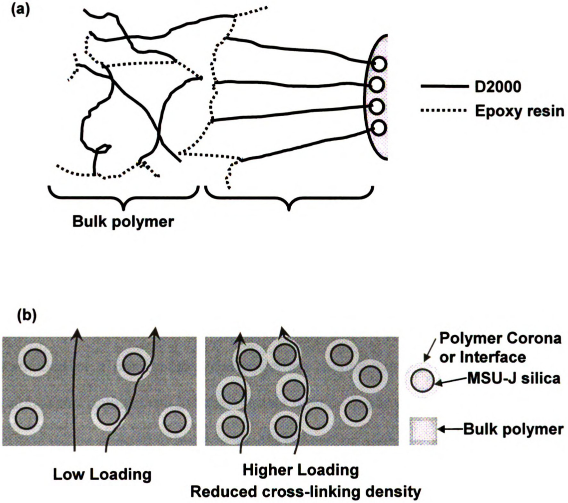

Figure 3.8 Schematic representations of (a) the proposed decrease in chain cross-linking density around the as-made MSU-J silica particles and (b) the proposed permeant gas pathways below and above ~ 5% (w/w) loading of as-made MSU-J silica.

a loading of ~30% (w/w).[22] For such membranes the zeolite pores are too small (< 1 nm) to be filled by polymer and the permeant traverses the 0.30 cm^3/g void volume of the zeolite at the percolation threshold. The small pore sizes and hydrophilic surface cause poor interaction with the polymer chains, resulting in inadequate zeolite particle dispersion.[40,41] The deteriorated mechanical properties of zeolite-epoxy composites[41] substantiate zeolite de-wetting by the polymer chains. Due to the poor zeolite particle dispersion, non-selective zeolite voids cannot provide facilitated diffusion pathway for entire membrane in the diffusion direction until the zeolite loading reaches a very high value (~30 wt%). In the present work, the pore size (5.3 nm) and pore volume (1.41 cm^3/g) of the inorganic phase are much larger than a zeolite, and consequently, the pore are filled with polymer. The high level of as-made MSU-J particle dispersion and the formation of a permeable polymer corona around the particles provides for a permeation pathway at a relatively low particle loading of 5% (w/w). Modeling efforts will be needed to better estimate the corona size.

3.5 Summary

As-made and calcined forms of large pore (5.3 nm) mesostructured silica with a wormhole framework structure, denoted MSU-J, have been used to form rubbery epoxy mesocomposites containing 1.0–12 % (w/w) silica. The tensile modulus, strength, toughness, and extension-at-break for the mesocomposites formed from as-made and calcined forms of MSU-J silica are systematically reinforced by up to 4.8, 5.7, 1.6, and 8.5 times, respectively, in comparison to the pure epoxy polymer. The composites represent the first examples wherein the reinforcement benefits provided by mesostructured silica particles are comparable to those provided by exfoliated organoclay nanolayers at equivalent loadings. Moreover, the reinforcement benefits are realized without the need for organic modification of the silica surface, and the increases in tensile properties occur with little or no sacrifice in optical transparency or thermal stability.

The oxygen permeability of the mesocomposites prepared form as-made MSU-J silica increases dramatically at loadings ≥ 5.0% (w/w), whereas the compositions made from the calcined form of the mesostructure show no permeation dependence on silica loading. For instance, the oxygen permeability of the mesocomposites containing 12 % (w/w) as-made MSU-J silica is six-fold higher than that of the silica-free epoxy membrane. Positron annihilation lifetime spectroscopy established the absence of free volume in the mesocomposites, thus precluding the possibility of facile oxygen diffusion through the framework pores of the silica. The increase in oxygen permeability is correlated with of the partitioning of curing agent between the as-made mesostructure and the liquid pre-polymer, which leads to coronas of permeable polymer with reduced chain cross-linking in the vicinity of the silica particles. Mesocomposites made from calcined forms of the mesostructured silica do not allow for curing agent partitioning, and the oxygen permeability is not significantly influenced by the silica loading.

Table 3.1 Tensile, thermal stability and oxygen permeability properties of pristine epoxy polymer and epoxy/MSU-J mesocomposites.

Sample	Silica loading (w/w%)	Tensile modulus (MPa)	Tensile strength (MPa)	Elongation (%)	Toughness (kJ m^{-3})	Thermal stability§ (°C)	Oxygen permeability (cc·mil·m^{-2}·day^{-1}/10^{4})
Pristine Polymer	0	2.96	0.60	21.1	71	269	2.3
As-made MSU-J Mesocomposites	1	5.74	1.10	22.1	132		2.4
	2	6.93	1.40	24.9	195		2.3
	3						2.2
	5	8.24	2.02	30.2	337		9.3
	7	9.84	2.63	32.1	477		12
	10						12
	12	11.9	3.41	33.8	601	320	14
Calcined MSU-J Mesocomposites	1	6.09	0.98	20.9	115		2.8
	2	5.17	1.01	25.9	137		2.8
	3						2.4
	5	8.37	1.66	29.5	259		2.8
	7	10.2	2.23	28.8	331		2.6
	10						3.0
	12	14.7	3.42	29.9	539		2.0

§ Temperature needed to achieve a weight loss of 1.5%.

3.6 References

(1) Novak, B. M. *Adv. Mater.* **1993**, *5*, 422.

(2) Giannelis, E. P. *Adv. Mater.* **1996**, *8*, 29.

(3) Kojima, Y.; Usuki, A.; Kawasumi, M.; Okada, A.; Fukushima, Y.; Kurauchi, T.; Kamigaito, O. *J. Mater. Res.* **1993**, *8*, 1185.

(4) Yano, K.; Usuki, A.; Okada, A.; Kurauchi, T.; Kamigaito, O. *J. Polym. Sci. Polym. Chem.* **1993**, *31*, 2493.

(5) LeBaron, P. C.; Wang, Z.; Pinnavaia, T. J. *Appl. Clay Sci.* **1999**, *15*, 11.

(6) Kresge, C. T.; Leonowicz, M. E.; Roth, W. J.; Vartuli, J. C.; Beck, J. S. *Nature* **1992**, *359*, 710.

(7) Shi, J. L.; Hua, Z. L.; Zhang, L. X. *J. Mater. Chem.* **2004**, *14*, 795.

(8) Lu, Y. F.; Yang, Y.; Sellinger, A.; Lu, M. C.; Huang, J. M.; Fan, H. Y.; Haddad, R.; Lopez, G.; Burns, A. R.; Sasaki, D. Y.; Shelnutt, J.; Brinker, C. J. *Nature* **2001**, *411*, 617.

(9) Nguyen, T. Q.; Wu, J. J.; Doan, V.; Schwartz, B. J.; Tolbert, S. H. *Science* **2000**, *288*, 652.

(10) Molenkamp, W. C.; Watanabe, M.; Miyata, H.; Tolbert, S. H. *J. Am. Chem. Soc.* **2004**, *126*, 4476.

(11) Li, G. T.; Bhosale, S.; Wang, T. Y.; Zhang, Y.; Zhu, H. S.; Fuhrhop, K. H. *Angew. Chem. Int. Ed.* **2003**, *42*, 3818.

(12) Kojima, Y.; Matsuoka, T.; Takahashi, H. *J. Appl. Polym. Sci.* **1999**, *74*, 3254.

(13) Ji, X. L.; Hampsey, J. E.; Hu, Q. Y.; He, J. B.; Yang, Z. Z.; Lu, Y. F. *Chem. Mater.* **2003**, *15*, 3656.

(14) He, J.; Shen, Y. B.; Yang, J.; Evans, D. G.; Duan, X. *Chem. Mater.* **2003**, *15*, 3894.

(15) Reid, B. D.; Ruiz-Trevino, A.; Musselman, I. H.; Balkus, K. J.; Ferraris, J. P. *Chem. Mater.* **2001**, *13*, 2366.

(16) Pinnavaia, T. J.; Beall, G. W. *Polymer-Clay Nanocomposites*. ed.; John Wiley and Sons: **2001**.

(17) Maier, G. *Angew. Chem. Int. Ed.* **1998**, *37*, 2961.

(18) Kulprathipanja, S.; Neuzil, R. W.; Li, N. N. Separation of Fluids by Means of Mixed Matrix Membranes. US Patent 4,740,219, **1988**.

(19) Jia, M. D.; Peinemann, K. V.; Behling, R. D. *J. Membrane Sci.* **1991**, *57*, 289.

(20) Duval, J. M.; Folkers, B.; Mulder, M. H. V.; Desgrandchamps, G.; Smolders, C. A. *J. Membrane Sci.* **1993**, *80*, 189.

(21) Gur, T. M. *J. Membrane Sci.* **1994**, *93*, 283.

(22) Suer, M. G.; Bac, N.; Yilmaz, L. *J. Membrane Sci.* **1994**, *91*, 77.

(23) Balkus, K. J.; Cattanach, K.; Musselman, I. H.; Ferraris, J. P. *Mater. Res. Soc. Symp. Proc.* **2003**, *752*, 91.

(24) Park, I.; Wang, Z.; Pinnavaia, T. J. *Chem. Mater.* **2005**, *17*, 383.

(25) Triantafillidis, C. S.; LeBaron, P. C.; Pinnavaia, T. J. *Chem. Mater.* **2002**, *14*, 4088.

(26) Shan, L.; Verghese, K. N. E.; Robertson, C. G.; Reifsnider, K. L. *J. Polym. Sci. Pol. Phys.* **1999**, *37*, 2815.

(27) Liang, W. J.; Kao, H. M.; Kuo, P. L. *Macromol. Chem. Physic.* **2004**, *205*, 600.

(28) Lee, J.; Yoon, S.; Oh, S. M.; Shin, C. H.; Hyeon, T. *Adv. Mater.* **2000**, *12*, 359.

(29) Lee, J.; Han, S.; Hyeon, T. *J. Mater. Chem.* **2004**, *14*, 478.

(30) Lan, T.; Pinnavaia, T. J. *Chem. Mater.* **1994**, *6*, 2216.

(31) Shi, H. Z.; Lan, T.; Pinnavaia, T. J. *Chem. Mater.* **1996**, *8*, 1584.

(32) Wang, Z.; Pinnavaia, T. J. *Chem. Mater.* **1998**, *10*, 1820.

(33) LeBaron, P. C.; Pinnavaia, T. J. *Chem. Mater.* **2001**, *13*, 3760.

(34) Ahmad, Z.; Sarwar, M. I.; Wang, S.; Mark, J. E. *Polymer* **1997**, *38*, 4523.

(35) Lan, T.; Kaviratna, P. D.; Pinnavaia, T. J. *Chem. Mater.* **1995**, *7*, 2144.

(36) Only 4 mol% of NH_2 groups of the D2000 molecules are protonated in the aqueous solution before the silica source is added. It is caculated using pK_b (~4) and the initial concentration (0.06 M) of the amine.

(37) Wind, J. D.; Staudt-Bickel, C.; Paul, D. R.; Koros, W. J. *Macromolecules* **2003**, *36*, 1882.

(38) Chung, T. S.; Chng, M. L.; Pramoda, K. P.; Xiao, Y. C. *Langmuir* **2004**, *20*, 2966.

(39) Robinson, J. P.; Tarleton, E. S.; Ebert, K.; Millington, C. R.; Nijmeijer, A. *Ind Eng Chem Res* **2005**, *44*, 3238.

(40) Zimmerman, C. M.; Singh, A.; Koros, W. J. *J. Membrane Sci.* **1997**, *137*, 145.

(41) Merkel, T. C.; Freeman, B. D.; Spontak, R. J.; He, Z.; Pinnau, I.; Meakin, P.; Hill, A. J. *Chem. Mater.* **2003**, *15*, 109.

CHAPTER 4

SILICA FOAM REINFORCED THERMOSET EPOXY MESOCOMPOSITES

4.1 Introduction

Thermoset epoxy polymers are used in a variety of applications, including coatings, adhesives and electronics due to their high chemical resistance, good adhesion, attractive optical properties and flexibility.[1, 2] Layered silicate clays have been widely investigated as reinforcing agents to improve mechanical,[3, 4] thermal,[5-7] optical,[7, 8] and barrier[9] properties for thermoset epoxy polymers. Complete dispersion (exfoliated) of individual clay nanolayers in the polymer matrix generally provides greater phase homogeneity, resulting in a better enhancement of properties in comparison to composites formed from intercalated clay nanoparticles.[8, 10]

To achieve complete exfoliation of clays[11] organically modified clays normally are used to import a hydrophobic environment to the clay layer surfaces that are normally hydrophilic in nature. However, only intercalated nanocomposites are obtained in many cases, despite the organic modification of clay surfaces.[2] Occasionally, delamination of clay layers is achieved under severe processing conditions (high temperature[12] or high pressure[13]) through the use of auxiliary solvents[14] or by processing under supercritical carbon dioxide[15]. The absence of X-ray reflections in the low 2θ range (> 10 nm layer separation) are often interpreted as an evidence for exfoliated clay morphology.[16] However, disordered clay layers or aggregates of aligned clay tactoids separated on a micron-scale by polymer voids are often observed in TEM images, even though no XRD reflections are detected in the low 2θ range of the XRD pattern of the composite.[16]

Mesostructured silica materials with one- or multiple-dimensional pore structures (e.g. MCM-41, SBA-15) have recently been used for the preparation of polymer-based nanocomposites exhibiting improved performances in diode[17], Li^+-battery[18], luminescence[19], and conductivity[20] applications. Relatively small monomers[17, 18] or polymerizable structure-directing agents[19-21] have typically been used to prepare (semi)conducting polymers for these applications. However, only a few attempts have been made for improving the mechanical properties of engineering polymers.[22-25] For instance, nylon 66 composites[22] prepared under high pressure (0.5 – 30 MPa) exhibited only two-fold increase in storage modulus at a 35 wt% loading of FSM (MCM-41) silica. Silylated MCM-41[23] and MCM-48[24] organosilicas were used as reinforcing agents for poly((3-trimethoxysilyl) propylmethacrylate and poly(vinyl acetate), respectively. In both cases tensile modulus and strength increased but elongation-at-break was sacrificed, so that no or a little improvement in toughness was observed. Recently polypropylene-filled MCM-41 composites prepared with aid of supercritical CO_2 have been reported.[25] However, no clear evidence for polymer filling in the mesostructure pore and only a few percents of reinforcement were observed in tensile properties.

The filling of small mesopore silica by polymer chains sequences forcing conditions such as high pressure[22], silyation of the pore walls[23, 24], or supercritical CO_2 as a solvent[25]. For instance, hexagonal MCM-41 mesostructured silica (pore size ~3 nm) with no organic modifier afforded brittle polyimide composites at high silica loading (>10 wt%),[26, 27] indicating poor interaction between the polymer chain and the internal surface area of the silica pores. Large-pore mesostructures are more likely to undergo pore filling by polymer chains without using organic modifiers or complicated processing conditions. Moreover, large-pore mesoporous silicas with high framework pore volume should provide polymer nanocomposites with improved homogeneity due to the low intrinsic density of the silica particles.

Recently, we reported epoxy mesocomposites reinforced by MSU-J silica with a wormhole framework structure. Mechanical properties of the composites were comparable to exfoliated clay-epoxy nanocomposites.[28] The as-made and calcined MSU-J silica particles (5.3 nm pore size) dispersed readily in the thermoset epoxy polymer. The mechanical properties of the resulting mesocomposites were reinforced at levels corresponding to 4.8-, 5.7-, 1.6-, and 8.5-fold increases in tensile modulus, strength, elongation and toughness, respectively, compared to pristine epoxy polymer. These improvements in tensile properties were realized despite the relatively isotropic particle morphology of the silica particles. The pore size of MSU-J silica is comparable to the d_{001} spacings found for intercalated clays in many polymer-clay nanocomposite systems.

Mesocellular silica foams (MCFs) have been synthesized from TEOS in the presence of a triblock copolymer surfactant (Pluronic P123) and 1,3,5-trimethylbenzene (TMB) as a cosurfactant in aqueous acid.[29] Nitrogen sorption, XRD, and TEM analyses confirmed that the MCF products possess cellular pores connected by windows. Subsequent studies[30] showed that increasing the content of TMB leads to microemulsion droplets that form spherical pore structures. Mesocellular foam structures exhibit very large cell sizes of 25–35 nm, window sizes of 7–18 nm and high pore volumes up to 2.4 cm^3/g. Another family of mesocellular silica foam structures, denoted MSU-F, have been prepared from cost-effective sodium silicate though electrically neutral assembly pathways.[31] This synthetic approach to MSU-F silica foams generates open cell foam structures with a relatively low cell to window size ratio (~1.5) after hydrothermal treatment at 100 °C for >8 h unlike closed cell structures of MCFs formed at similar post-synthetic conditions.[32]

In the present study a calcined mesocelluar silica foam (MSU-F) is used as a reinforcing agent for a thermoset rubbery epoxy polymer. The MSU-F silica foam exhibits very large pore size (cell size; 27 nm and window size; 15 nm) comparable to clay layer separation of >10 nm in exfoliated clay-polymer nanocomposites. The relatively high pore volume of the silica (2.2 cm^3/g) also provides a low intrinsic density of silica particles, promoting the formation of homogeneous nanocomposites. The tensile modulus, strength, elongation, and toughness of the resulting rubbery epoxy-MSU-F mesocomposites systematically are enhanced up to 3.7, 6.8, 2.2, and 20.6 times at relatively low silica loading (9 wt%) compared to silica-free epoxy polymer. Although the modulus enhancement is lower than the enhancement provided by epoxy-MSU-J mesocomposites, the fractural properties of the MSU-F counterparts are more improved due to a more uniform distribution of silica in the matrix. Moreover, no or little loss of optical transparency and thermal stability was observed for the epoxy-MSU-F mesocomposites.

4.2 Experimental

Epoxy resin EPON 828, a diglycidyl ether of bisphenol (Resolution Performance Products), was used for the preparation of epoxy–MSU-F silica mesocomposites. The *α,ω*-diamine–terminated polypropylene oxide $H_2NCH(CH_3)CH_2[OCH_2CH(CH_3)]_xNH_2$ (x = ~33.1) with an average molecular weight of ~2000 was obtained from Huntsman Chemical Co. under the trade name Jeffamine D2000. For the synthesis of MSU-F silica foam, a triblock copolymer (Pluronic P123, $EO_{20}PO_{70}EO_{20}$, BASF) was used as a surfactant. Sodium silicate (27% SiO_2, 14% NaOH solution) and 1,3,5-trimethylbenzene (TMB) were purchased from Aldrich and used as a silica precursor and a pore expander, respectively, for the preparation of MSU-F mesostructured silica foam.

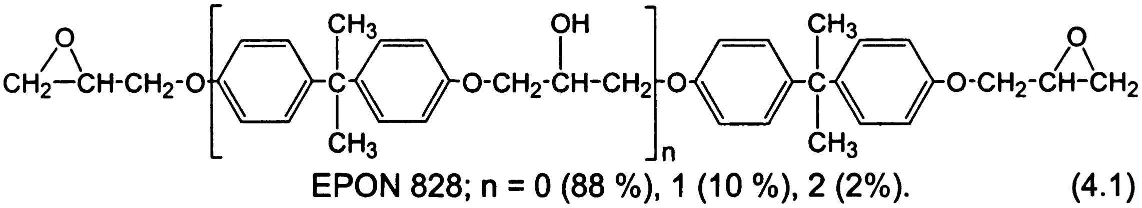

EPON 828; n = 0 (88 %), 1 (10 %), 2 (2%). (4.1)

A large pore mesostructured silica foam, denoted MSU-F, was assembled from sodium silicate and P123 as the structure-directing porogen according to previously described methods.[32] The P123 porogen was mixed with an amount of aqueous acetic acid solution equivalent to the NaOH content of the silicate source and stirred for 2 h. TMB was added to the porogen solution and the mixture was stirred for an additional hour. The silica source was then added to the porogen solution containing the pore expander (TMB) under vigorous stirring at ambient temperature and the mixture was allowed to age at 25°C for 24 h. The reaction mixture was then heated at 100°C for 24 h under static reaction conditions. The porogen-intercalated as-made mesostructured product was recovered by filtration and dried in air at ambient temperature. The molar composition for the formation of as-made MSU-F was 1.0 SiO_2 : 0.78 NaOH : 0.017 P123 : 0.83 CH_3COOH : 0.69 TMB : 230 H_2O. A porogen–free analog of the mesostructure, denoted calcined MSU-F, was obtained by calcination of as-made MSU-F at 600°C for 4 h. The calcined form of the mesostructure was ground to a powder for future use.

For the preparation of the rubbery epoxy polymer nanocomposites, a pre-determined amount of calcined MSU-F silica foam was added to the epoxy resin (EPON 828) and mixed at 50°C for 10 min. A stoichiometric amount of Jeffamine D2000 curing agent was then added to the mixture and mixed at 50°C for another 10 min. The resulting suspensions were out-gassed under vacuum and transferred to an aluminum mold. Pre-curing of the mesocomposite was carried out under nitrogen gas flow at 75°C for 3 h, followed by an additional 3 h cure at 125°C to complete the crosslinking.

N_2 adsorption-desorption isotherms were obtained at 77 K on an ASAP 2010 volumetric adsorption analyzer. Calcined MSU-F silicas were outgassed at 150°C overnight. Pore size distributions were determined by applying the BdB-FHH2 model[33] to the adsorption and desorption isotherms.

Transmission electron microscopy (TEM) images were taken on a JEOL JEM-100CX II microscope with a CeB_6 filament and an accelerating voltage of 120 kV. Sample grids of calcined mesoporous silicas were prepared via sonication of a powdered sample in ethanol for 10 min and evaporating 2 drops of the suspension onto a holey carbon film supported on a 3 mm, 300 mesh copper grid.

Tensile measurements on individually molded samples were performed at ambient temperature according to ASTM standard D3039 using an SFM-20 United Testing System. The dog-bone shaped specimens used in the tensile testing were 28 mm long in the narrow region, 3 mm thick, and 3 mm wide along the center of the casting. At least six stress-strain data points with good precision were obtained and the results averaged. The errors in tensile data are based on the 95 % confidence interval for the mean values.

Thermogravimetric analyses (TGA) were performed using a computer controlled Shimadzu TGA-50 thermal analyzer. Typically, a 50 mg sample was placed in a quartz bucket and heated an ambient temperature to 800°C at a rate of 5 °C/min in a nitrogen flow of 50 mL/min.

Refractive indices of calcined MSU-F silica foam and pristine rubbery epoxy sample were determined using liquid testing methods. Carbon tetrachloride (n = 1.46, Aldrich, 99.8%), benzene (n = 1.50, Baker, 99.9%) and benzyl alcohol (n = 1.54, Fisher Scientific Co.) were used as references. A 0.2 g quantity of calcined MSU-F silica was added to 20 g of solvent. A pristine rubbery epoxy sample (dog-bone sample used for tensile tests) was scratched with sand paper to generate an opaque surface and then immersed in each solvent to judge refractive index matching.

4.3 Results

Figure 4.1 presents the nitrogen adsorption-desorption isotherm and the pore-size distribution for calcined MSU-F silica foam assembled at ambient temperature for 24 h and then subjected to hydrothermal treatment at 100 °C for additional 24 h. The isotherm curve and the relatively narrow hysteresis loop in good agreement is consistent with a typical open cell foam structure.[32] The pore volume and BET surface area are 2.2 cm^3/g, and 540 m^2/g, respectively, and the cell size (26.5 nm) and window size (14.9 nm) were judged using the BdB-FHH2 model.[33] TEM images in Figure 4.2 verify the spherical pore structure and the cell size matching the nitrogen sorption isotherm.

Tensile data were obtained from dog-bone-shaped specimens containing 1.0–9 wt% calcined MSU-F silicas. A comparison of stress-strain curves (more accurately load-displacement curves because the load is not normalized with respect to cross sectional area of the specimens) as a function of silica loadings for the rubbery epoxy mesocomposites is provided in Figure 4.3. The mesostructure provides composites with improved mechanical performance. The modulus, strength, elongation and toughness of the epoxy composites prepared

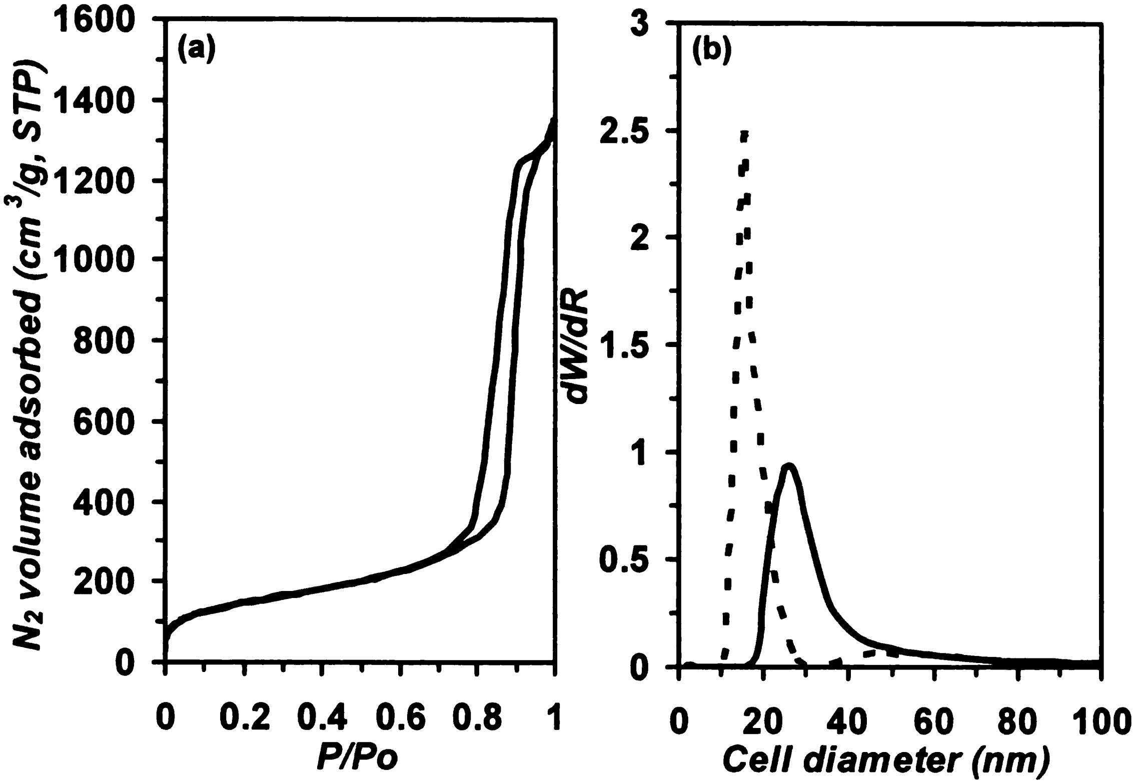

Figure 4.1 (a) Nitrogen adsorption-desorption isotherm for calcined MSU-F silica foam prepared from postsynthesis hydrothermal treatment of the as-synthesized MSU-F for 24 h at 100 °C. (b) Corresponding cell size (solid line) and window size (dash line) distributions obtained from adsorption and desorption branches, respectively. The distributions were determined by applying the BdB-FHH2 model.[33]

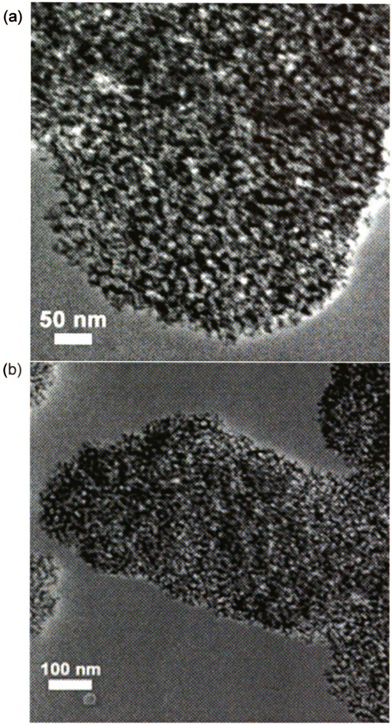

Figure 4.2 Transmission electron microscope (TEM) images of a calcined MSU-F silica foam synthesized through postsynthesis treatment at 100 °C for 24 h. Images (a) and (b) are taken with high and low magnifications, respectively.

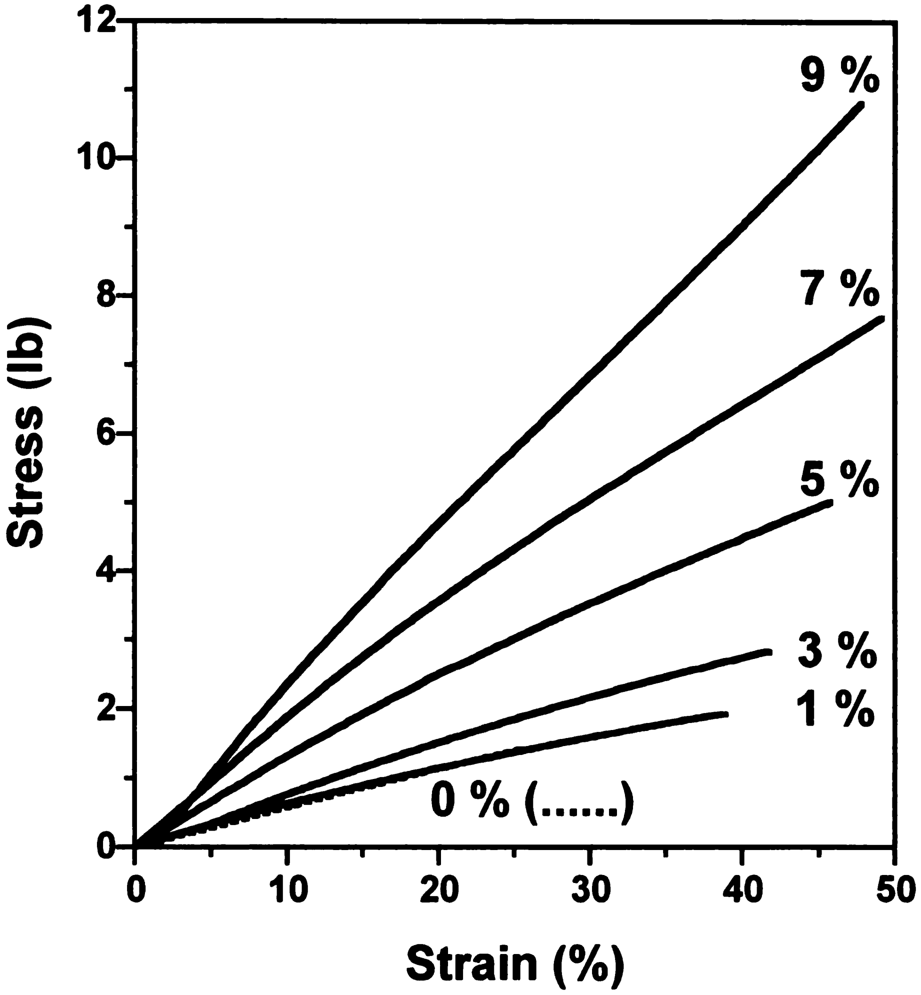

Figure 4.3 Comparison of stress-strain curves for pristine epoxy (......) and MSU-F-epoxy mesocomposites containing different silica loadings.

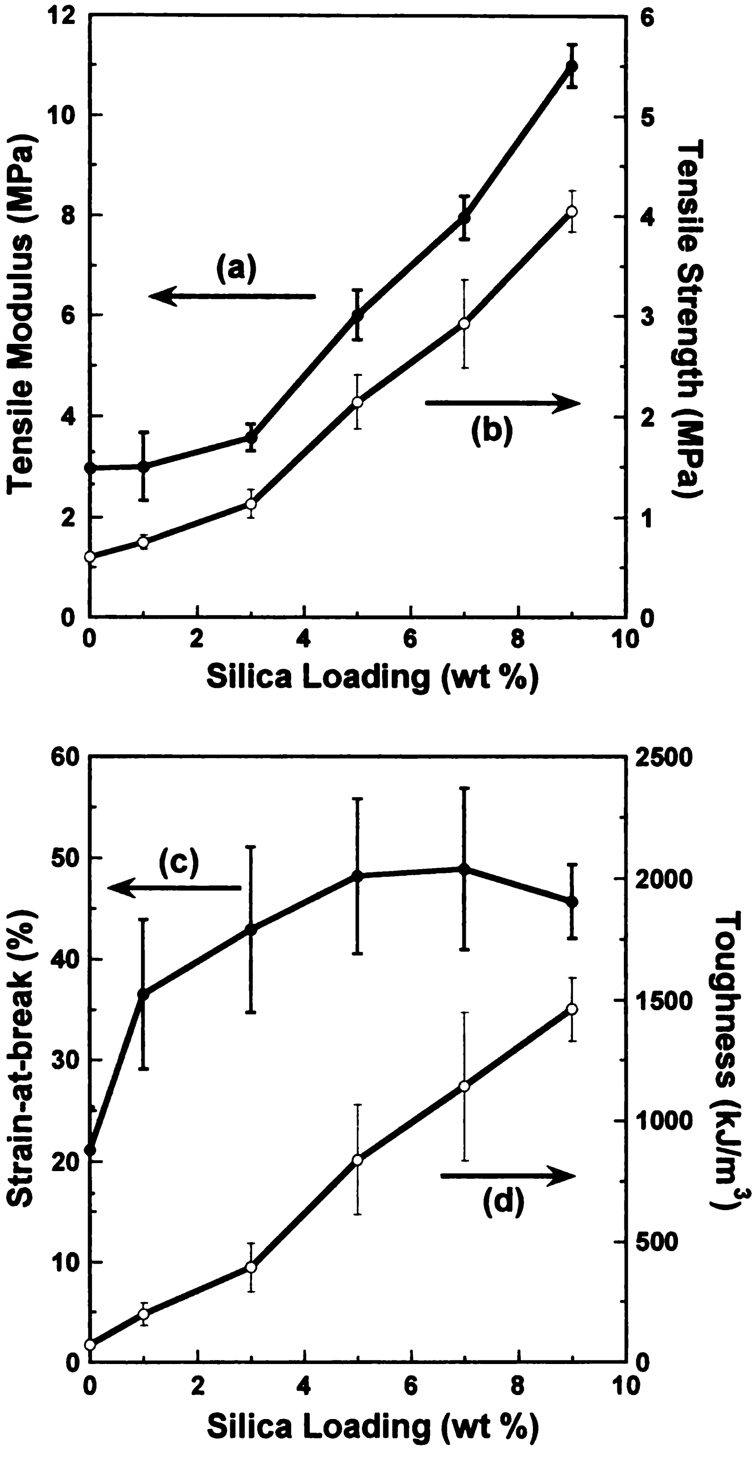

Figure 4.4 Loading dependence of the (a) tensile moduli, (b) tensile strengths, (c) strain-at-break and (d) toughness for rubbery epoxy mesocomposites prepared from calcined MSU-F silica.

from the calcined MSU-F silica generally increase with increasing silica loadings (Figure 4.4). The values are summarized in Table 4.1 at different silica loadings. All the tensile properties of epoxy-MSU-F mesocomposites generally increase with increase in silica loadings. Although the elongation shows little dependence on high silica loadings, the toughness is increased in proportion to the silica loading, because toughness is a combined property of strength and elongation.

In addition to the remarkable improvement in the mechanical properties another significant benefits derived from MSU-F silica foam is the retention of optical transparency and thermal stability compared to pristine epoxy polymer. Optical photographs of pristine epoxy polymer and epoxy-MSU-F mesocomposite samples containing 5 and 9 wt% silica are shown in Figure 4.5 demonstrating the refraction index of the MSU-F silica nearly matches that of the epoxy matrix. Liquid emersion testing methods were carried out to determine refractive indices for the pristine epoxy polymer and calcined MSU-F silica foam. The white color of the silica disappears in CCl_4 solvent (n = 1.46) indicating the refractive index of the silica foam is nearly 1.45 as predictable.[34] Figure 4.6 shows that MSU-F silica foam does not promote nor hinder thermal degradation of the epoxy polymer. The temperatures at the maximum degradation rate, as determined by the first derivatives of the corresponding TGA curves, are 362 °C for both samples.

Table 4.1 Tensile and thermal properties of pristine epoxy polymer and epoxy–MSU-F mesocomposites.

Sample	Silica loading (wt%)	Tensile modulus (MPa)	Tensile strength (MPa)	Elongation (%)	Toughness (kJ/m^3)	Thermal stability (°C)[a]
Pristine Rubbery	0	2.96	0.60	21.1	71	362
Epoxy–MSU-F Mesocomposites	1	2.99	0.75	36.5	199	
	3	3.57	1.13	42.9	394	
	5	6.01	2.14	48.2	839	
	7	7.96	2.92	48.9	1140	
	9	11.0	4.05	45.7	1460	362

[a] The temperatures at maximum degradation rate were determined from the first derivative of the corresponding TG curves.

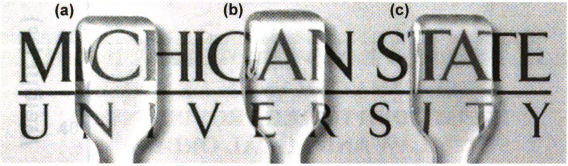

Figure 4.5 Optical images illustrating differences in the transparency of (a) pristine rubbery epoxy polymer and epoxy composites prepared from calcined MSU-F silica at (b) 5 and(c) 10 wt%.

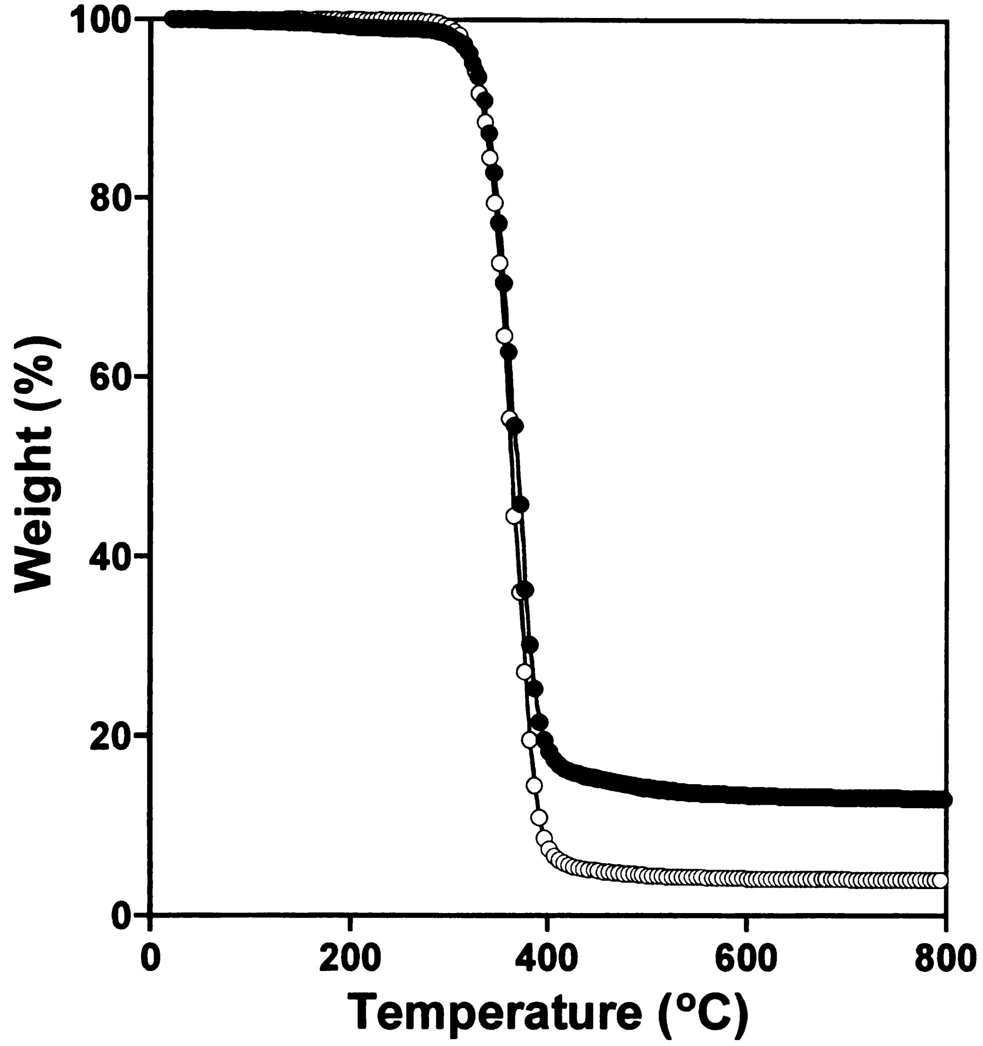

Figure 4.6 Thermogravimetric analysis curves in nitrogen for the silica-free epoxy polymer (open circles) and the epoxy mesocomposites (solid circles) prepared from calcined MSU-F silica at a loading of 9 wt%.

4.4 Discussion

A mesocellular silica foam (MSU-F) assembled under a near neutral pH conditions is a good candidate as a polymer reinforcing agent due to its very large pore size and pore volume. The large pore >10 nm of calcined MSU-F silica is comparable to the average separation of exfoliated clay nanolayers in polymer-clay nanocomposites. The improved mechanical properties for the resulting mesocomposites are realized without need of organic modifiers. Calcined MSU-F silica is readily dispersed in the polymer matrix and no observable particle aggregates are found in the cured mesocomposites at 1–9 wt % silica loadings. Previously reported epoxy–MSU-J mesocomposites exhibit nearly identical XRD patterns between top and bottom of dog-bone specimens demonstrating little or no settling of the mesophase during curing process.[28] Positronium annihilation lifetime spectroscopic (PALS) analysis substantiated the absence of voids in the epoxy-MSU-J mesocomposites representing filled MSU-J silica mesopores with epoxy polymer chains. Although the degree of dispersion of MSU-F silica particles in a polymer matrix is not sensitive to the XRD technique owing to the absence of Bragg reflections, the mesocelluar pores are certainly filled due to large pore size. Retention of the silica foam structure in the epoxy polymer matrix is confirmed by the nearly identical nitrogen sorption[35] properties (not shown) of the recovered MSU-F silica obtained by calcinating 9 wt% epoxy-MSU-F mesocomposite sample. The isotherm of the recovered silica was nearly identical to pristine MSU-F silica (c.f. Figure 4.1).

Good particle dispersion and the filling of the mesostructured pores with polymer are required to maximize the interfacial interactions between the polymer chain and the silica surface for reinforcing resulting mesocomposites. Previously reported attempts to form nanocomposites using MCM-41 type silicas with one-dimensional pore structure sacrificed elasticity and toughness. In this respect, the composites behaved like conventional reinforced composites in exchange for benefits in modulus and strength.[36] Calcined HMS (pore size 2.8 nm) and MCM-48 (pore size 3.2 nm) silicas with three-dimensional pore network have been used as reinforcing agents for thermoset epoxy polymers.[37] However the unmodified silicas presented low level of dispersion in the polymer matrix. Thus the dispersion of silica was not uniform composite materials. It is important to note that large pore mesostructures are highly desired for high quality of reinforced polymer nanocomposites without using organic modifier or auxiliary processing steps to obtain cost- and labor-efficiency.

Significant improvements in mechanical properties have been obtained for the epoxy-MSU-F mesocomposites (c.f. Figure 4.4 and c.f. Table 4.1) compared to silica-free rubbery epoxy polymer. The 3.7-fold increase in tensile modulus for the mesocomposites at 9 wt% is comparable to that of MSU-J (~4-fold increase) counterpart at the same loading. The higher surface area of MSU-J mesoporous silica (~950 m^2/g) facilitates interfacial interaction between the polymer and the silica surface providing slightly higher modulus at the beginning stage in stress-strain behavior. However, the fracture properties, tensile strength and elongation, of the epoxy-MSU-F mesocomposites are superior to MSU-J composites. Moreover the 6.8-fold increase in tensile strength of MSU-F composites is even higher relative to exfoliated organo-montmorillonite nanocomposites (5.3-fold increase)[38] at same silica loading (9 wt%). The highly improved tensile strength is presumably provided by high homogeneity resulting from a high pore volume (2.2 cm^3/g) of the mesocelluar structure. MSU-F silica with lower intrinsic density compared to MSU-J particles, occupy a larger volume of the mesocomposites leading to reduced distances between silica particles. It is also noteworthy that the epoxy-MSU-F mesocomposites exhibit ~50% elongation at 5–9 wt% silica loadings, despite the isotropic particle morphology. In comparison a more limited elongation (~30% at 12 wt% silica loading) was obtained for epoxy-MSU-J mesocomposites. The enhancement in strain-at-break for MSU-F composites is comparable to 40–60 % elongation provided by anisotropic exfoliated nanolayers aligning in the direction of applied stress.[38] Thus, the high pore volume and more uniform dispersion of silica throughout the entire polymer matrix results in improved fractural properties for epoxy-MSU-F mesocomposites.

The modulus of amorphous silica (~10 GPa) is much larger than the modulus of the epoxy matrix (~3 MPa). The simple rule of mixture theory (eq. 4-1) does not fit the observed moduli of the mesocomposites (see dash-dot line in Figure 4.7). In many cases, a super-linear dependence of the Young's modulus E_c is observed as a function of the particulate volume fraction v_p.[39, 40]

$$E_c = E_m(1 - v_p) + E_p v_p \qquad (4\text{-}1)$$

, where E_m and E_p are the moduli for the matrix and the particulate, respectively. According to Elsheby's prediction[40] the bulk modulus of a composite (K_c) and the shear modulus of a composite (G_c) at a volume fraction of particulate are given by:

$$K_c = \frac{K_m}{1 - Av_p}, A = \frac{K_p - K_m}{(K_p - K_m)\alpha + K_m}, \alpha = \frac{1 + \nu_m}{3(1 - \nu_m)} \qquad (4\text{-}2)$$

$$G_c = \frac{G_m}{1 - Bv_p}, B = \frac{G_p - G_m}{(G_p - G_m)\beta + G_m}, \beta = \frac{2}{15}\frac{4 - 5\nu_m}{1 - \nu_m} \qquad (4\text{-}3)$$

, where K_m and K_p are the bulk modulus values for the matrix and the particulate, respectively, and G_m and G_p are the shear modulus values of the matrix and the particulate and v_m is the Poisson ratio for the matrix. The bulk modulus is the inverse of compressibility. Young's modulus (E) for an isotropic, linearly elastic composite containing spherical particulates is related to K, G, v through the equations below, but we need Poisson ratios of the rubbery epoxy polymer and amorphous silica to compute K_m, K_p, G_m and G_p.

$$E = \frac{9KG}{(3K + G)}, G = \frac{E}{2(1 + \nu)}, K = \frac{E}{3(1 - 2\nu)}, \nu = \frac{3K - 2G}{2(3K + G)} \qquad (4\text{-}3)^{41}$$

We know the approximate Poisson ratio for amorphous silica (~0.2)[42] and a rubber has a value near 0.5,[41] the maximum value of Poisson's ratio. As seen in equations (4-2) and (4-3), K and G are independent of the Poisson ratio for the particulate.

If the Poisson's ratio of the polymer is taken to be 0.5, K_m approaches infinity and G_m will be ~$E_m/3$ (namely, E_m ~$3G_m$). Accordingly, the difference in predicted Young's modulus (E_c) for the polymer at v_m=0.5 (actually 0.49999) and at 0.45 is 20 % (10 MPa vs. 8 MPa), where the Young's modulus for the mesoporous silica is ~10 GPa.[43, 44] In Figure 4.7, the experimental Young's

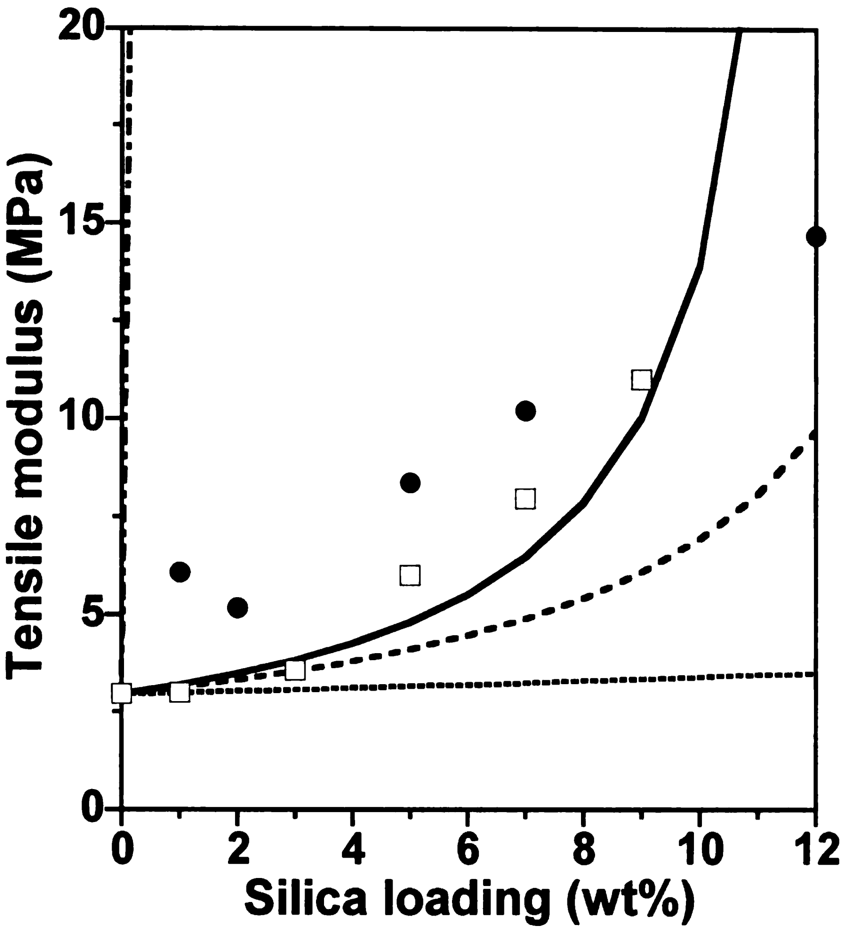

Figure 4.7 Experimental (symbols) and computed (lines) values of Young's modulus as a function of silica loadings. Solid circles: composites made from calcined MSU-J and open squares: composites made from calcined MSU-F. Dot line: Computed dependence taking only the silica wall volume as the particulate volume fraction; dash line: assuming the particulate volume to be the silica wall volume plus the pore volume of MSU-J; solid line: assuming the particulate volume to be the silica wall volume plus the pore volume of MSU-F. The prediction (dot-dash line) based on a simple rule of mixture is also plotted.

moduli for composites prepared from as-made MSU-J, calcined MSU-J and calcined MSU-F are indicated with symbols. The dependence computed from equations (4-2 – 4-4) assuming only the wall volume of the silica alone as the particulate volume (dot line) provides a poor prediction of the experimental data. A better correspondence to the data is obtained based on the filling factor of the particulate to be the combined volume of the silica walls and the pore volume of the mesostructure. Thus, it is clear that the entire volume of the mesostructured silica particle (walls plus pores) contribute to the reinforcement. Moreover, the Eshelby model predicts the silica with the lower structural density to provide more reinforcement (see the predicted curves for MSU-F and MSU-J with foam and wormhole structure, respectively). However, the denser MSU-J wormhole structure is observed to provide more reinforcement than the foam structure. Also, the experimental moduli are larger than the predicted values based on the Eshelby model. This latter model assumes the reinforcing particles to be solid rigid spheres. The mesostructured silicas used as reinforcement agents in the present study provide a substantially larger surface area than expected on the basis of solid spherical particles. Accordingly, the additional interfacial interactions between the particulate and the polymer matrix should lead to greater stiffness, in agreement with the higher moduli found for composites made from MSU-J (950 m^2/g) in comparison to MSU-F (540 m^2/g). Moreover, the Eshelby prediction values are higher than other advanced models (see examples in Reference 40) indicating that the interfacial interactions must be taken into account in these mesocomposites. However a molecular dynamic simulation study for the dependence of Young's modulus on particle size may be required as smaller particulates generally provide an increased composite modulus compared to larger particlulates.[40]

Liquid test results show the approximate refractive index of the rubbery epoxy polymer is ~1.50, nearly matching that of benzene. Both calcined MSU-J and MSU-F mesostructures possess identical refractive index (n ~ 1.45), as confirmed by the disappearance of silica in CCl_4 solvent. This result indicates that the transparency of the silica particles is dependent not on the porosity but on refractive index of the silica wall. A glassy epoxy polymer[45] prepared form EPON 826 and Jeffamine 230 exhibits ~1.55 refractive index so that glassy epoxy nanocomposites containing calined MSU-F silica lose their transparency at >5 wt% silica loading due to a mismatch of refractive indices between the polymer and the silica.[37] However, the epoxy-MSU-F mesocomposites show more transparency compared to the epoxy-MSU-J mesocomposites at the same silica loadings. Consequently, the large separation of the silica walls allows complete pore filling by polymer and this leads to improved transparency for the epoxy-MSU-F mesocomposites in comparison to MSU-J and montmorillonite composites. The transparent composite samples obtained from exfoliated clay nanolayers as approved to transparent clay analogues[8], can be explained on the basis of similar consideration. Moreover, the high transparency at 9 wt% silica loading also substantiates the complete dispersion of MSU-F silica particles in the entire epoxy matrix.

4.5 Summary

Mechanically improved thermoset epoxy mesocomposites have been prepared from calcined silica foam, MSU-F which exhibits surface area of 540 m^2/g, cell size of 26.5 nm (14.9 nm window size) and pore volume of 2.2 cm^3/g. Despite the absence of a surface organic modifier, the calcined MSU-F silica foam is well dispersed in the epoxy matrix due to its very large pore diameter and low intrinsic density. The cellular foam structure is retained in the polymer matrix as judged by nitrogen sorption isotherm analysis of the residue silica obtained by calcining the 9 wt% mesocomposite.

The tensile modulus, the tensile strength, the strain-at-break, and the toughness for the resulting rubbery epoxy mesocomposites are systematically enhanced up to 3.7, 6.8, 2.2, and 20.6 times, respectively, at relatively low silica loading (9 wt%) relative to the silica-free rubbery epoxy polymer. The remarkable mechanical enhancements are contributed by the large window and cell sizes of the MSU-F silica foam which are comparable to the layer separation (>10 nm) of the exfoliated clay layers in the polymer-epoxy nanocomposites. Moreover, the mechanical improvements for the epoxy mesocomposites obtained from the calcined MSU-F silica verify that mesostructured silica having a very large pore size and a large pore volume is a good reinforcing agent for thermoset epoxy polymers.

Although the modulus enhancement obtained with MSU-F foam particles is less than the modulus increase observed for MSU-J wormhole particles, the fractural properties of the MSU-F mesocomposites are substantially improved due to homogeneous dispersion. The fracture properties, tensile strength and elongation, of the epoxy-MSU-F mesocomposites are superior to MSU-J composites. Moreover the 6.8-fold increase in tensile strength of MSU-F composites is even higher than the tensile strength benefit obtained for to exfoliated organo-montmorillonite nanocomposites (5.3-fold increase) at same silica loading (9 wt%). The highly improved tensile strength is presumably provided by the high homogeneity resulting from high pore volume of the mesocelluar structure and the good dispersion of the foam particles. MSU-F silica particles occupy a larger volume of the mesocomposites due to the lower intrinsic density of the foam structure in comparison to the MSU-J wormhole structure. The lower density of the foam structure leads to reduced distances between silica particles and to better overall reinforcement of the polymer matrix. It is also noteworthy that the epoxy-MSU-F mesocomposites exhibit ~50% elongation at 5–9 wt% silica loadings despite the isotropic particle morphology whereas limited elongation (~30% at 12 wt% silica loading) was obtained for the epoxy-MSU-J mesocomposites.

The 3.7-fold increase in tensile modulus for the MSU-F mesocomposites at 9 wt% loading is comparable to that of the MSU-J (~4-fold increase) counterpart at the same loading. The relatively higher surface area of MSU-J mesoporous silica (~950 m^2/g) facilitates interfacial interaction between polymer chains and the silica surface, providing a slightly higher modulus at the beginning stage in stress-strain behavior. Theoretical modulus predictions established for particulate-filled polymer composites were performed in order to investigate the effects of the interfacial interactions and the pore volumes on the modulus behavior. The experimental modulus values for both mesocomposites prepared from each calcined MSU-J and MSU-F mesostructure are higher than the theoretical values derived from a consideration of the volume fractions occupied by silica walls only, as well as by the volume fraction occupied by the entire mesostructured particle (silica walls + polymer-filled pores). The results demonstrate that mesostructured silica particles function as reinforcement agents by providing volume fractions beyond the volume fractions provided by non-porous silica particulates at the same weight loading. Moreover, the large surface area of the mesostructured particles increases the interfacial interactions between the particulate and the polymer matrix and this leads to greater stiffness. The importance of surface area in providing stiffness is verified by the higher moduli found for composites made from MSU-J (950 m^2/g) in comparison to MSU-F (540 m^2/g).

4.6 References

(1) Lange, J.; Nicolas, B.; Galy, J.; Gerard, J. F. *Polymer* **2002**, *43*, 5985.

(2) Becker, O.; Simon, G. P. *Adv. Polym. Sci.* **2005**, *179*, 29.

(3) Lan, T.; Kaviratna, P. D.; Pinnavaia, T. J. *Chem. Mater.* **1995**, *7*, 2144.

(4) Messersmith, P. B.; Giannelis, E. P. *Chem. Mater.* **1994**, *6*, 1719.

(5) Kelly, P.; Akelah, A.; Qutubuddin, S.; Moet, A. *J. Mater. Sci.* **1994**, *29*, 2274.

(6) Lee, D. C.; Jang, L. W. *J. Appl. Polym. Sci.* **1998**, *68*, 1997.

(7) Wang, Z.; Pinnavaia, T. J. *Chem. Mater.* **1998**, *10*, 1820.

(8) Brown, J. M.; Curliss, D.; Vaia, R. A. *Chem. Mater.* **2000**, *12*, 3376.

(9) Osman, M. A.; Mittal, V.; Morbidelli, M.; Suter, U. W. *Macromolecules* **2004**, *37*, 7250.

(10) Wang, Z.; Massam, J.; Pinnavaia, T. J. In *Polymer-Clay Nanocomposites*, Edited by Pinnavaia, T. J. Beall, G. W., Wiley, New York, **2001**.

(11) LeBaron, P. C.; Wang, Z.; Pinnavaia, T. J. *Appl. Clay Sci.* **1999**, *15*, 11.

(12) Liang, Z. M.; Yin, H.; Xu, H. H. *Polymer* **2003**, *44*, 1391.

(13) Vargas, E. S.; Lynch, M. W.; Ruda, M. J.; Chandrashekar, V. *US Patent 6602966*, **2003**.

(14) Kotsilkova, R. *J. Appl. Polym. Sci.* **2005**, *97*, 2499.

(15) Li, C. Y.; Yang, J. *J. Appl. Polym. Sci.* **2005**, *98*, 22.

(16) Vaia, R. A. In *Polymer-Clay Nanocomposites*, Edited by Pinnavaia, T. J. Beall, G. W., Wiley, New York, **2001**.

(17) Park, J. H.; Kim, S.; Kim, Y. C.; Park, O. O. *Nanotechnology* **2005**, *16*, 1793.
(18) Xi, J. Y.; Tang, X. Z. *Electrochim Acta* **2005**, *50*, 5293.

(19) Nguyen, T. Q.; Wu, J. J.; Doan, V.; Schwartz, B. J.; Tolbert, S. H. *Science* **2000**, *288*, 652.

(20) Li, G. T.; Bhosale, S.; Wang, T. Y.; Zhang, Y.; Zhu, H. S.; Fuhrhop, K. H. *Angew. Chem. Int. Ed.* **2003**, *42*, 3818.

(21) Lu, Y. F.; Yang, Y.; Sellinger, A.; Lu, M. C.; Huang, J. M.; Fan, H. Y.; Haddad, R.; Lopez, G.; Burns, A. R.; Sasaki, D. Y.; Shelnutt, J.; Brinker, C. J. *Nature* **2001**, *411*, 617.

(22) Kojima, Y.; Matsuoka, T.; Takahashi, H. *J. Appl. Polym. Sci.* **1999**, *74*, 3254.

(23) Ji, X. L.; Hampsey, J. E.; Hu, Q. Y.; He, J. B.; Yang, Z. Z.; Lu, Y. F. *Chem. Mater.* **2003**, *15*, 3656.

(24) He, J.; Shen, Y. B.; Yang, J.; Evans, D. G.; Duan, X. *Chem. Mater.* **2003**, *15*, 3894.

(25) Wang, N.; Li, M. T.; Zhang, J. S. *Mater. Lett.* **2005**, *59*, 2685.

(26) Reid, B. D.; Ruiz-Trevino, A.; Musselman, I. H.; Balkus, K. J.; Ferraris, J. P. *Chem. Mater.* **2001**, *13*, 2366.

(27) Balkus, K. J.; Cattanach, K.; Musselman, I. H.; Ferraris, J. P. *Mater. Res. Soc. Symp. Proc.* **2003**, *752*, 91.

(28) Park, I.; Peng, H. G.; Gidley, D. W.; Xue, S.; Pinnavaia, T. J. *Chem. Mater.* **2005**, *ASAP*.

(29) Schmidt-Winkel, P.; Lukens, W. W.; Zhao, D. Y.; Yang, P. D.; Chmelka, B. F.; Stucky, G. D. *J. Am. Chem. Soc.* **1999**, *121*, 254.

(30) Lettow, J. S.; Han, Y. J.; Schmidt-Winkel, P.; Yang, P. D.; Zhao, D. Y.; Stucky, G. D.; Ying, J. Y. *Langmuir* **2000**, *16*, 8291.

(31) Kim, S. S.; Pauly, T. R.; Pinnavaia, T. J. *Chem. Comm.* **2000**, 1661.

(32) Karkamkar, A.; Kim, S. S.; Pinnavaia, T. J. *Chem. Mater.* **2003**, *15*, 11.

(33) Lukens, W. W.; Schmidt-Winkel, P.; Zhao, D. Y.; Feng, J. L.; Stucky, G. D. *Langmuir* **1999**, *15*, 5403.

(34) Blanco, A.; Chomski, E.; Grabtchak, S.; Ibisate, M.; John, S.; Leonard, S. W.; Lopez, C.; Meseguer, F.; Miguez, H.; Mondia, J. P.; Ozin, G. A.; Toader, O.; van Driel, H. M. *Nature* **2000**, *405*, 437.

(35) Pore volume, BET surface area, cell size and window size of the recovered MSU-F silica foam are 2.1 cm^3/g, 509 m^2/g, 26.9 nm, and 15.3 nm, respectively.

(36) Ahmad, Z.; Sarwar, M. I.; Wang, S.; Mark, J. E. *Polymer* **1997**, *38*, 4523.

(37) Park, I.; Pinnavaia, T. J. *Unpublished data*.

(38) Lan, T.; Pinnavaia, T. J. *Chem. Mater.* **1994**, *6*, 2216.

(39) Richard, T. G. *J. Composite Mater.* **1975**, *9*, 108.

(40) Monette, L.; Anderson, M. P.; Wagner, H. D.; Mueller, R. R. *J. Appl. Phys.* **1994**, *75*, 1442.

(41) *Handbook of Polymer Testing*, edited by R. Brown, **1999**, Marcel Dekker, New York.

(42) Williford, R. E.; Addleman, R. S.; Li, X. S.; Zemanian, T. S.; Birnbaum, J. C.; Fryxell, G. E. *J. Non-Cryst. Solids* **2005**, *351*, 2217.

(43) Jung, S. B.; Han, C. K.; Park, H. H. *Appl. Surface Sci.* **2005**, *244*, 47.

(44) Yamada, K.; Oku, Y.; Hata, N.; Seino, Y.; Negoro, C.; Kikkawa, T. *J. Electrochem. Soc.* **2004**, *151*, F248.

(45) Triantafillidis, C. S.; LeBaron, P. C.; Pinnavaia, T. J. *Chem. Mater.* **2002**, *14*, 4088.

CHAPTER 5

MESOPOROUS SILICA STRUCTURES ASSEMBLED FROM JEFFAMINE AND TOMAH3 SURFACTANTS

5.1 MSU-J Wormhole Mesostructures

Electrically neutral supramolecular assembly pathways using primary amine surfactants generally produce mesoporous materials with wormhole framework structures as discussed in Chapter 1. Wormhole mesostructures typically exhibit enhanced catalytic activity due to the three-dimensional pore network[1] and the improved textural porosity[2] relative to hexagonal mesostructures prepared through strong electrostatic interactions.

Large-pore wormhole mesostructures (MSU-J) have been synthesized from Jeffamine D2000 and D4000.[3] The pore size and pore volume of MSU-J silicas are in range of 5.3–14.3 nm and 1.4– 2.3 cm^3/g, respectively, comparable to those of SBA-15 silicas (see Chapter 2 for details). This appendix describes other members of the MSU-J family of mesostructured silicas prepared frin diverse Jeffamine and Surfonamine surfactants (see structures 5.1–5.4).

Three series of Jeffamine (M, D, and T series) surfactants are provided by Huntsman Chemical. The prefix M, D, and T represent the presence of one (mono-), two (di-), and three (tri-) amine groups, respectively, in the chemical structures. The number designation after the prefix corresponds to the approximate molecular weight. Basically, the Jeffamine surfactants are based on a propylene oxide (PO) or mixed PO/EO backbone. The Surfonamines (see

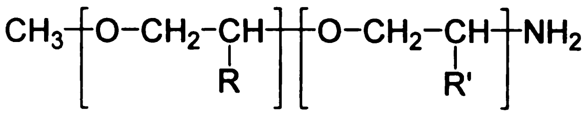

$CH_3-[O-CH_2-CH(R)]-[O-CH_2-CH(R')]-NH_2$

Jeffamine™ M2005:
R, R' = H or CH_3
Molar ratio of PO/EO = 39/6
M_w = ~2000

(5.1)

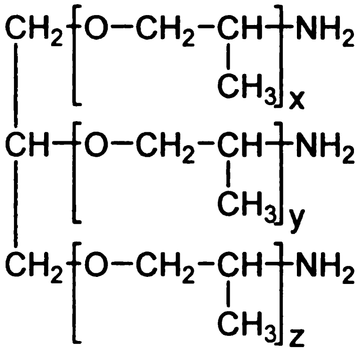

Jeffamine™ T3000:
x + y + z = 50
M_w = ~3000

Jeffamine™ T5000:
x + y + z = 81
M_w = ~5000

(5.2)

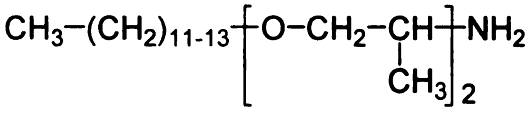

$CH_3-(CH_2)_{11-13}-[O-CH_2-CH(CH_3)]_2-NH_2$

Surfonamine™ ML300:
M_w = ~300

(5.3)

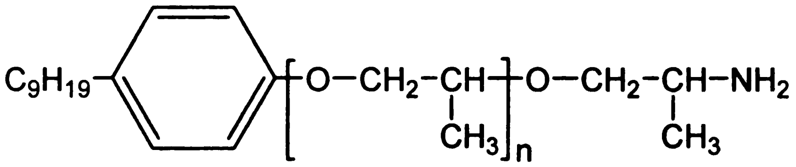

(5.4)

Surfonamine™ MNPA1000:
n = 13.5
M_w = ~1000

structures 5.3 and 5.4) are monofunctional amines similar to the M-series but they possess long-alkyl groups at the end of the hydrophobic tails. A commercially available sodium silicate (Aldrich, 27% SiO_2, 14% NaOH) solution was used as the silica precursor. Sodium silicate compared to another silica source, such as TEOS, is cost-effective and suitable the use of the silica as a reinforcement agent to enhance mechanical property of polymers. The experimental procedures for the preparation of the MSU-J silicas in this appendix are same as those of Chapter 2 except for the Surfactant/Si ratios (see Table

5.1). Numerous survey experiments indicated that the optimum Surfactant/Si ratios provide intense XRD reflections, large surface areas and high yields.

Table 5.1 Physical properties for mesostructured wormhole silicas prepared from sodium silicate and Jeffamine or Surfonamine surfactants.

Surfactant	Surf./Si molar ratio	Temp./time (°C/hour)	d_{001}[†] (nm)	S_{BET} (m^2/g)	Pore size (nm)	Pore volume (cm^3/g)
M2005	0.062	25 / 20	6.5 / 5.9	632	3.5	0.5
		45 / 20	7.9 / 7.0	673	4.8	0.9
		65 / 20	-[‡] / 7.1	885	6.1	1.4
T3000	0.083	25 / 20	6.4 / 5.9	936	5.0	1.3
		45 / 20	6.6 / 6.4	964	6.0	1.5
		65 / 20	6.2 / 7.2	881	6.7	1.8
T5000	0.033	25 / 20	-[‡]	1030	5.2	1.5
		45 / 20	-[‡]	882	8.2	2.0
ML300	0.25	25 / 20	4.6 / 4.2	770	2.8	1.1
MNPA1000	0.12	25 / 20	5.6 / 6.0	1012	5.1	1.4

[†] Basal spacings of as-made and calcined MSU-J silicas are separated by a slash (as-made / calcined).

[‡] The XRD reflections are not resolved.

The XRD patterns of as-made and calcined MSU-J silicas prepared from the sodium silicate and M2005, T3000, T5000, ML300 and MNPA1000 are illustrated in Figures (5.1–5.4). Typical of wormhole mesostructures (e.g. HMS and MSU-X), each sample exhibits a typical XRD pattern consisting of an intense and relatively broad low angle reflection and a weaker, higher angle broad shoulder due to lack of long-range order. Although a few MSU-J silicas do not show well-resolved reflections in their XRD patterns (see Table 5.1), an intense reflection characteristic of a regular pore spacing is in the 2θ range 1–1.5°. The

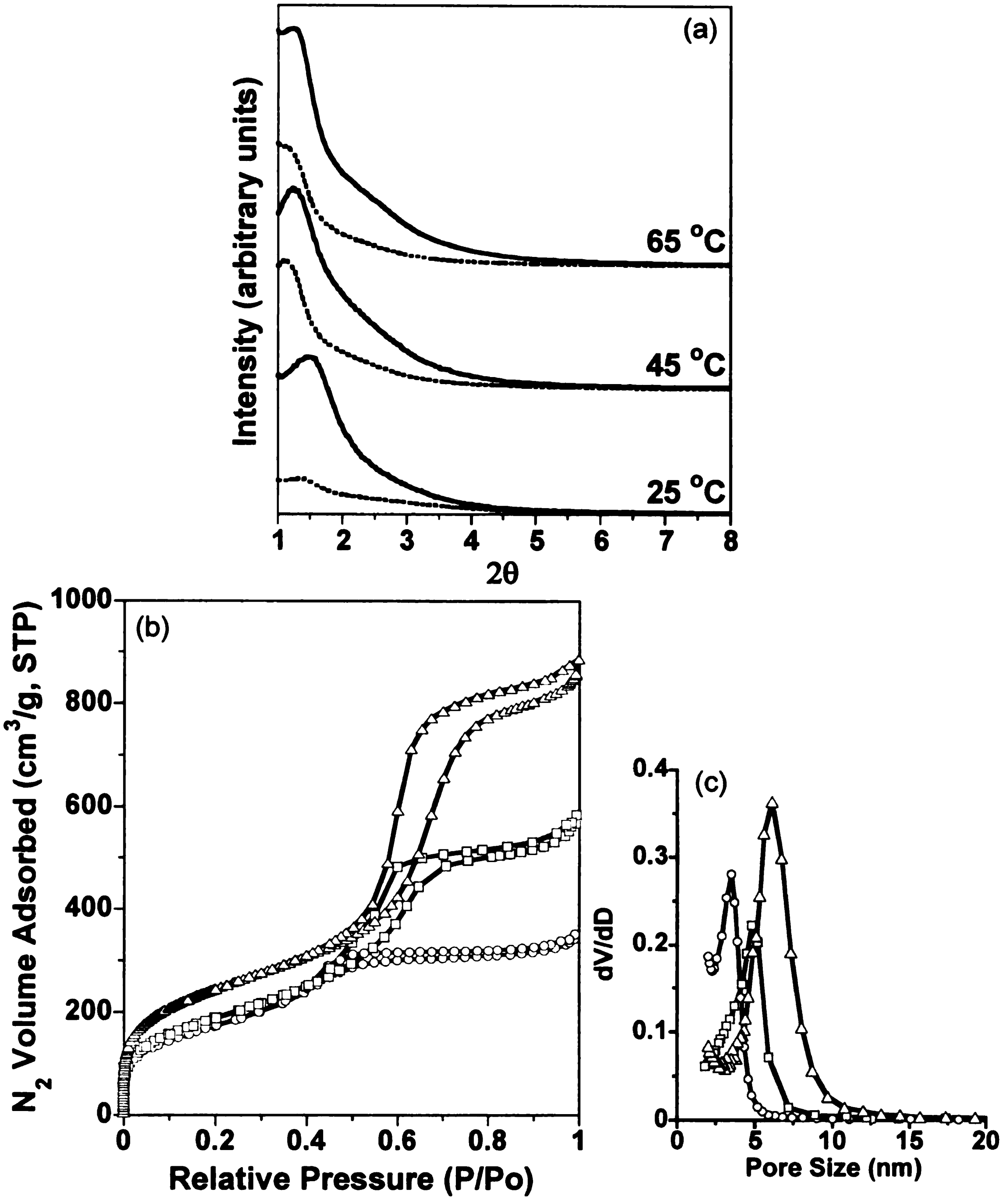

Figure 5.1 (a) XRD patterns, (b) N_2 sorption isotherms, and (c) pore size distributions for MSU-J silicas prepared from sodium silicate and M2005. The dotted (····) and solid (–) XRD scans represent as-made and calcined MSU-J silicas at different synthesis temperatures. Isotherms are measured for calcined MSU-J silicas synthesized at 25 (○), 45 (□), and 65 (Δ) °C.

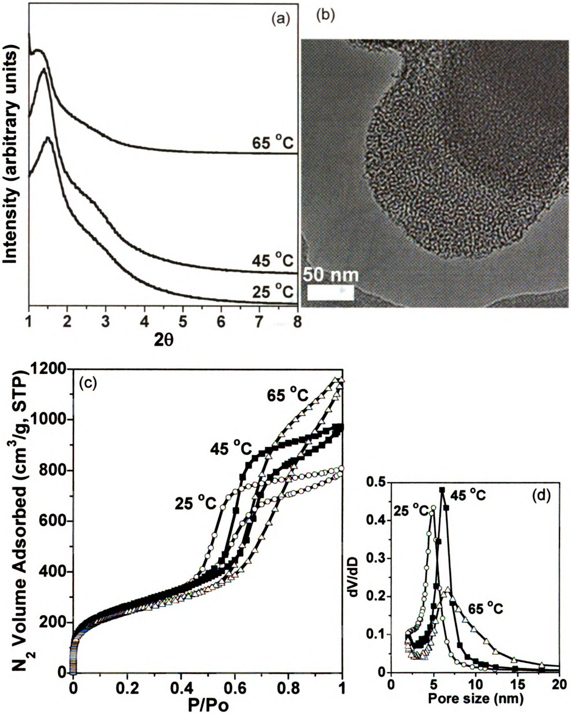

Figure 5.2 (a) XRD patterns, (b) a TEM image (synthesized at 25 °C), (c) N_2 sorption isotherms, and (d) pore size distributions for MSU-J silicas prepared from sodium silicate and T3000. The synthesis temperatures are indicated as 25 (○), 45 (■), and 65 °C (Δ) (c and d).

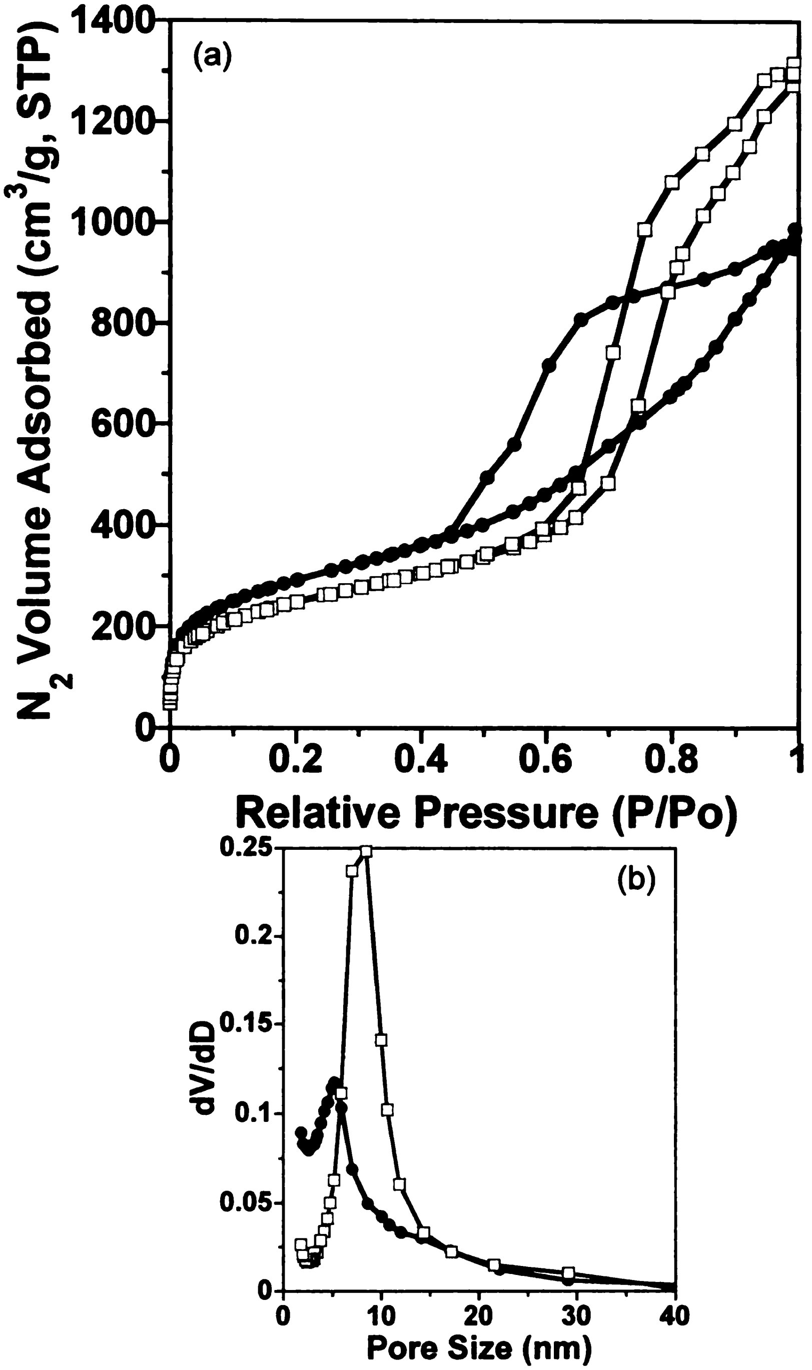

Figure 5.3 (a) N_2 sorption isotherms and (b) pore size distributions for MSU-J silicas prepared from sodium silicate and T5000. The synthesis temperatures are indicated as 25 (●), and 45 (□) °C.

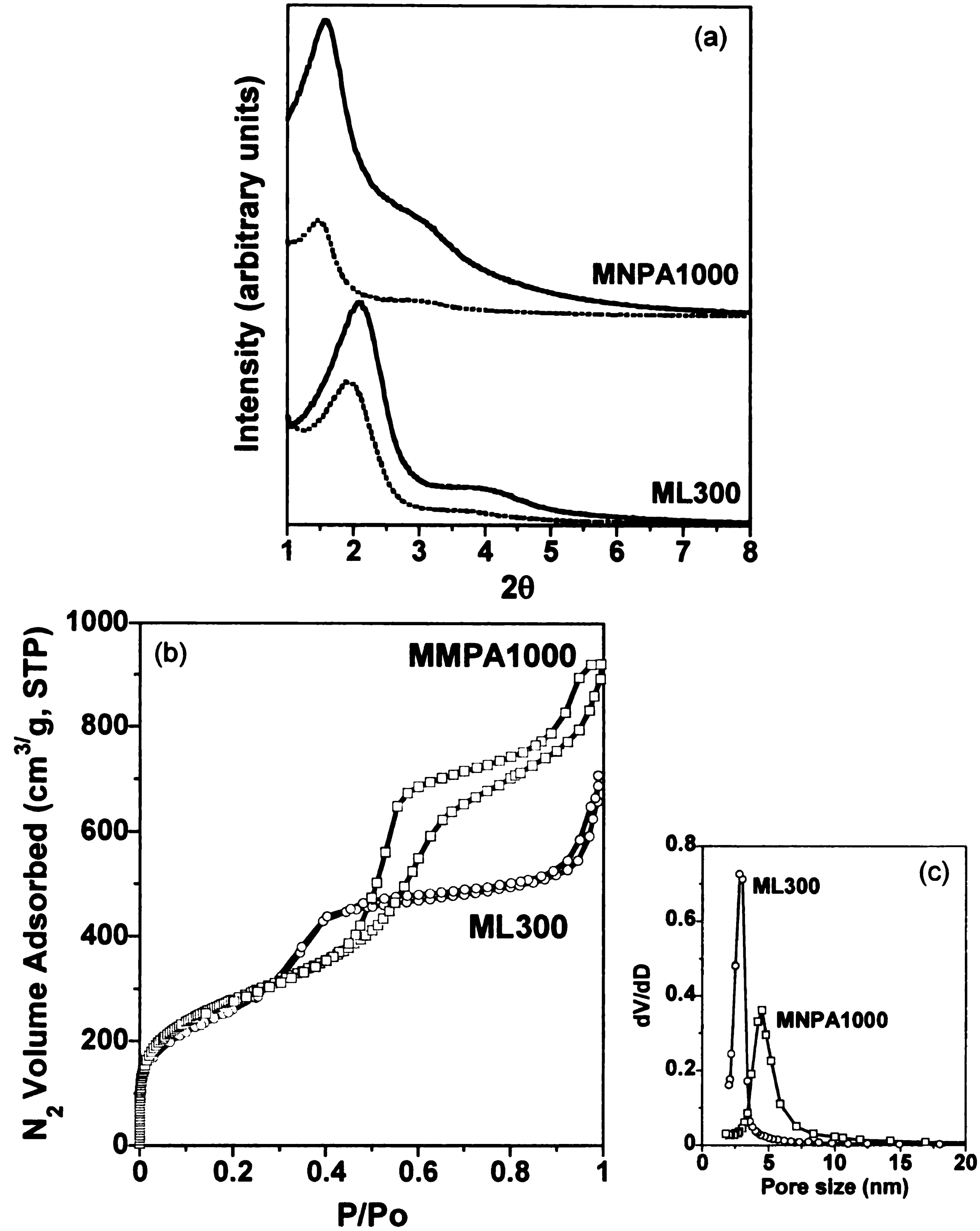

Figure 5.4 (a) XRD patterns (as-made; ···· and calcined; –), (b) N_2 sorption isotherms, and (c) pore size distributions for MSU-J silicas prepared from sodium silicate and Surfoamine surfactants (ML300; ○ and MNPA1000; □ in b and c).

TEM image of the MSU-J silica prepared form sodium silicate and T3000 at 25 °C shows typical wormhole framework morphology with a regular pore size (Figure 5.2b).

As shown in Chapter 2 the pore diameter of calcined MSU-J silicas generally expands accompanied by increase of the pore volume with increasing synthesis temperature over the range 25–65 °C. The temperature dependence of MSU-J pore sizes is associated with a decrease in H-bonding at the silica-surfactant interface with increasing temperature (details in Chapter 2).

The above results show that large-pore wormhole mesostructures have been successfully synthesized through the supramolecular assembly of neutral amine surfactants without the need for an auxiliary pore expander. Jeffamines are well-known curing agents for thermoset epoxy polymers[4] and the diverse Jeffamine chain lengths afford epoxy polymers with diverse mechanical properties and glass transition temperatures. Therefore, the as-made and calcined MSU-J wormhole mesostructures can be promising candidates as reinforcement agents for the corresponding thermoset epoxy polymers. Moreover, the mechanical properties of the epoxy polymers can be systematically modified by the controlling pore size, pore volume and surface area of the MSU-J silicas.

5.2 MSU-G Type Lamellar Mesostructures (Tomah3 Surfactants)

A family of mesoporous molecular sieves (MSU-G) with vesiclelike hierarchical structures has been prepared through a supramolecular assembly pathway using electrically neutral gemini surfactants as the structure-directing progens (composition 5.5) and a silica precursor, TEOS.[5] The electrically neutral

$C_nH_{2n+1}NH(CH_2)_2NH_2$ n = 10, 12, 14 (5.5)[5]

H-bonding assembly pathway based on the hydrolysis of TEOS in the presence of the gemini surfactants form vesiclelike silica mesostructures analogous to a L_α (bilayer lamellar phase) or L_3 (wormhole or spongelike phase) intermediate. The MSU-G vesicles exhibit unprecedented thermal (up to 1000 °C) and hydrothermal (>150 hours at 100 °C) stabilities due to their very high degree of framework (SiO_4) crosslinking, as comfirmed by ^{29}Si MAS NMR spectroscopy (Q^4/Q^3 ~7). Moreover, redox-active Ti(IV) and acidic Al(III) centers have been incorporated into the MSU-G framework without altering the lamellar framework or the vesicular hierarchical structure. The Al-substituted (2 mol%) MSU-G derivatives are more efficient acid catalysts than Al-MCM-41 (2 mol%) for the conversion of 2,4-di-*tert*-butylphenol and cinnamyl alcohol to a flavan.[6] For gemini derivatives with n = 12, 14 and m = 3, 4 (composition 5.6) hierarchical vesicles have been prepared analogous to those assembled from the gemini surfactants with m = 2.[7] However, for n = 10, a new coiled slab structure (m = 3) and an onion-like core-shell structure (m = 4) are formed.

$C_nH_{2n+1}NH(CH_2)_mNH_2\,(C^0_{n+m+0})$ n = 10, 12, 14 and m = 3, 4 (5.6)[7]

In this appendix, MSU-G type silica vesicles were synthesized from TEOS in the presence of commercially available gemini surfactants, DA1214 and DA14. The DA series of gemini surfactants provided by Tomah3 Chemical Inc. are alkyloxypropyl-1,3-diaminopropanes. The number after DA represents the number of carbon and oxygen atoms in tail group (compositions 5.7 and 5.8).

DA1214 $C_nH_{2n+1}O(CH_2)_3NH(CH_2)_3NH_2$ n = 8 and 10 (5.7)

DA14 $(CH_3)_2(CH_2)_8O(CH_2)_3NH(CH_2)_3NH_2$ (5.8)

The chemical structures of the surfactants are provided by Tomah3 Inc. DA1214 is a mixture of octyl- (50 mol%) and decyl- derivatives. A distinct difference between the DA gemini series and the former gemini surfactants (composition 5.6) used to prepare MSU-G silicas is the presence of an oxygen atom at the γ-position from the secondary amino group.

The synthesis procedure for the preparation of vesicular MSU-G silicas is similar to that of previously reported MSU-G mesostructures.[5] In a typical synthesis 0.8 g of DA1214 was dissolved in an ethanol/water solvent mixture (2 mL/18 mL) and 2.52 g of TEOS was then added to the surfactant solution. The reaction mixture was stirred at ambient temperature for 30 min. and then heated at 100 °C in an autoclave for 72 h under static conditions. The solid product was filtered, washed with water, and dried in air. The surfactant was removed by calcination at 600 °C for 4 h. The molar ratio of each reaction mixture was 1.0 Si : 0.25 Surfactant : 4.3 EtOH : 78 H_2O. Partially protonated amine surfactants were used by adding 1.0 mL of 1.0 M HCl solution (H^+/Si = 0.083).

An as-made mesoporous material prepared from TEOS in the presence of the neutral and protonated forms of DA1214 surfactant shows an intense low angle reflection in the XRD pattern (not shown) similar to the diffraction feature of the previously reported MSU-G vesicles. The TEM images (Figure 5.6 a, b) of

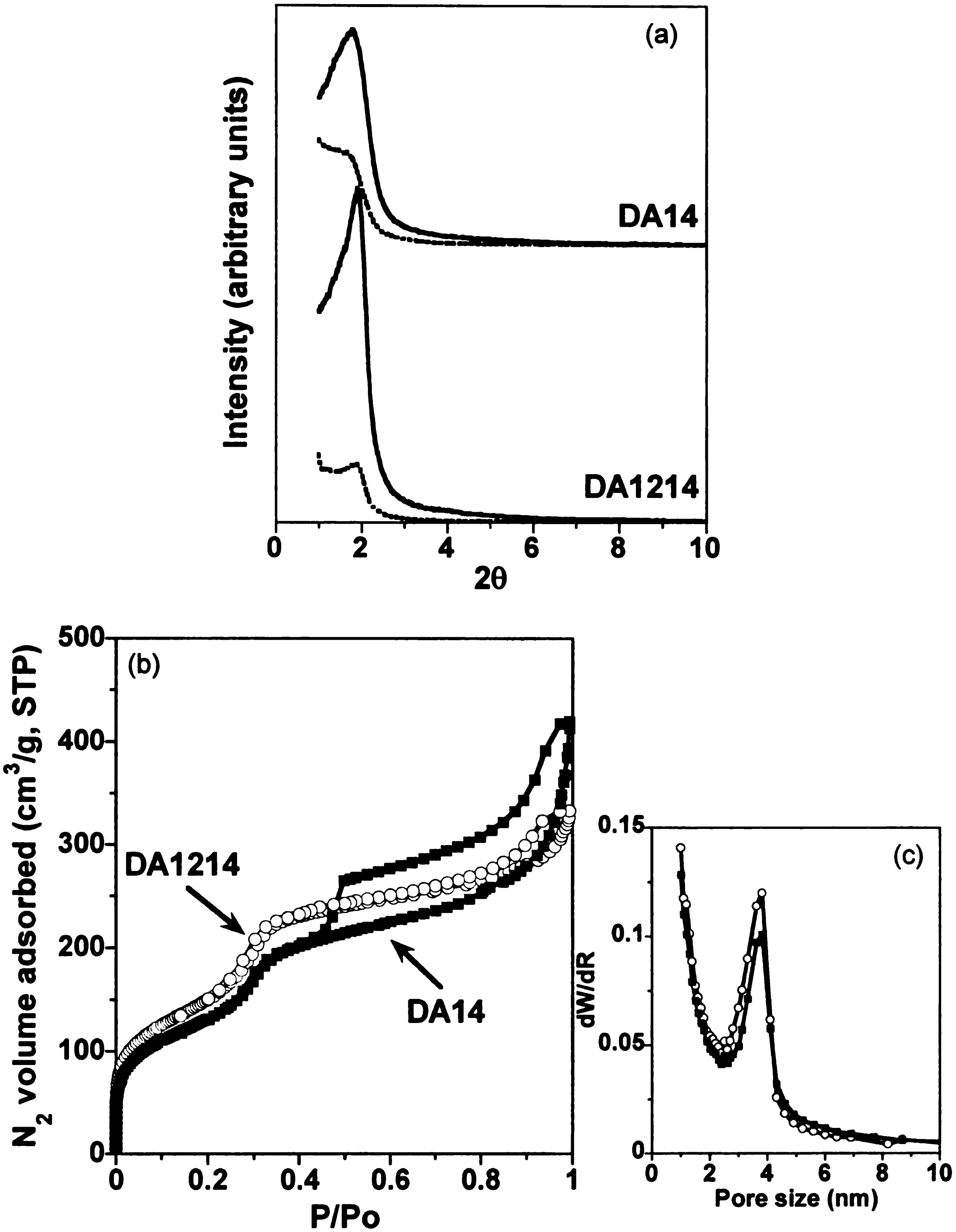

Figure 5.5 (a) XRD patterns (as-made; ···· and calcined; –), (b) N_2 sorption isotherms, and (c) pore size distributions for silica vesicles prepared from TEOS and partially protonated Tomah3 DA surfactants (DA1214; ○ and DA14; ■ in b and c).

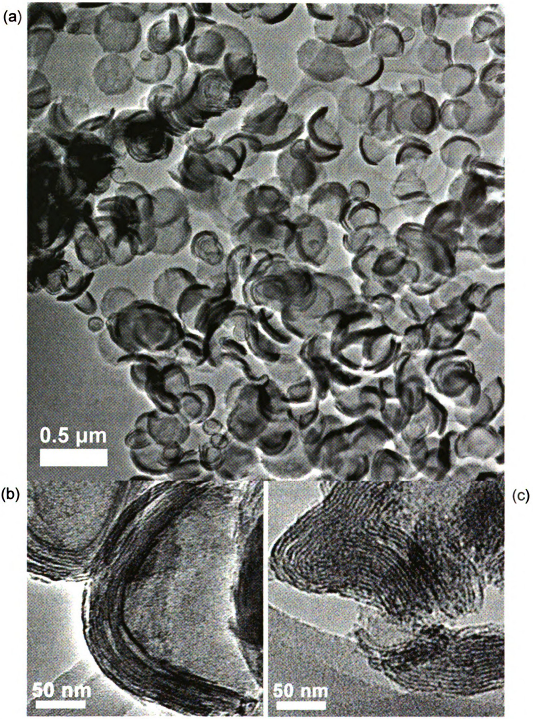

Figure 5.6 (a) TEM images with low and (b) high magnification of MSU-G type lamellar vesicles formed from TEOS and neutral DA1214 surfactant (as-synthesized). (c) A TEM image of the calcined lamellar silica structure assembled from partially protonated DA1214 surfactant.

the as-made mesostructure assembled under electrically neutral conditions illustrate the vesicular morphology containing 5–20 silica layers in the vesicular walls. Almost all of the particles (100–400 nm size) are broken vesicles. However, the lamellar structure is collapsed by removing surfactant indicating lack of pillars in the gallery region of the layers. In contrast, the partially protonated DA1214 surfactant formed by adding a small amount of hydrochloric acid (H^+/Si molar ratio = 0.0083 – 0.083) to the reaction mixture leads to lamellar silica nanoparticles. Figure 5.5a (bottom) illustrates the well-ordered lamellar structures and the XRD patterns of the as-made and calcined lamellar mesostructure assembled from protonated DA1214 gemini surfactant (H^+/Si = 0.083). The maximum in the HK pore size distribution curve occurs at 3.8 nm, corresponding to capillary condensation of liquid nitrogen at a relative pressure ~0.3 (see Table 5.2). Although the silica assembled from the partially protonated gemini surfactant possess a lamellar framework structure and textural properties similar to those of MSU-G silica, the particle morphology cannot be described as being a vesicle. However, the size of the lamellar silica particles is relatively more uniform (100–200 nm) and each particle has a more regular number of silica layers (~15).

No mesoporous materials with well-resolved XRD reflections were synthesized from neutral DA14 gemini surfactant. From the XRD pattern (Figure 5.5a, top) and N_2 sorption properties (Figure 5.5b) of the calcined silica assembled from protonated DA14 surfactant may be comparable to the lamellar silica form by protonated DA1214 with same amount of acid in physical properties. However, more detailed studies including TEM are required to determine the framework structures of the silica prepared from the DA14 gemini surfactant.

Table 5.2 Textural properties for lamellar silica vesicles assembled by TEOS in the presence of Tomah gemini surfactants.

Surfactant	HCl/Si molar ratio	*d* spacing[a] (nm)	S_{BET} (m^2/g)	Pore size (nm)	Wall thickness[b] (nm)	Pore volume (cm^3/g)
DA1214	0.0	5.1 / -[c]	464	-[d]	-	0.39
	0.083	4.8 / 4.7	543	3.8	1.9	0.47
DA14	0.0	-[c] / -[e]	418	-[d]	-	0.98
	0.083	-[c] / 5.0	479	3.8	2.2	0.65

[a] Basal spacings of as-made and calcined MSU-J silicas are separated by a slash (as-made / calcined).

[b] The framework wall thickness is determined by subtracting the HK pore size from the d spacing of calcined sample.

[c] A low-intensity hump (one third of intensity of the as-made sample) in range of 1.5–2° 2θ.

[d] No observable peaks in HK pore size distributions.

[e] No evident XRD reflections.

The protonated amine group possibly plays an important role in forming silica bridges between silica layers. The tail of tomah3 surfactants contains an ether (oxygen atom) group with a partial negative charge which causes a weaker van der Waals interaction between the surfactant tails in comparison to the previous gemini surfactants containing alkyl tail groups. The corresponding increase in the surfactant chain volume results in an increase in the effective packing parameter (*g* value, Figure 1.3). Thus only silica lamellar layers in absence of pillars in gallery region are generated. Once a small amount of acid (H^+/NH_2 = 0.0166–0.166) is added to the reaction mixture the larger effective head group area of the partially protonated amino groups decreases the packing parameter, to produce bridges between silica layers. However, lamellar silica framework structures are not formed at higher concentrations of ammonium groups (H^+/NH_2 >0.166), as confirmed by XRD and N_2 sorption analyses (not shown).

Mesostructured molecular sieves with a lamellar framework structure have been synthesized from TEOS and commercially available gemini surfactants in partially protonated form. A relatively low molar fraction of protonated amino groups in the surfactants generates pillared lamellar silica frameworks. The mesostructures are predicted to exhibit improved thermal and hydrothermal stability and high catalytic performance as shown in previously in the published literature[5, 6]. However, a more detailed analysis such as XRD, TEM and ^{29}Si NMR is needed to complete the characterization of the novel materials. Also, a more detailed study of the reaction stoichiometry required for a more complete description of the assembly reactions.

5.3 References

(1) Lee, J.; Yoon, S.; Oh, S. M.; Shin, C. H.; Hyeon, T. *Adv. Mater.* **2000**, *12*, 359.

(2) Pauly, T. R.; Liu, Y.; Pinnavaia, T. J.; Billinge, S. J. L.; Rieker, T. P. *J. Am. Chem. Soc.* **1999**, *121*, 8835.

(3) Park, I.; Wang, Z.; Pinnavaia, T. J. *Chem. Mater.* **2005**, *17*, 383.

(4) Pinnavaia, T. J.; Lan, T. US Patent 5,801,216, **1998**.

(5) Kim, S. S.; Zhang, W. Z.; Pinnavaia, T. J. *Science* **1998**, *282*, 1302.

(6) Kim, S. S.; Liu, Y.; Pinnavaia, T. J. *Micropor. Mesopor. Mater.* **2001**, *44*, 489.

(7) Karkamkar, A. J.; Kim, S. S.; Mahanti, S. D.; Pinnavaia, T. J. *Adv. Funct. Mater.* **2004**, *14*, 507.

APPENDIX

HIGH OXYGEN GAS BARRIER CLAY-EPOXY COMPOSITE FILMS

A.1 Introduction

Improving the gas barrier of polymers and plastics to small molecules (e.g. O_2, H_2, H_2O, CO_2 etc.) is an important need for a vast number of applications, such as food and beverage packaging, liquid hydrogen storage and transportation, moisture and air-proof coatings, etc. As mentioned in Chapter 1 the high aspect ratio of impermeable exfoliated clay nanolayers in a polymer matrix presents an increased tortuous path length for permeant gas molecules. For instance, PET (polyethylene terephthalate)-monmorillonite nanocomposites exhibits up to 70% reduction in oxygen permeability compared to the pristine polymer, depending on the degree of clay exfoliation, nanolayer orientation and aspect ratio of the clay platelets.[1]

In this appendix, a new method is described for fabricating highly oxygen-impermeable polymer composites by impregnating smectite clay films with the thermoset epoxy polymer. The glassy epoxy polymer described in this study can have significant practical applications for the manufacturing of liquid hydrogen and methane storage tanks and transfer pipes. The reduction in oxygen permeability measured for the different epoxy–clay composite films were 2–3 orders of magnitude lower than for the pristine polymer. A recent study[2] on the permeability of epoxy-montmorillonite nanocomposites demonstrated a 70% reduction of oxygen permeability coefficient at 5 vol% loading. The barrier properties of the described epoxy–clay composite films were far better than those for classical epoxy–clay nanocomposite samples[3], which were also prepared and tested for comparison.

A.2 Sample Preparation

The epoxide resin used for the formation of the pristine glassy epoxy polymer and the epoxy–clay composite films was EPON 826 (see structure 1.3) and the curing agent was Jeffamine D230 (D230, structure 1.4). An industrially purified Na^+-montmorillonite (PGW, Nanocor Inc.) with a cation exchange capacity (CEC) of 120 meq/100 g was used as the pristine clay for the preparation of the Na^+–montomorillonite clay films. A synthetic Li^+-fluorohectorite clay (FH, Corning Inc.) with a CEC similar to that of the PGW montmorillonite was used as the pristine fluorohectorite clay for the preparation of the Li^+–fluorohectorite clay films in this study.

For the preparation of the self-supported Na^+–montomorillonite clay film 190 mL of an aqueous suspension containing 10.0 g of Na^+-montmorillonite (PGW) was blended at room temperature for 1–2 min to form a clay colloidal suspension (with clay concentration of 5 wt%). The colloidal suspension was then cast on a glass plate and was dried at room temperature and atmospheric conditions for a period of 2 days. The formed clay film was then carefully peeled of the glass plate. In this way a smooth, self-supported, continuous, semi-transparent Na^+-montmorillonite clay film with a uniform thickness of 60 μm was produced. The thickness of the film could be varied depending on the initial concentration of the aqueous clay colloidal suspension. For example, a 3 wt% clay suspension resulted in a 35 μm thick film. Li^+–fluorohectorite films were prepared in the same fashion as the Na^+–montmorillonite films.

Pristine glassy epoxy polymer disks were prepared by mixing the epoxy monomer with the curing agent at 50°C for ~30 min, outgassing the liquid mixture at room temperature and curing the mixture on an aluminum disk mold by using an appropriate relief-coat at 75°C for 3 h and at 125°C for an additional 3 h under nitrogen. The formed epoxy disks were polished to an average thickness of ~0.2 mm (~8 mil).

For the preparation of the epoxy–clay composite films the self-supported clay films were impregnated with a mixture of uncured EPON 826 and D230 and were then cured to form flexible epoxy–clay composites in which the clay film was encapsulated in the epoxy polymer in a sandwich-like fashion. The Na^+–montmorillonite film with dimensions approximately 8 cm × 8 cm was dipped in a mixture of EPON 826 epoxy resin and D230 curing agent at room temperature until it was well-wetted on both sides. The epoxy–D230 mixture was prepared by mixing the liquid EPON 826 resin with the D230 at 50°C, for 30 min, under stirring. Before dipping the clay film in the pre-polymer, the uncured epoxy–D230 mixture was outgassed at room temperature for 30 min. The dipped clay film was then suspended vertically at room temperature in air so that excess uncured mixture was allowed to drop from the film. After 1 day of aging in air the epoxy resin was partially cured. The epoxy–clay composite film was then heated in the oven at 60°C for 3 h and 125°C for 3 h in a nitrogen atmosphere so that the epoxy resin was completely cured. The produced cured epoxy–clay composite film was smooth, flexible, semi-transparent and uniformly covered on both sides with cured epoxy polymer.

In order to estimate the tortuosity factor of the film the weight content of the impregnated epoxy polymer in the Na^+-montmorillonte clay film was calculated by measuring the thickness and weight of the clay film, the pristine epoxy disk, and the composite sample. The weight content of clay was converted to a volume fraction using the bulk densities of the Na^+-montmorillonite film (2.0 g/cm^3) and the pristine epoxy polymer (1.18 g/cm^3). The void volume of the Na^+-montmorillonite film prepared from a 3 wt% clay suspension was also estimated using the bulk density of Na^+-montmorillonite (2.6 g/cm^3)[4]. The external epoxy polymer coating of the composite film was excluded from the calculation of the volume fraction.

X-ray diffraction (XRD) patterns were obtained on a Rigaku rotaflex 200B diffractometer equipped with Cu K_α X-ray radiation and a curved crystal graphite monochromator, operating at 45 KV and 100 mA. The diffraction patterns were collected between 1 and 12° at a scanning rate of 1°/min. Samples of the Na^+-montmorillonite powder and film were prepared by mounting the films on a glass holder and a glass slide, respectively.

Oxygen permeability measurements were performed on a Mocon Ox-tran 2/60 oxygen permeability instrument with a 100% oxygen as test gas. The specimens tested were the pristine epoxy polymer disks and the epoxy–clay nanocomposite disks with an average thickness of ~0.2 mm (~8 mil), and the epoxy–clay composite films with an average thickness ranging from ~0.10 to ~0.15 mm.

A.3 Results and Discussion

Different types of pristine clays have been cast from aqueous suspensions into opaque (fluorohectorite) and semi-transparent (montmorillonite) films. The clay film made from montmorillonite has a light brown color and is smooth, continuous, flexible and semi-transparent. Self-supported films with different lateral dimensions could be fabricated in this way. Optical images of the self-supported Na^+-montmorillonite film with a thickness of 35 μm are shown in Figure A.1. The fluorohectorite films prepared from 5 wt% suspension by the same method had a white color and a mean thickness of ~65 μm.

The XRD patterns of the Na+-montmorillonite powder and the form of the clay film prepared from 3 wt% water suspension are shown in Figure B.2. Although base line corrections for each pattern are necessary to compare the reflection intensities, the 001 peak of the film sample (Figure A.2 b) exhibits five times higher intensity than that of the powder sample, indicating the nanolayers are stacked in the film sample with high ordering along the c axis. In addition, the intensity of the 004 peak for the film sample is 25 times higher than the corresponding peak of the powder sample. Consequently the exfoliated individual clay nanolayers are stacked with highly ordered perpendicular to the layer plane.

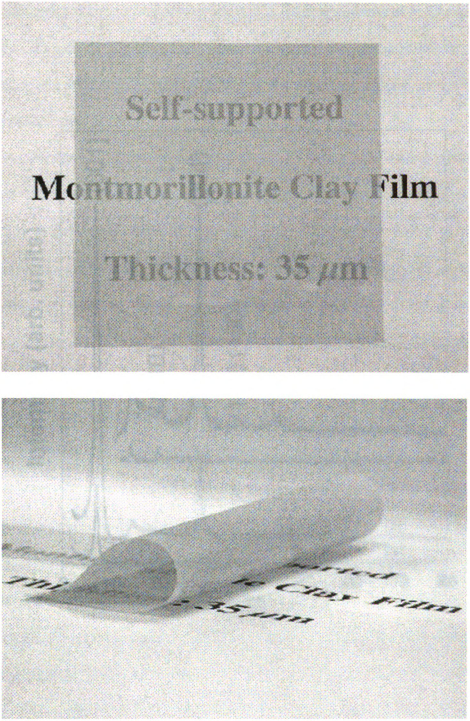

Figure A.1 Optical images of a self-supported Na^+-montmorillonite clay film with a thickness of 35 μm prepared from a 3 wt% aqueous suspension.

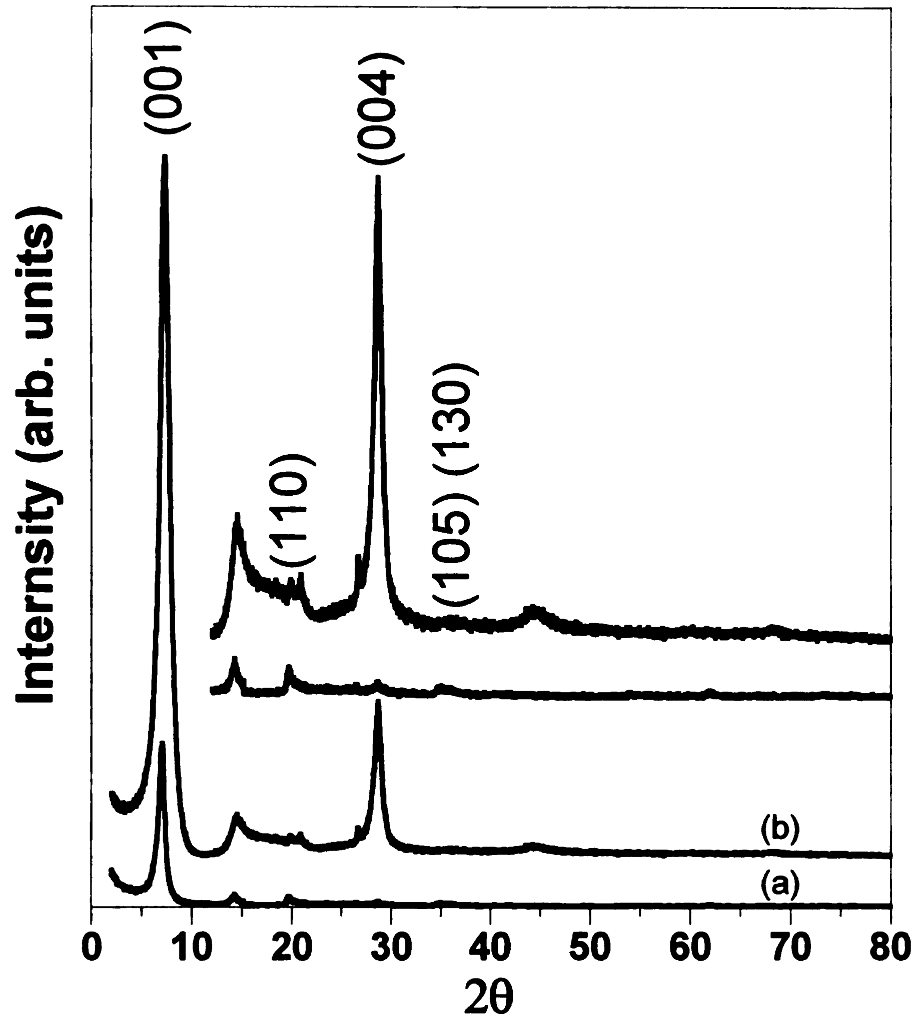

Figure A.2 X-ray diffraction patterns of (a) Na$^+$–montmorillonite powder and (b) the Na$^+$–montmorillonite film prepared from a 3 wt% water suspension. The intensity of the patterns from 12° to 80° was multiplied three-fold and shown as an insert for clarity. Offsets are 500 counts for both sets of scans.

A proposed restacked clay structure formed in films is illustrated in Figure A.3 (a). From SEM images of the clay films (not shown) the clay films possess micro or sub-micro voids which may generate the extremely high oxygen permeability (> 6000 $cc \cdot mil \cdot m^{-2} \cdot day^{-1}$).

The barrier properties of polymer–clay nanocomposites have been initially described based on a relatively simple tortuous path model[5], as is presented in Chapter 1. In this model the silicate platelets obstruct the diffusion of gases through the polymer matrix. The improvement in the barrier properties based on this model is a function of the volume fraction and of the aspect ratio of the platelets. Moreover, it is generally considered that a parallel orientation of the clay platelets to the surface of the polymer–clay nanocomposite film is necessary for improving the barrier properties of the polymers. This prerequisite is usually difficult to achieve, especially in thermoset polymer–clay nanocomposites such as epoxy nanocomposites, where the exfoliated individual clay nanolayers with thickness of ~1 nm are randomly oriented upon curing of the polymer resin.

The dependence of the oxygen permeability of a classical epoxy–clay nanocomposite on the clay content has been examined. The nanocomposites were prepared from organically modified montmorillonite and fluorohectorite with Jeffamine D2000 (see structure 1.7) and the same epoxy polymer.[3] The nanocomposite specimens had a thickness of ~0.2 mm (~8 mil) and the clay nanolayers in the polymer matrix were intercalated or exfoliated depending on the degree of onium ion exchange. The reduction in oxygen permeability is achieved with the increase in the degree of nanolayer exfoliation but it was never

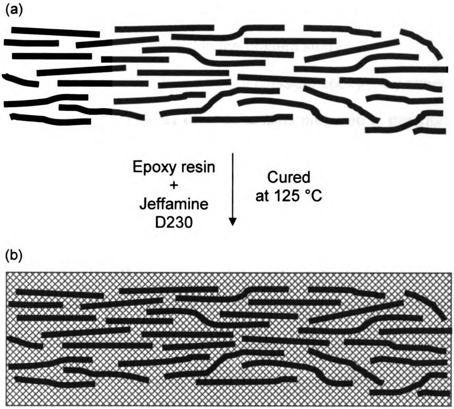

Figure A.3 Proposed clay nanolayer structure of an oriented clay film in (a) pristine and (b) epoxy-impregnated form. The mixture of epoxy resin and D230 represented by hatched pattern is impregnated in voids of the clay films and cured at 125 °C to form high gas barrier composite films. Sodium ions in the gallery regions of the clay are omitted for clarity.

higher than ~20% at 6 wt% clay loading. Higher clay loadings had a small additional effect on the barrier properties of the nanocomposites. Although greater reductions in gas permeability have been previously reported[1, 6-8], they refer to the reduction achieved for more permeable pristine polymers (such as PET and rubbers) and/or to permeants (e.g. water vapor) different from the epoxy and oxygen system of interest in the present study.

In contrast to the barrier properties of classical epoxy–clay nanocomposite samples, the oriented epoxy–clay composite films prepared in this work showed a dramatic decrease in oxygen permeability, reaching 2–3 orders of magnitude lower than the permeability of the pristine epoxy. This enormous increase of the barrier properties of the produced epoxy composites was achieved by impregnating the extremely permeable clay films (oxygen permeability $\geq 6 \times 10^3$ $cc \cdot mil \cdot m^{-2} \cdot day^{-1}$) with the permeable pristine epoxy polymer. The oxygen permeability data for the epoxy–clay composite film specimens prepared from different clay films are shown in Table A.1. In most cases, the reduction in oxygen permeability is 2–3 orders of magnitude in comparison to the pristine epoxy polymer and 3–4 orders of magnitude compared to the pristine clay films. The reduction in permeability was not significantly affected by the thickness of the composite clay film since a ~10 μm sodium montmorillonite composite clay film resulted in a similar decrease in oxygen permeability as an epoxy–clay composite film with a thickness of ~60 μm (see Table A.1). In general, the differences in permeability among different composite film samples are difficult to identify because the low oxygen transmission rates are subjected to relative high standard deviation of the mean values.

Table A.1 Oxygen Permeability data of the epoxy–clay composite films.

Sample	Thickness of Clay Film (mm)	Thickness of Epoxy–Clay Composite film (mm)	Oxygen Permeability (cc·mil·m^{-2}·day^{-1})
Pristine Epoxy	-	0.20	98.9
Epoxy–(Na^+-montmorillonite)	0.060	0.11	≤ 0.1
Epoxy–(Na^+-montmorillonite)	0.035	0.10	0.97
Epoxy–(Li^+-fluorohectorite)	0.065	0.14	1.2

On the bases of the density of a Na^+-montmorillonite platelet and the bulk density of a montmorillonite film, the void volume fraction in the Na^+-montmorillonite film is calculated to ~0.19. This is consistent with the volume fraction of the impregnated epoxy polymer (~0.21) in the clay film which is used for tortuosity factor estimation. If clay disk plates of diameter L and width W are dispersed in a parallel fashion in a polymer matrix, the widely used tortuosity factor[5] and the relative permeability are given in equation 1.6. Typical aspect ratio for natural montmorillonite is 200 (200 nm in length and 1 nm in thickness).[9] Thus, the tortuosity factor for the Na^+-monmorillonite–epoxy composite film is 76 and its predicted permeability is 1.3 cc·mil/m^2·day. This is slightly higher than the oxygen permeability data shown in Table A.1. However, equation 1.6 is applicable only in dilute ($\alpha\varphi$<<1) regime.[10] The more developed version (equation 1.7)[11] includes a quadratic term and provides a more reliable prediction (0.07

cc·mil/m^2·day) of extremely low oxygen permeabilities consistent with the observed values.

The high barrier properties of epoxy–clay composite films results from the confinement of epoxy in the voids between stacked clay layers and the voids formed between layer edges and folded layers (see Figure A.3). The impregnation of the clay films by the liquid, uncured epoxy polymer precursors occurs through diffusion into the voids of sub-micron dimensions that exist on the surface of the clay films. Such cracks, which were observed by SEM images (not shown here), allow the liquid epoxy resin to approach the inorganic clay nanolayers in the center of the clay film.

A.4 Conclusion

A new concept in barrier technology is presented in this work wherein the appropriate combination of two permeable materials resulting in a composite with extremely low gas permeability. This unprecedented increase of barrier properties can be achieved by impregnating an inorganic clay film with the polymer precursors resulting in a cured composite that contain a central phase consisting of highly oriented clay nanolayers. The high volume fraction of parallel oriented clay nanolayers in impregnated epoxy polymer cause the permeability of the polymer phase to be significantly lower than that of the bulk polymer, and to contribute also to the extremely high barrier properties.

A.5 References

(1) Matayabas Jr, J. C.; Turner, S. R. In *Polymer-Clay Nanocomposites*, Edited by Pinnavaia, T. J. Beall, G. W., Wiley, New York, **2001**.

(2) Osman, M. A.; Mittal, V.; Morbidelli, M.; Suter, U. W. *Macromolecules* **2004**, *37*, 7250.

(3) Triantafillidis, C. S.; LeBaron, P. C.; Pinnavaia, T. J. *Chem. Mater.* **2002**, *14*, 4088.

(4) Osman, M. A.; Mittal, V.; Lusti, H. R. *Macromol. Rapid Comm.* **2004**, *25*, 1145.

(5) Nielsen, L. E. *J. Macromol. Sci. (Chem.)* **1967**, *A1*, 929.

(6) Messersmith, P. B.; Giannelis, E. P. *Chem. Mater.* **1994**, *6*, 1719.

(7) Strawhecker, K. E.; Manias, E. *Chem Mater* **2000**, *12*, 2943.

(8) Kojima, Y.; Fukumori, K.; Usuki, A.; Okada, A.; Kurauchi, T. *J Mater Sci Lett* **1993**, *12*, 889.

(9) Yano, K.; Usuki, A.; Okada, A.; Kurauchi, T.; Kamigaito, O. *J. Polym. Sci. Part A: Polym. Chem.* **1993**, *31*, 2493.

(10) Fredrickson, G. H.; Bicerano, J. *J Chem Phys* **1999**, *110*, 2181.

(11) Cussler, E. L.; Hughes, S. E.; Ward, W. J.; Aris, R. *J. Membrane Sci.* **1988**, *38*, 161.